TAMPEREEN TEKNILLINEN YLIOPISTO
TAMPERE UNIVERSITY OF TECHNOLOGY

NIDA RIAZ

DIELECTRIC CHARACTERIZATION OF BI-AXIALLY ORIENTED POLYPROPYLENE INSULATIONS

Master of Science thesis

Examiner: Adjunct prof. Kari Lahti
Examiner and topic approved by the Council of the Faculty of Computing and Electrical Engineering on 8th June 2016

Abstract

TAMPERE UNIVERSITY OF TECHNOLOGY
Master's Degree Programme in Electrical Engineering
Nida Riaz: Dielectric characterization of bi-axially oriented polypropylene insulations
Master of Science Thesis, pages 101
December 2016
Major: Smart Grids
Examiner: Adjunct prof. Kari Lahti
Keywords: Polymer, degradation, sputtering, dielectric spectroscopy, capacitor, thin film insulation, BOPP, nanocomposite, dielectric strength, loss factor, permittivity, electric field, thermal stress, humidity, polarization.

Recent advancement in the field of thin film polymer insulations have brought limelight in the usage of bi-axially oriented dielectric thin films for high voltage capacitors and insulations. The reason of this popularity and extensive acceptance of bi-axially oriented thin films is their peculiar characteristics and optimum balance in the thermal, electrical and mechanical properties. Moreover, the demand of high energy density for capacitors and operation of dielectrics near breakdown voltage further prominent the importance of bi-axially oriented thin films as a dielectric material and insulation. In this thesis, the dielectric material under consideration is bi-axially oriented polypropylene (BOPP) thin film and its nanocomposite. BOPP has low dielectric loss with permittivity around 2.2 and relatively high energy density because of the ability to operate near breakdown voltage because of self-healing property when used with in metallized electrodes.

The focus of this thesis is to establish the optimum procedure of sample preparation of BOPP dielectric films for dielectric spectroscopy using Novocontrol device. It has been observed that thin film or the considered material behavior and characteristics vary with respect to the physical condition and potential stresses during experiments. Thus, to minimize these stresses, various methods have been tried by varying different physical parameters which are discussed in detail in chapter 5. An optimum testing procedure has also been proposed for precise experimental results. A detailed portion on estimating reliability and repeatability of the measurements has been introduced which tries to establish the validity of measurements and comment on the possible sources of errors and uncertainties.

After establishing the testing procedures, the next phase of the thesis includes the dielectric characterization of BOPP and its nanocomposite. Since BOPP thin films can be customized by altering the polymer material composition resulting in nanocomposite and micro composites. The comparison of nanocomposites with respect to pure BOPP has also been made and explained. The effect of moisture and ambient humidity has been analyzed at different levels of relative humidity e.g. 0%, 30%, 75%, 90% and 100% RH. The degradation of the dielectric properties of polymer due to moisture absorption is studied in Chapter 6. This chapter is also comprised of dielectric behavior of BOPP and its

nanocomposite as a function of temperature, frequency and applied field. The operation of pure BOPP and its nanocomposite has been studied over a temperature range of -60°C to 130°C. Moreover, the aging of BOPP w.r.t temperature has been analyzed. The degradation of dielectric properties of thin film sample due to continuous application of wide range of temperatures from -60°C to 130°C during temperature test has also been observed and discussed. This aspect has been identified when these results were compared with the results found during the application of only a certain temperature and not a series of different temperatures. The last phase of the thesis includes the dielectric response of BOPP as a function of applied field as the energy density and voltage endurance are of prime importance these days in high voltage applications.

PREFACE

Under the department of Electrical Engineering of Tampere University of Technology, I have completed my masters of science thesis in the year 2016. This thesis elaborates the dielectric behavior of Bi-axially oriented thin film polypropylene insulation.

I would like to pay my heartiest regards and thanks to Adjunct Professor Mr. Kari Lahti for his valuable supervision and guidance during thesis. As he helped me a lot in understanding the thesis and also flourished my knowledge with the background of the topic and made the path convenient for me being a student of Smart Grids. I also want to show my gratitude for the entire staff of High Voltage research group of department especially postdoctoral researcher Ilkka Rytöluoto and doctoral student Mikael Ritamäki for their support in learning how to use the novo control device and sputter coater as well as their assistance in handling different problems and scenarios during the experimental and analytical phases of the thesis. Also, I want to thank doctoral student Minna Niittymäki for her moral and professional assistance.

Finally, I also want to thank all the laboratory assistants, technicians and staff from different departments who took part in some way in any phase of the thesis. Also, I thank doctoral student Hannes Ranta who reserved time and came to help me using profilometer. I am grateful to all my friends, family and those who think that they have contributed in this thesis some way.

Tampere, 16.09.2016

Nida Riaz

CONTENTS

TERMS AND DEFINITIONS

A	Area
AC	AC Alternating current
$Å$	Angstrom (10^{-10} m)
Al_2O_3	Alumina
$BOPP$	Bi-axially oriented polypropylene
C	Capacitance
C_0	Vacuum capacitance per unit area, coupling capacitance
C_a	Equivalent capacitance
D_e	Electric displacement
DC	Direct current
DF	Dissipation factor
d_n	Dipole moment
d	Distance
d_A , d_B	Thickness of the material
DL	Dielectric Loss
DP	Degree of polymerization
$E_{threshold}$	Threshold energy
E	Electric field
E	Energy
ESL	Equivalent Series Inductance
ESR	Equivalent Series Resistance
EMI	Electromagnetic interface
f	Frequency (Hz)
G	conductance
HV	High voltage
$HVAC$	High voltage alternating current
$HVDC$	High voltage direct current
I	Current
ΔI_{xc}	Unbalance capacitive current component
I_{xr}	Dissipation current
I_c	Charging current
I_l	Loss current
ICC	Intraclass correlation
k	Boltzmann's constant
L	Inductance
LV	Low voltage
l	length
m	Molecular mass
$\overline{Mz}$	Z-average molecular weight
$\overline{Mv}.$	Viscosity-averaged molecular weight
$\overline{Mw}$	Weight-averaged molecular weight.
$M_i.$	Molecular weight of component
$\overline{Mn}$	Number-averaged molecular weight
$MgCl_2$	Magnesium chloride
MgO	Magnesium Oxide

N	Number of dipoles/unit volume
N_A	Avogadro's number
$NaCl$	Sodium chloride
NANOPOWER	Novel polymer nanocomposites for power capacitors
n_i	No. of component i in the sample
P	Polarization
p	Pressure
p_n	Dipole
p_i	Dipole moment per unit volume
P_{evap}	Vapor pressure
PD	Partial discharge
PA	Polyamide
PET	Polyethylene terephthalate
PP	Polypropylene
PS	Polystyrene
PVC	Poly vinyl chloride
PVD	Physical vapor deposition
POSS-EP	Polyhedral Oligomeric Silsesquioxane Ethylene Propylene
Q	Reactive power, charge
q	Magnitude of the charge
QDC	Quasi DC current
R	Radius, Resistance
RMS	Root mean square
R_{ESR}	Series equivalent resistance
SD	Standard deviation
SEM	Scanning electron microscope
SPSS	Statistical Package for the Social Sciences
SiO_2	Silica
SR	Silicon Rubber
sq	Square
T	Temperature
T_g	Glass transition temperature
T_m	Melting temperature
TUT	Tampere University of Technology
TiO_2	Titania
V	Voltage
Δv	Unit volume
VAr	Volt ampere reactive
wt-%	Weight percent
W	Energy (Watt)
w_i	Mass of component i in the sample
W_e	Electrostatic energy
X_c	Capacitive reactance
XLPE	Cross-linked polyethylene
Y	Young's modulus
Z	Impedance of the sample
α	Polarizability, thermal expansion
β	Weibull shape parameter
α-form	Configuration of polymers

β-form	Configuration of polymers
γ-form	Configuration of polymers
ε_0	Permittivity of free space ($8.85\times10^{-12}\mathrm{Fm}^{-1}$)
ε_r	Relative permittivity
ε	Total permittivity
ε'	Real part of the complex permittivity
ε''	Imaginary part of the complex permittivity
ε^*	Complex permittivity
φ	Rotation angle (degrees) in polymer conformation
θ	Phase angle
μ_i	Mobility of charge carriers
ω	Angular frequency
δ	Loss angle
ρ	Charge density
σ	Surface tension
χ	Electrical susceptibility
∇H	Enthalpy change

1. INTRODUCTION

Electrical insulation is a material that has resistivity to the current flow. All kind of electrical equipment needs insulation and thus improving the properties of insulating materials can easily create a significant impact. Electrical insulation is widely used as a dielectric between capacitors plates for restricting the current flow but dielectric material at the same time gets polarized in the presence of field. Some of the major electrical properties on which the material of insulation is selected are Electric breakdown strength, permittivity and dielectric loss. The importance of these characteristics is dependent on the application whereas the Dielectric strength is required in all areas of application. [1]

During the past few years the use of traditional insulations like ceramics, glass, mica etc. have been superseded by polymer insulations and currently the installed insulating materials in North America is comprised of 70% of polymer insulations. The reason of this change is the discriminating electrical, mechanical and chemical properties of polymer. There exists one more peculiar property of self-healing in metallized thin film which increases the service life of insulation whereas a sudden breakdown in traditional insulations can cause huge financial loss and outage. Moreover, polymer insulations have good thermal, electrical and optical properties. The common applications of insulators include electrical cables insulation both overhead and underground, film capacitors, reactors, submarine telephone cables, inverter fed motors, switchgears etc. The role of insulation in high voltage applications is very crucial and high operating temperature requirements are of the main concern. Polymer insulating materials have reached to 105°C (in BOPP) to 200°C in some other polymer materials. The estimated life span of metallized film insulations is around 30 to 40 years.[1][2][3]

Considering different applications, it has always been a major issue to alter the properties of polymer insulators. Thus, the use of filler materials with polymers can change different electrical, thermal and optical properties. This gave rise to the introduction of polymer composites. The polymers up to 60wt-% micro sized fillers can alter the thermal, mechanical and flammability properties but these micro sized fillers if enhances one property degrades the other properties as for example electrical strength. The attempts were also made to increase the energy density of capacitors by increasing the permittivity as energy density is linearly proportional to permittivity and square of electrical field. Thus, another improvement has been made by introducing the polymer nanocomposites. The inclusion of around 3 to 9wt-% of inorganic filler material can enhance the dielectric properties without degrading other properties of polymer nanocomposites. This is because the interfacial area is dominating because of large surface to volume ratios of nanoparticles and properties of interfacial area covers the whole nanocomposite properties.[4][5]

The theme of the thesis revolves around two major phases. The first phase involves the fabrication of best possible method of testing the samples. The sample materials under consideration are BOPP (Bi-axially oriented polypropylene) and its nanocomposite including Tervakoski RER, RERT, NPO30 BOPP nanosilica composite and its reference unfilled polymer NPO49. Polypropylene has high breakdown strength and low dissipation factor as compared to other films but the maximum operating temperature is around 105°C [6]. The bi-axial orientation of polypropylene enhances the dielectric, optical, mechanical and barrier (to water and gases) properties, increases the tensile strength and helps in making the thinner film capacitors. Moreover, the use of fillers has also altered mechanical and thermal properties and thus BOPP is different from conventional propylene. The experimental sections which help in concluding the optimum testing methods in the first phase are sample preparation, its pretreatment, setting up the sputtering routines and optimum parameters, post sputtering treatment of electrodes, vacuuming routines, repeatability and reliability of results are studied and tested. The second phase involves the dielectric characterization of BOPP and its nanocomposite films as a function of temperature, frequency, humidity, moisture etc.[1][7]

The thesis is lengthening up to six chapters. The first chapter is the overall introduction of the thesis. In the 2nd chapter the basic chemistry of polymers is introduced including the structural and physical properties. There is a brief introduction of classification, conformation and configuration of polymers and some basic terminologies. The second chapter is an extension of chapter 1 including the electrical properties and terms such as polarization, space charge, dielectric loss and permittivity. Moreover, it also discusses about the capacitor fundamental and polymer morphology. Chapter 4 is comprised of polymer nanotechnology discussing the science of nanocomposite matrix interface, its behavior and nature w.r.t the content of nanofiller percentage. It discusses about the models related to this interface and applications in different scenarios. The chapter describes in detail about the electrical properties of nanocomposites in comparison with pure polymer. To enhance the explanation and understanding, experimental results from thesis about BOPP and its nanocomposite have been included. Testing procedures and methods have been described in chapter 5 where the optimum procedures of pre-vacuum, pretreatment of samples, sample preparation, sputtering routines and setting up the best possible parameters have been studied. Vacuuming procedures and different possibilities are tried and tested. A detailed statistical discussion on reliability and uncertainty has been made including; interrater reliability, test-retest reliability, parallel forms reliability and internal consistency reliability estimation. Chapter 6 comprises of analysis based on experimental results. It starts with the moisture and humidity effect then discusses the dielectric behavior as a function frequency, temperature and applied voltage.

Before conclusion, Chapter 7 discusses about the validity of results and measurements and it explains the intrinsic and extrinsic uncertainties, shortcomings and limitations discovered during the thesis. To wrap up the thesis in a nutshell, a brief conclusion in chapter 8 explains all the findings and achievements made through the thesis.

2. BASICS OF POLYMERS

Polymer as a name consists of two parts i.e. poly means many and 'mers' means units. Polymer is a large molecule that comprises of many small repeating molecules that are chemically joined together in the form of covalent bonds. These small molecules are the basic building blocks of polymer and are known as 'monomers'. A monomer can be a single atom or a group of atoms that repeat itself in the backbone of polymer in a specific fashion. The process of converting monomers into polymers is known as polymerization. If 'X' is the monomer(base molecule) then the corresponding polymers (also called macromolecule can be represented as (-X-X-X-X-X-X-X-X-X-X-X-) or (-X-)n, where n is known as the degree of polymerization[8][9]. The list of different polymers and their monomers are represented in the Table 2.1;

Table 2.1. Examples of polymers and their respective monomers[8].

Polymer	*Monomer*	*Repeat Unit*
Polyethylene	**Ethylene,** $CH_2{=}CH_2$	$—CH_2—CH_2—$
Polypropylene	**Propylene,** $CH_2{=}CH(CH_3)$	$—CH_2—CH(CH_3)—$
Polystyrene	**Styrene,** $CH_2{=}CH(C_6H_5)$	$—CH_2—CH(C_6H_5)—$
Poly (vinyl chloride)	**Vinyl chloride,** $CH_2{=}CH(Cl)$	$—CH_2—CH(Cl)—$
Poly (viny acetate)	**Vinyl acetate,** $CH_2{=}CH(OCOCH_3)$	$—CH_2—CH(OCOCH_3)—$
Polyacrylonitrite	**Acrylonitrite,** $CH_2{=}CH(CN)$	$—CH_2—CH(CN)—$

Polymerization is the process in which the double covalent breaks into single covalent bond and rearrange into long chains. Polypropylene in the table 2.1 is formed from propylene monomers when its double bond breaks and turns into single bond and the remaining free valencies combine with other propylene monomers.

The length of the polymer is described by the degree of polymerization (DP), which is the average number of monomers or repeating base units in the polymer chain. The degree of polymerization is usually in hundreds and thousands and thus justifies the name of the macromolecule for polymer. The molecular weight of the polymer is generally the product of the molecular weight of the repeating units. Polymers with the molecular weights in the range of 10000 to 20000 are low polymers whereas the polymers with the weight above 20000 are termed as high polymers[8][10].

The L/D or L: D (Length to diameter) ratio of the polymers is very high which corresponds to higher tensile strength, entanglement, melting point and elongation. The difference in L/D between monomer and the corresponding polymers creates the difference in the physical properties.

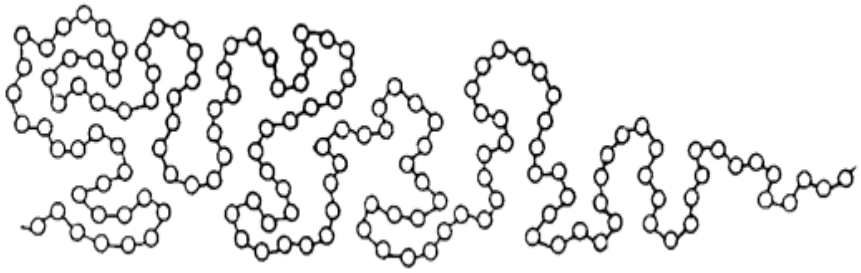

Figure 2.1. Polymer molecule structure (a chain of several monomers) [8].

2.1 Molecular Weight

Molecular weight is one other way to estimate the size of the polymer chain. The molecular weight of a single molecule of polymer can be generally represented as DP*MW of a monomer, where DP is the degree of polymerization and MW is the molecular weight. But this is not as straight forward for a large sample of polymer material as it is for a single molecule. The chain lengths are not uniform on material level and the individual polymer chains do not have the same length and weights. Thus the distribution of molecular weight in a polymer material is important to be found out and there are statistical methods available for calculating the average molecular weight of the real sample of polymer[7] [9] [10].

Number-averaged molecular weight, $\overline{Mn}$ is the simplest type of averaging the molecular weight by counting the number of molecules or it can also be estimated using the relative molar mass. The possible method of deterring the distribution of molecular weight in this type of averaging is MP (melting point) dispersion, BP (boiling point) elevation or osmotic pressure. The large number of small molecular weight species presence can be seen in the figure below;

$$\overline{Mn} = \frac{\sum_i n_i M_i}{\sum_i n_i} \tag{2.1}$$

In the above equation, n_i is the no. of components in the sample with the molecular weight M_i.

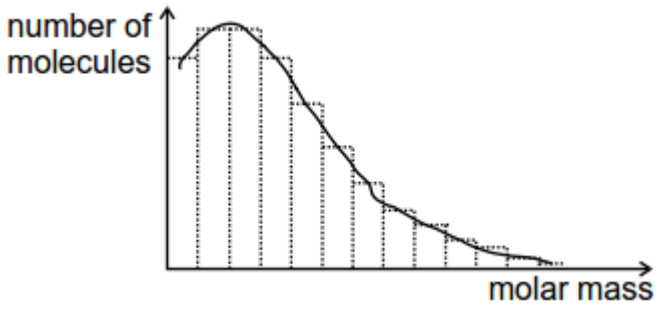

Figure 2.2. The effect of distribution of number-averaged molecular mass due to molecules with smaller weight[11].

One other way of estimating the distribution of molar mass is the weight-averaged molecular weight, $\overline{Mw}$ in which the effect of large molecules is more effective and has more contribution in the molecular unlike number-averaged molecular weight. The equation below gives the weight-averaged molecular weight.

$$\overline{Mw} = \frac{\sum_i w_i M_i}{\sum_i w_i} \tag{2.2}$$

$$\overline{Mw} = \frac{\sum_i n_i M_{i^2}}{\sum_i n_i M_i} \tag{2.3}$$

In the above equation, w_i is the mass of components in the sample with the molecular weight M_i.

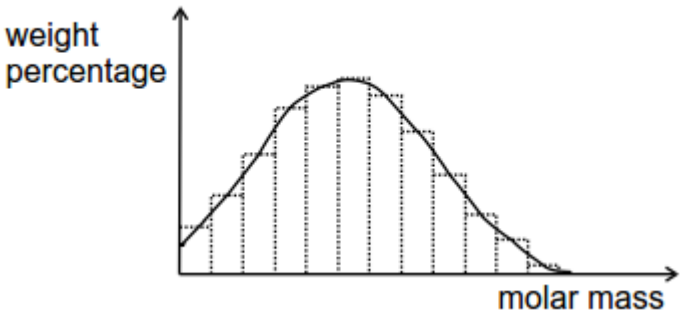

Figure 2.3. Distribution of molecular weight in weight-averaged molecular weight indicating the presence of effect of heavy molecules[11].

From the figure 2.2 and 2.3. it can be interpreted that the for the same material, the small molecular weight molecules which are present in large number affects the number-average molecular weight whereas the heavier big molecules which are smaller in number affects the weight averaged molecular weight[11].

Some other methods of calculating the molecular weights are z-average molecular weight $\overline{Mz}$ and viscosity-averaged molecular weight $\overline{Mv}$.

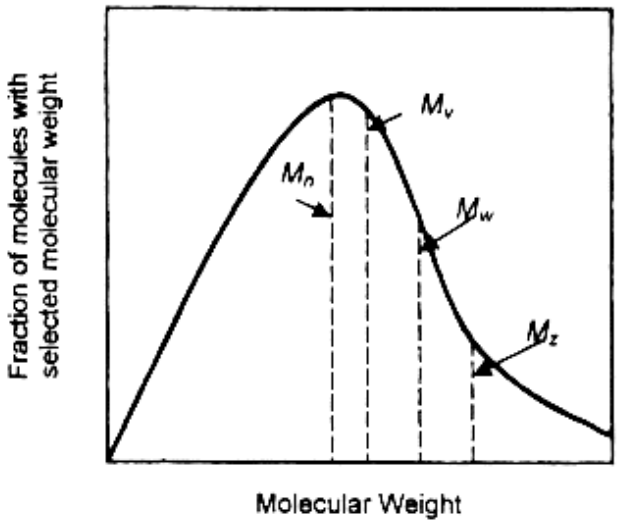

Figure 2.4. Average molecular weight fraction[9].

The figure 2.4. shows that the average molecular weights for a same material can be in the order of $Mn \leq Mw \leq Mz$. The value of *Mv* is between *Mn* and *Mw*. The spread of polymer distribution can be found out by the ration of *Mw* and *Mn* which is also known as polydispersity. If the value of the ratio is 1, it means that all the molecules in the material sample are of the same molecular weight. Larger values interpret wide spread of the molecular weight towards both sides[9].

2.2 Classification of polymers

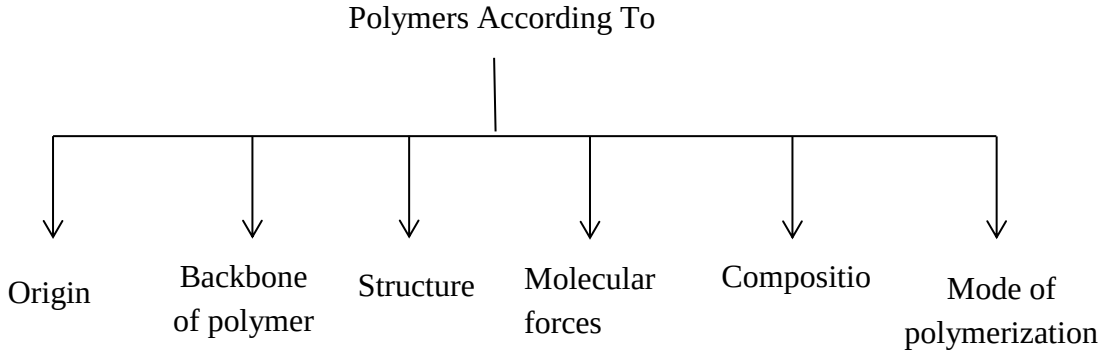

- **Origin**

Natural polymers: are found in plants and animals for example protein, starch, rubber etc.

Semisynthetic polymers: are chemically formed using natural polymers for example cellulose including cellulose nitrate, cellulose acetate and its other derivatives, hydrogenated rubber etc.

Synthetic polymers: are prepared chemically by humans including polyethylene, polypropylene, PVC (Polyvinyl Chloride)

- **Backbone of the Polymer**

Organic Polymers: are those polymers whose backbone chains are made of carbon whereas the side valencies of the backbone carbon atoms are mostly Hydrogen, Nitrogen, and Oxygen etc. Synthetic polymers are usually organic polymers.

Inorganic Polymers: are those polymers whose backbone does not have Carbon atoms. For example, glass.

- **Structure**

Linear polymers: The polymers comprised of long finite straight chains with repeating units in sequence. They can be derived from condensation polymerization of bi-functional monomers. These are soft or like rubber.

Branched Polymers: are the polymers with some Finite branches (short and long) of repeating units which are resulted due to some uncontrolled reactions. These branched polymers have branch points from where different length of branches originate. There are tree or star or dendrimers types of branch polymers based on their structure.

Cross linked Polymers: These polymers can be represented by their network structures e.g. planner or space network structure. These are insoluble and have higher molecular weight. They have strong covalent bonds and are formed from bi and tri functional polymers e.g. epoxy resins.

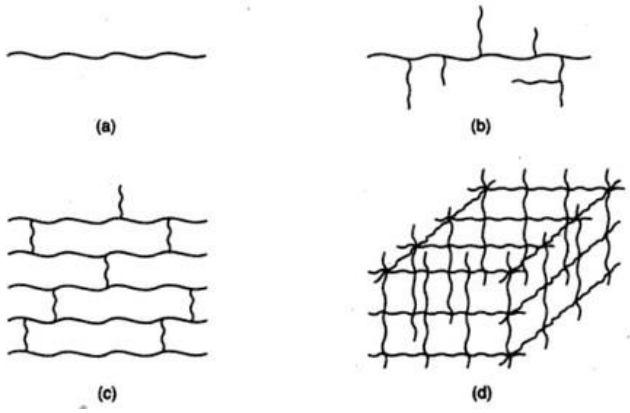

Figure 2.5. (a) Linear, (b)branched, (c)planar (d)space network polymer structures [8].

- **Molecular Forces**

The polymer mechanical properties are based on type of bonding forces between molecules for example, Van der Waal forces, hydrogen bonding, covalent bonds etc. Based on these forces polymers are classified into Elastomers, thermoplastics, thermosets, Plastics, Fibers.

- **Composition**

Homopolymers: These polymers are made up of single type of repeating units or monomers.

Copolymers: when two or more types of monomers are combined in one polymer chain, they result in forming a copolymer. Copolymers are also called heteropolymers. Polymers following an alternating fashion are called alternating copolymers. Random copolymers have their monomers in any order. Block copolymers have their monomers grouped together according to their type. Graft polymers are kind of branched polymers with two types of homopolymer chains. One type of homopolymer exists in the main chain and the other type in the side branches.

2.3 Configuration of polymers

Polymers can have different geometrical arrangement even if they have the similar chemical composition. The variation in which the same polymer molecules arrange themselves is known as isometry. The configuration or arrangement of the polymer when formed is permanent unless the covalent bonds are disintegrated or reformed[11].

Isomers consists of two main types; structural and stereo isomers. In structural isomers, the molecules tend to form different covalent bonds and result in different properties. The other type is the spatial or stereoisomers in which the molecules have similar covalent but different spatial arrangement of the side groups or adjacent groups or the characteristic group. This spatial arrangement or stereo regularity can affect the polymer properties and can further be explained as tacticity. Polymers which have their characteristic group arranged always on the same side of the backbone chain (also called main chain) are termed as isotactic polymers. Ziegler-Natta polymerization is very controlled and result in isotactic polymers. As shown in the figure 2.6. (b) that in isotactic polypropylene, the methyl group i.e. $-CH_3$is on the same side of the main polymer chain. Isotactic polypropylene can be further classified into α-form, β-form and γ-form. α-form of polypropylene form cross hatched helical structures and these form spherulites. They are produced under normal conditions. β-form consists of hexagonal cell structure and their lamella does not result in a cross hatched structure. They have lower modulus of elasticity and higher impact strength as compared to α-form. Moreover, in this form polypropylene can be crystallized at low temperature. γ-form unit cell has orthorhombic structure and its lamella is crossed and non-parallel. Moreover, it doesn’t exist in normal processing condition as α-

form. Under normal atmospheric pressure it exists and if the pressure increases γ-form also start forming but in lower molecular weight materials. Unlike isotactic polymers if the characteristic group arranges itself in an alternating fashion in the main chain then it is called *syndiotactic polymer*. Their unit cell structure is orthorhombic with zig zag helices. They have more flexibility due to which they have better tensile strength, better UV radiation resistance. If the characteristic group does not follow any routine and are arranged in random orders in the main chain as shown in figure 2.6. (a) then it is termed as *atactic polymer*. Due to random arrangement atactic polypropylene molecules cannot crystallize themselves in any order and are amorphous unlike isotactic molecules which are highly crystalline[10],[12].

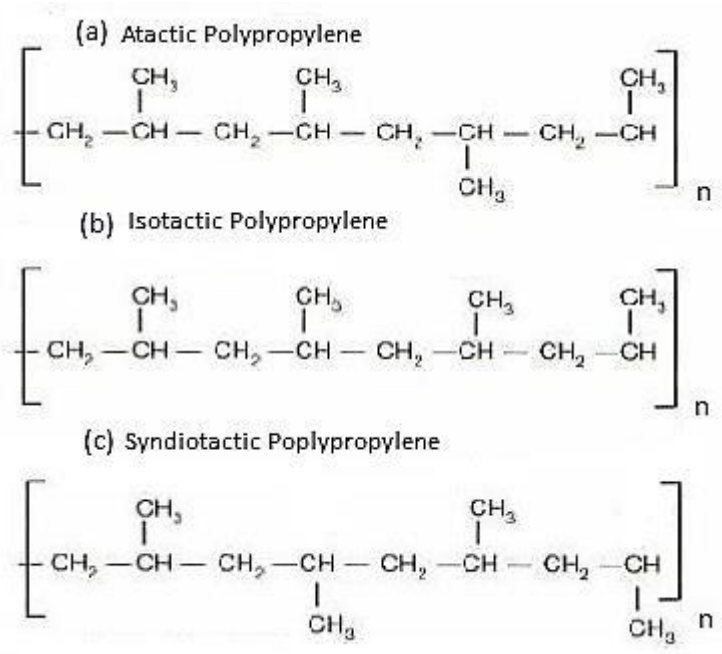

Figure 2.6. Tacticity in polypropylene.

2.4 Conformation of polymers

Conformation is the rotational orientation of the segments or constituents of the polymer chains around the primary covalent bond or central carbon-carbon bond. This carbon-carbon covalent bond stabilized because of the spatial rotation of side species attached to the side valencies. In general polymer chains conform themselves according to the lowest potential energy in order to stabilize the polymer. Since configuration is very difficult to break and almost permanent unless the chemical bonding is reformed but conformation can easily be reorganized or changed under stress at moderate temperatures because of the presence of weak energy barrier. Conformation is dependent on many factors like length of the side chains, dimensions and type of crystallization etc.[4], [11].

Bloor et al. [15] in his book gives an example of n-butane conformation as shown in the figure. The potential energy curve w.r.t the angle of rotation around the primary covalent bond helps in understanding the stability and conformation. The rotation of the methyl groups with primary carbon-carbon bonds describes the stability of conformation. The fully eclipsed conformation where the methyl groups are on the same side as shown in the figure and the angle of rotation φ=180˚, the potential energy is maximum and the conformation is highly unstable. Whereas the Trans- conformation where the angle of rotation φ=0˚ and the methyl groups are on the opposite sides, the potential energy is minimum and the conformation is the most stable. Two intermediate stability conformations also exist namely; gauche conformation and eclipsed conformation as shown in the figure 2.7(a) and figure 2.7 (b) respectively[15].

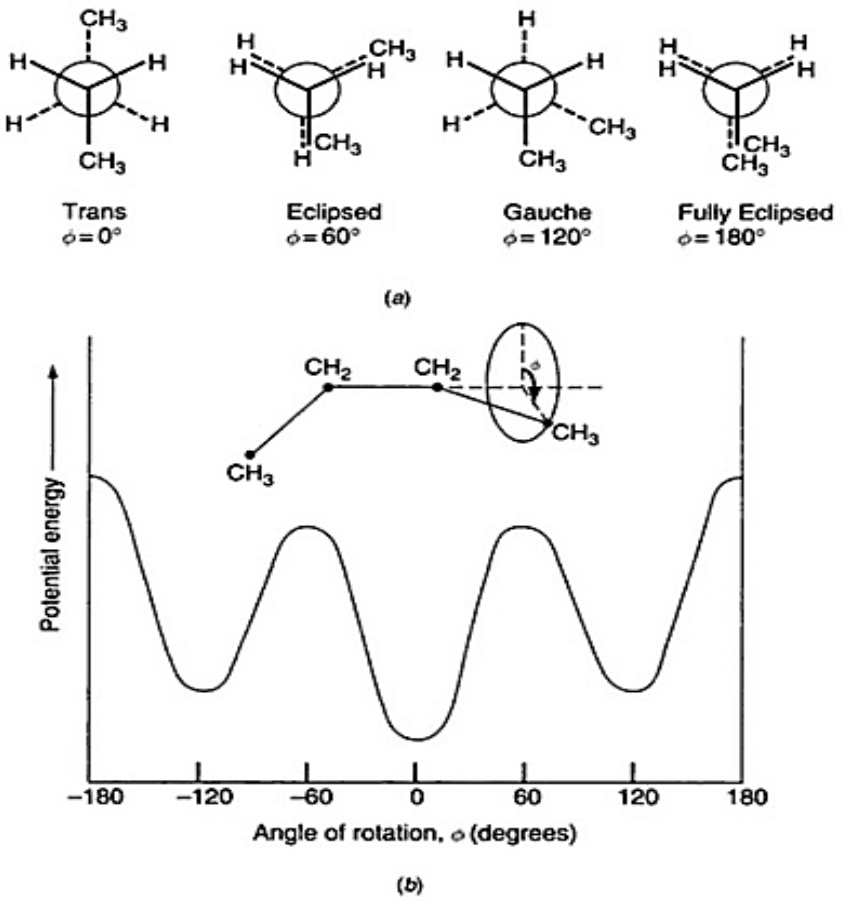

Figure 2.7. (a) Conformations of n-butane, (b) potential energy w.r.t the rotation angle φ(degrees)[15].

In conjugated polymer for example polyacetylene, the conformational rotation is very difficult and it is governed by the electronic forces of the primary carbon-carbon bond. The polymer molecule remains planar and is termed as flat conformation. Moreover, the molecules with larger side chains cannot have planar conformation and they tend to form three dimensional structures due to less space available.

2.5 Polymer morphology

The idea of polymer morphology arises with the irradiance of the X ray beam. Sharp reflections and series of sharps circular rings on the background screen indicate the crystal structure. Whereas the diffused halos and liquid like diffraction indicates defects and disorders in the polymer structure which gives the evidence of amorphous regions. Crystallinity is the regular packing of chain with uniformity when the polymer is cooled from its molten state. The opposite of crystallinity is amorphous region which evolve when the polymer chains are tangled and randomly arrange in some order. Amorphous polymers are not totally disordered; they could be better termed as less ordered. Because of differences in configuration, conformation, chain lengths and dimension, flexibility etc., none of the polymers are absolutely crystalline, though they may be semi-crystalline. Degree of crystallinity tells about the extent to which the material is crystallized. Many atactic polymers are amorphous. Crystalline structures are responsible for particular electrical, thermal and mechanical properties of a polymer material.

2.5.1 Crystalline, semi crystalline and amorphous states

The morphological structure originates when the polymer in the molten state starts to get cooled down. In the melt state the polymer mixture is like entangled chains and they freedom of conformation. In the melt state the polymer is liquid. As it starts to cool down, its viscosity increases and when the temperature cools down to a point where the polymer chains develop strong attraction then the polymer solidifies to crystallites. Now if the temperature further decreases from this point, the polymer chain left behind now gets solidified in an abrupt order and makes an amorphous region.[9]

Different models have been developed to explain the morphology of polymer. One of the initial models were '*Fringed Micelle Model'* as shown in the figure 2.9. which describes the existence of many parallel polymer chains which run through many amorphous and crystallites. This model describes many properties of semi crystalline polymers but has been discarded as later the electron microscopy does not support this theory[16]. This model is true for stiff polymers but not for flexible polymers and Ziegler and Natta stereo regular polymers, therefore another explanation of *fold surface model in figure 2.8.* (a surface where molecules turn back and forth) was given where the polymer chains tend to form a 3 dimensional lamella[12][17].

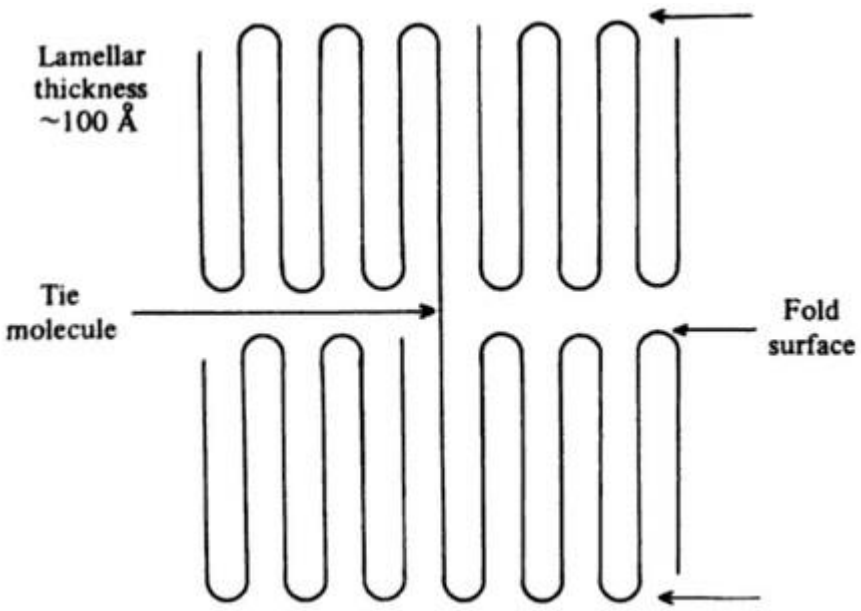

Figure 2.8. Fold chain model[17].

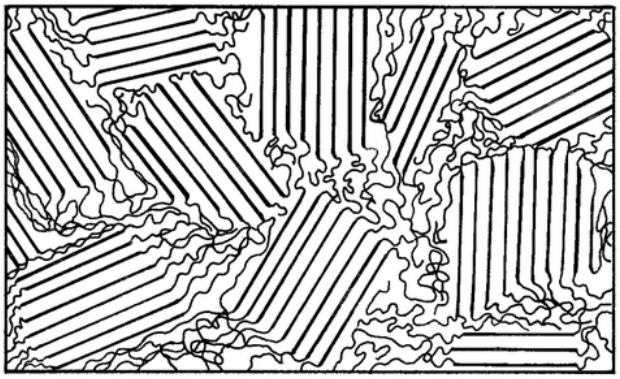

Figure 2.9. Fringed micelle model [16].

Crystallization starts with the formation of nucleus when the polymer molecules overcome the thermal stress and form cluster. Crystallization can be controlled by managing the physical conditions e.g. temperature and pressure. Moreover the process of crystallization depends on[9];

- Polymer chain symmetry
- Intermolecular forces
- Tacticity
- Length and dimension of branches
- Average molecular weight

After the formation of nucleus, the crystal starts to grow and form semi crystalline and amorphous regions. These crystals form long ribbon like folding structures called lamella. Lamella form inter-crystalline links and bend. During crystallization some of the lamella

start to form their own nucleus called spherulites which are sphere shaped fiber like structures[4]. The exact reason of spherulite formation is unknown but they grow until they collide with each other and they are volume fillers. If the polymer melt is cooled down gradually, the growth rate of spherulite would be more and the material would be rigid as compared to sudden cooling of polymer melt. In the latter case, the spherulite will not find any time to grow up. Spherulites affect the properties of the material. Spherulites are composed of pure polymer and reject the impurities to the outer boundary leading to a heterogeneous structure[11].

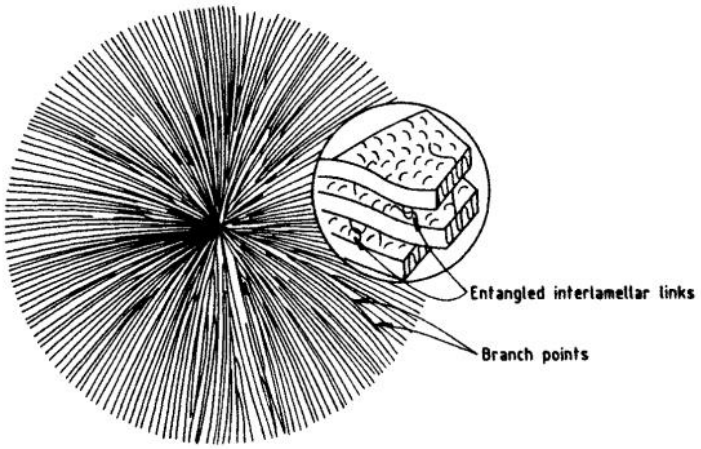

Figure 2.10. Structure of spherulites [16].

2.5.2 Thermal phase transition

The crystalline structure of a semi crystalline solid dissolves at the melting point (Tm). The phase change occurs as the melting point is achieved and the polymer turns into a viscous liquid from solid state. Different physical properties including density, viscosity, refractive index, heat capacity change with the phase change. Polymer usually does not melt at a certain point rather they melt over a temperature range because of variation of lamella thickness in the same material. Melting point decreases with the lower crystallinity. Syndiotactic polymers have lower melting point as compared to their respective isotactic polymers. Higher melting points provide resistance against softening of the material at higher operating temperatures e.g. polypropylene can operate up to 105°C. The other important factor in the thermal range of polymers is the glass transition temperature which has a relation to the free volume present in the polymer. Molecules with temperature higher than glass transition vibrate and enter in the non-crystalline region whereas at glass transition temperature only low vibrations can occur and possess the restricted free volume. For polymers the temperature between melting and glass transition temperature is examined.[14]

As already discussed that the phase transition with temperature change, affects many physical properties. Specific volume change is illustrated in the figure 2.11. As the semi

crystalline polymer cools down suddenly at its melting temperature there is a drastic drop in the specific volume whereas the specific volume of the amorphous polymer does not drop at the melting point rather it has a linear drop. Between melting and glass temperature, both the polymers have rubber state. Below the glass transition temperature the specific volume drops very slowly[4].

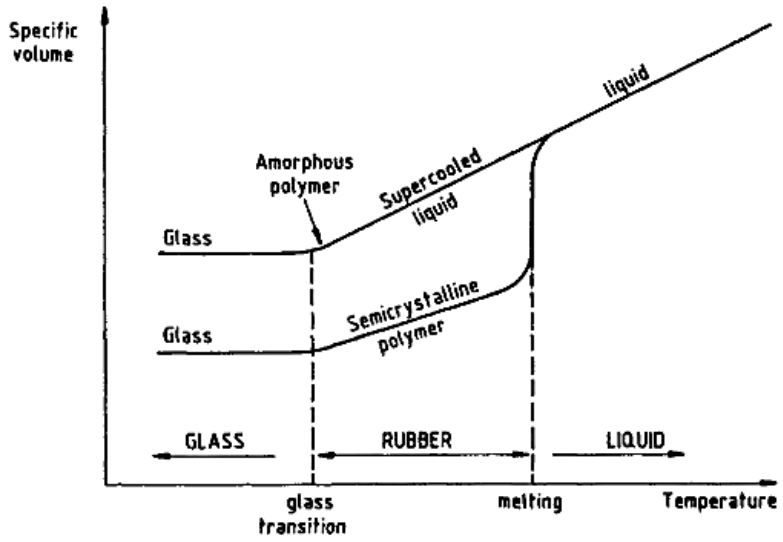

Figure 2.11. Thermal transition of polymers w.r.t specific volume[4]

3. ELECTRICAL PROPERTIES OF POLYMERS

3.1 Electrostatics of dielectrics

The dielectric materials are generally neutral because the positive and negative charges are arranged in a bounded way that they keep the overall material neutral. If a dielectric material is placed in an electric field, the field tends to penetrate the dielectric material. This is because of immobile nature of the bond charges. This contrasts with a conductor which when placed in an electric filed does not allow the field to enter the conductor material. The movable charges in the conductor align themselves according to the applied field in a way that the internal field remains equal to zero. This penetration of electric fields alters the internal charge density of the dielectric material. Dipoles are formed when the negative charges gets displaced with respect to the positive center of an atom or molecule.[18]

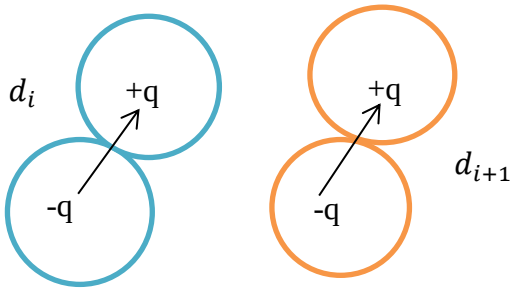

Figure 3.1. Formation of dipoles

$$p_n = q d_n \tag{3.1}$$

In the above equation p_n is the dipole, q is the magnitude of the charge and d_n is the dipole moment. If every dipole and its magnitude of charge can be known, then the microscopic model could be built but it is not possible and practical. Therefore, the macroscopic model is realized which is based on the average of thousands of molecules.

$$P = \lim_{\Delta v \to 0} \left(\frac{p_i}{\Delta v} \right) = \lim_{\Delta v \to 0} \left(\frac{1}{\Delta v} \sum_{i=1}^{N \Delta v} p_i \right) \tag{3.2}$$

In the above equation p_i is the ith dipole moment per unit volume Δv and the N is the number of dipoles/unit volume. The macroscopic charge density can be represented as;

$$\rho = \lim_{\Delta v \to 0} \left(\frac{1}{\Delta v} \sum_{i=1}^{N \Delta v} q_i \right) + \rho_{free} \tag{3.3}$$

In the above equation, q_i is the net charge of the molecules and ρ_{free} is the charge density of the freely moving molecules which are very few in dielectric materials as most of the molecules are neutral and average charge is zero. On macroscopic level, the electric field can be build up. Let us consider a macroscopically small volume element Δv. Each of these volume elements has charges +q and –q and is termed as dipoles. These dipoles collectively build up the charge distribution. If all the segments (Δv) are integrated, then the potential at point y can be given as;

$$\Phi(y) = \frac{1}{4\pi\varepsilon_0} \int_{v\prime}^{v\prime} \frac{[\rho(y') - \nabla'.P(y\prime)}{|y - y\prime|} \tag{3.4}$$

The charge distribution (ρ-∇.P) has been resulted in this potential build up. Since we know that

$$E = -\nabla\varphi \tag{3.5}$$

Where E is the electric field which can be represented as $\frac{V}{d}$ for a capacitor where V is the applied voltage across the plates and d is the distance between the plates. Now the fundamental free space postulates need to be modified for the dielectric material. According to Maxwell equation;

$$\nabla \cdot E = \frac{1}{\varepsilon_0} (\rho - \nabla \cdot P) \tag{3.6}$$

The effects of the polarization can be illustrated by electric displacement and can be given as;

$$D_e = \varepsilon_0 E + P \tag{3.7}$$

ε_0 is the permittivity of free space and its value is $8.85\times10^{-12}\text{Fm}^{-1}$. The collective effect of Dielectric polarization and vacuum polarization (without dielectric material) can be explained with the equation;

$$\varepsilon = \varepsilon_0 \varepsilon_r \tag{3.8}$$

ε_r is the relative permittivity which is a function of frequency, temperature and electric field;

$$\varepsilon_r = \frac{\varepsilon_0 E + P}{\varepsilon_0 E} = 1 + \frac{P}{\varepsilon_0 E} = 1 + \chi \tag{3.9}$$

In the above equation, χ is electrical susceptibility. For a linear and isotropic material, the dielectric polarization can be written as;

$$P = \varepsilon_0 \chi E \tag{3.10}$$

Now the electric displacement can be rewritten as;

$$D = \varepsilon_0 (1+\chi) E = \varepsilon_0 \varepsilon_r E \tag{3.11}$$

If we consider that the dielectric material is homogeneous then its susceptibility is constant and independent of electric field intensity direction. Therefore, Maxwell divergence equation can be reduced as;

$$\nabla \cdot E = \frac{\rho}{\varepsilon_0 \varepsilon_r} \tag{3.12}$$

The above equation shows that the applied electric field intensity in case of a homogenous, isotactic and linear dielectric material is $\frac{1}{\varepsilon_0}$ times less than that of free space. With the insertion of dielectric material between two electrodes as commonly done in case of a capacitor, the dielectric material introduces electric field intensity inside the material which cancels out a portion of applied electric field and thus increases capacitance. Thus, the dielectric material can store more energy. The electrostatic energy can be given as;

$$W_e = \frac{1}{2} \int D \cdot E \, dv \tag{3.13}$$

$$W_e = \frac{1}{2} \int \varepsilon_0 E^2 \, dv \tag{3.14}$$

3.2 Polarization mechanism

Before discussing the polarization mechanisms, it is required to know the difference between polarization and conduction mechanisms. Both are closely related in their concepts with some difference. Polarization results from the displacement of charges in an electric field whereas conduction is the result of average velocity of charges in an electric field. Thus, polarization results in conduction only when there is a strong electric field and continuous conduction is not possible.

3.2.1 Electronic polarization

According to the fundamental theory, an atom is composed of nucleus which acts as a center and electrons which revolve around the nucleus in different orbits. Ideally electrons and nucleus and equal and opposite charges and keep an atom neutral. When such an atom is subjected to an electric field then the charges face an electric force and consequently nucleus and electron cloud displace with respect to each other. A dipole moment is produced from negative charge to the nucleus. This dipole can be given as;

$$P = (4\pi\varepsilon_0 R^3) E = \propto_{optical} E \tag{3.15}$$

In the above equation, R is the radius of an atom which is a conductive sphere. α or the term under brackets is polarizability and is related to the volume of the sphere or atom[18].

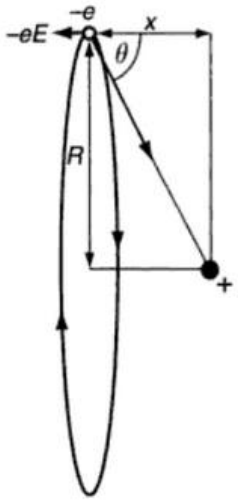

Figure 3.2. An electron displacement resulting in a dipole[15].

Thus, electronic polarization is the dipole moment produced per unit electric field and is the measure of ease with which the charges displace from their center.

3.2.2 Molecular or atomic polarization

Atomic polarization results as a displacement or distortion of nucleus because of the application of an electric field. Molecules have higher electronic polarization due to bigger electronic cloud and their polarization is related to the bond angles, turns and symmetry. This type of polarization occurs in the molecules that have zero dipole moment before the application of electric field[19]. This type of polarization occurs in polar substance. The huge difference in the mass of nucleus and electron cloud has resulted in the formation of two groups. One group is related to electrons displacement w.r.t nuclei in an optical frequency region and another group that is related to the electrons displacement w.r.t nucleus in an infra-red frequency region. Due to elastic displacement, the application of an electric field introduces a dipole moment which can be given by;

$$P = (\propto_{optical} + \propto_{infra-red}) E \tag{3.16}$$

In the above equation, $\propto_{optical}$ and $\propto_{infra-red}$ are electronic and atomic polarization respectively. Few examples of polar substances are carbon dioxide CO_2 and ionic crystals (salts) e.g. sodium chloride NaCl show higher atomic polarization.[18]

3.2.3 Orientational polarization

This polarization phenomenon takes place when an electric field is applied to a dipolar material. The dipolar material possesses a permanent dipole which can reorient itself after the application of an electric field. In the absence of an electric field the dipoles are randomly oriented and net polarization is zero. This type of polarization weak and it's the effect of electric field is not very strong and the thermal rotational movements are stronger. The static polarization among weak interactions of dipolar molecules can be represented as a combined effect of orientation, optical and infra-red polarization;[18]

$$\propto_t=(\frac{P^2}{3k_BT})+\propto_{Optical}+\propto_{infra-red} \tag{3.17}$$

In the above equation T is the temperature and P is the permanent dipole moment. Molecules like H_2, Cl_2 are di atomic and possess no permanent dipole whereas molecules like water H_2O, HCL are polar and possess a dipole of 1.08D and 1.84D respectively.[19]

3.2.4 Interfacial polarization

Interfacial polarization is related to the accumulation of charges at the interfacial region between two materials or between crystalline and amorphous regions. This is also called Maxwell-Wagner polarization where an inhomogeneous structure inside the polymer material results in charge accumulation. This type of polarization takes place at lower frequencies and is the slowest among all polarization types. Charged particles with reduced mobility travel a longer distance. Interfacial polarization is further discussed in Chapter 4 of nanodielectric science.

One other type of polarization is hopping charge polarization which is actually the result of hopping charges. This resembles permanent and introduced by dipoles and free mobile charges. Due to thermal vibrations hopping charges can jump through the potential barriers. This jump is further dependent on the distance between transit locations. This transit can be changed while applying an electric field. If the charges travel through the polymer surface, then it results in a DC current.

In the figure 3.3., the mechanism of polarization w.r.t frequency has been illustrated. It can be observed that as the frequency increases the dipolar polarization decreases and under lower frequency dispersion below 1 kHz, all types of polarizations take effect. The relative permittivity has the same trend. [15]

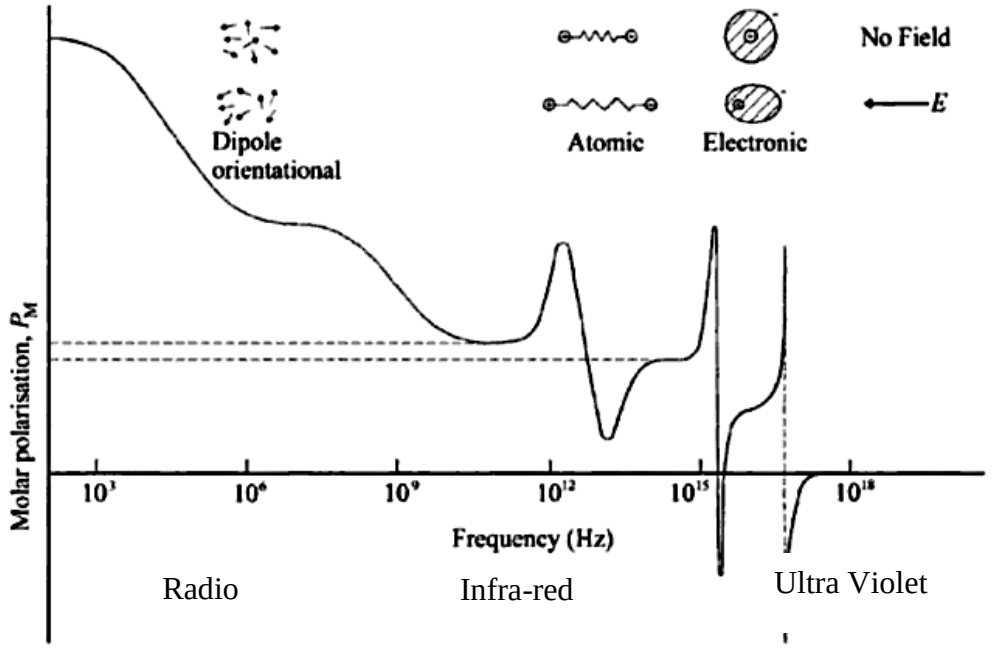

Figure 3.3. Polarization mechanism w.r.t frequency range [15].

The polarization effect takes time to build up after the application of an electric and the dipoles do not suddenly revert their orientation to original after the removal of electric field because of inertia. This time is called relaxation time and the phenomenon is dielectric relaxation.

3.3 Space charge

Space charge is produced locally in a material. It results whenever the rate of charge accumulation is more than the rate of charge removal. This charge accumulation arises due to the drift of electrons or charges, charge trapping and generation. Space charges are both because of trapped and moving charges. Let us consider a capacitor with a polymer dielectric between its electrodes. There exists a potential barrier between the electrodes and an electric field is required for the charges to pass the barrier. But large ions or electrons fail to pass the barrier. These ions from DC excitation accumulate and result in a localized field. The equation for accumulation rate of space charge can be given by space charge density ρ; [11], [19], [20]

$$\frac{d\rho}{dt} = - \nabla \cdot J \tag{3.18}$$

The application of an electric field to a capacitor or a dielectric material with space charges can positively or negatively affect the applied field. The localized field due to the space charges can interrupt the applied fields and can reduce or enhance the field. Space charges have two types; heterocharge and homocharge. The formation of these types of charges occur if the electrode has a space charge of opposite polarity which could be

trapped while moving from the other electrode. Polymer material has voids, impurities and imperfections and the charge moving from the surface of the lamella traps in it easily. Heterocharge is a situation when positive ions accumulate at negative electrode and vice versa. Heterocharge increases the electric field at the areas close to electrode and decreases it in the middle areas of the dielectric material. Heterocharge increases the localized electric field and reduces dielectric breakdown strength.[9] [10][19] [20]

The other type of space charge that generates is homocharge. Homocharge is dependent on the electrode material and its capability to inject and accept the charge, temperature, electrode insulation connection etc. Homocharge means the accumulation of same polarity charge for example electron at cathode. Homocharge reduces the electric field and thus enhances the apparent breakdown strength of the polymer but unlike heterocharge, the electric field at the electrode reduces and in the middle of the dielectric material the field increases and can cause a small breakdown there. Space charge accumulation is prominent under DC conditions. Nelson et al. [20] has given a pictorial overview of charge accumulation and recombination activities as shown in the figure 3.4.

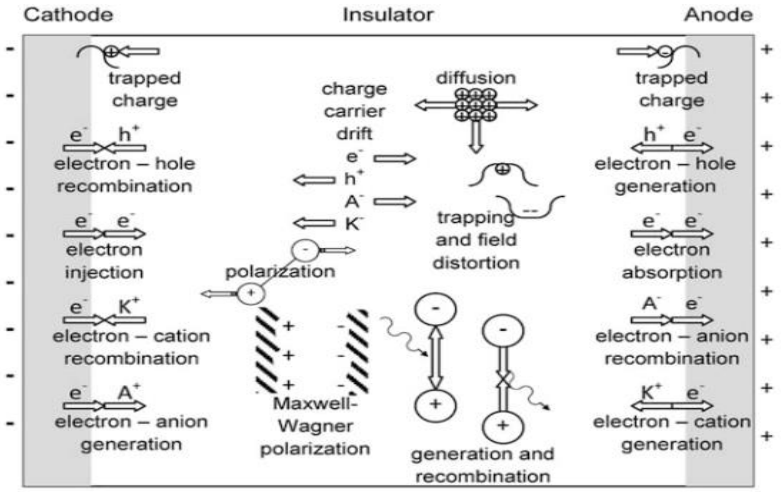

Figure 3.4. Charge accumulation and recombination at insulator-electrode interface [20].

Some of the techniques used to measure space charge are mentioned by Mizutani et al. [21] which are laser induced pressure pulse method, piezo-electrically induced pressure step method, and pulsed electroacoustic method, thermal Pulse method, thermal step pulse method and the laser intensity modulation method.

3.4 Dielectric loss and relative permittivity

Dielectric materials have properties between conductors and insulators. Therefore, these materials are not perfect insulators and have some conductivity in certain conditions. Many dielectric materials have dielectric constant greater than 1 and thus possess dielectric loss under ac voltage. In high voltage applications these factors play a prominent role as both of these are dependent on magnitude and frequency of the applied voltage[22]. Complex permittivity is an important factor to figure out the changes in dielectric loss and permittivity w.r.t frequency variations. A lossy dielectric can be modelled as a capacitor with parallel resistance i.e. parallel RC equivalent circuit.

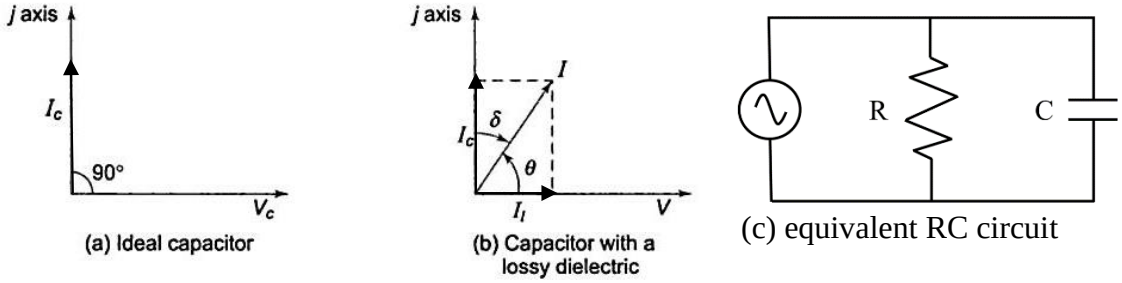

Figure 3.5 Phasor diagram of (a) ideal and (b) lossy capacitor[22].

A capacitor is connected to a sinusoidal voltage supply of V= v$e^{-j\omega t}$ which has angular frequency ω=2πf and it stores a charge of Q=C_0V and it draws a charging current of I_C=jω$c_0 v$. C_0 is the vacuum capacitance. As we know that in an ideal capacitor current leads the voltage by 90°[22].

Let us replace the vacuum with a dielectric material. Dielectric material will increase the capacitance of the material to

$$C=C_0 \frac{\varepsilon'}{\varepsilon_0}. \tag{3.19}$$

As shown in the figure 3.5., V is the applied voltage and I_c is the corresponding charging current in case of true capacitance. But in case of lossy capacitance, there will be one component of loss current that I_l and the resultant current would be

$$I= I_c + I_l = (j\omega C + G)\, V \tag{3.20}$$

In the above equation G is the conductance of parallel RL circuit and is equal to 1/R and I_l=GV. In loss less capacitor the current leads the voltage by 90° but in lossy capacitor the current leads the voltage by an angle θ which is less than 90°. Therefore loss factor would be[10][21];

$$\tan\delta = (90-\theta)\ ^\circ \tag{3.21}$$

Loss factor depends on frequency, capacitance and resistance in this model.

$$\text{Tan}\delta = D = \frac{I_l}{I_c} = \frac{1}{\omega CR} \tag{3.22}$$

The permittivity of the material is complex and can be represented as;

$$\varepsilon^* = \varepsilon' - \varepsilon''$$

Where $\varepsilon'$is the real part of the complex permittivity and ε'' is the imaginary part. ε'' is also called loss factor and represents the loss due to polarization and conductivity. Dissipation factor gives the ratio between imaginary and real parts of permittivity and tells that how much the dielectric material is deviated from ideal behavior.

$$\text{Tan}\delta = \frac{\varepsilon''}{\varepsilon} \tag{3.23}$$

Moreover, the resultant current can be given as;

$$I = (j\omega\varepsilon' + \omega\varepsilon'')\frac{C_0}{\varepsilon_0}v \tag{3.24}$$

The complex permittivity can be given as;

$$\varepsilon^*(\omega) = \varepsilon'(\omega) - \varepsilon''(\omega) \tag{3.25}$$

Also, the dissipation factor tanδ is a function of frequency.

$$\text{Tan}\delta = \frac{\varepsilon''(\omega) + \frac{\sigma}{\varepsilon_0 \omega}}{\varepsilon_r(\omega)} \tag{3.26}$$

3.5 Polypropylene in detail

Polypropylene has been discovered in 1954 and it is being widely used in food, packaging, high voltage sector. This popularity is because of the peculiar characteristics of polypropylene including chemical resistance, High temperature resistance and mechanical properties. It is environment friendly and non-toxic and has replaced Poly vinyl chloride (PVC) in different sectors. This is because it does not release any toxic gases when burnt as PVC releases chlorine gas[11]. Polypropylene is formed because of polymerization of propylene. Propylene is an unsaturated hydrocarbon. The gaseous petrochemical propylene when polymerized in the presence of a catalyst under set temperature and pressure results in polypropylene. During polymerization the double bond between carbon atoms of propylene break into single bond and a linear long polymer chain is resulted with a methyl (-CH_3) molecule attached to alternate carbon atoms.[23][24]

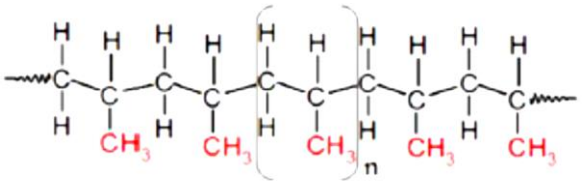

Figure 3.6. Structural view of polypropylene chain[23].

There are many reasons that make polypropylene superior to other polymers including; Polypropylene is one of the best materials for long life electrical and mechanical applications because of its high melting temperature, chemical inertness, low density, lower cost etc. Polypropylene can generate various mechanical properties according to the applications. Polypropylene can have different morphologies and can be modified also by using micro and nano sized filler or reinforcing agents to get the desired characteristics as required by the application area. Some of the examples are silica filled polypropylene, elastomer modified polypropylene, flame retardant polypropylene etc. polypropylene is present in isotactic, syndiotactic and atactic states and their tacticity can be controlled. Commercial grade polypropylene is highly isotactic and its degree of crystallization is around 96%. Ziegler-Natta polymerization results in homopolymers of polypropylene. Branching of linear polypropylene can be done which results in higher molecular weight product with higher tensile strength, higher modulus of rigidity and higher heat resistance.[23][12]

Table 3.1. Characteristics of capacitor grade polymer film[25].

Polymer film	ε_r	**Maximum temperature (°C)**	**Breakdown strength (MV/m)**	**Energy density (J/cm^3)**	**Dissipation factor% 1Hz**
Polypropylene (PP)	2.2	105	640	1-1.2	<0.02
Polyester (PET)	3.3	125	570	1-1.5	<0.50
Polycarbonate (PC)	2.8	125	528	0.5-1	<0.15
Polyphenylene sulphide (PPS)	3	200	550	1-1.5	<0.03
Polyvinylidene fluoride (PVDF)	12	125	590	2.4	<1.8

One of the growing applications of polypropylene in high voltage industry is in capacitor dielectric. Bi-axially oriented polypropylene (BOPP) isotactic film is under consideration in this thesis as a capacitor grade film. Films can be uniaxial or bi-axial in orientation.

When polymer crystallizes in the absence of any external forces then the molecules arrange themselves randomly. In uniaxial orientation film is stretched in machine direction only whereas in biaxial orientation the film is stretched both in machine direction and transverse direction. Biaxial orientation is also known as balanced orientation. In orientation process, spherulites break because lamellae rotate and slide out. Moreover, the polymer chains slide each other and orient in same direction. Crystallites form long thin films as a consequence. As shown in the table 3.1., PP film has highest breakdown strength and lower dielectric loss among all the capacitor grade film. It has low permittivity relative to other films and energy density is around 1.2 J/cm^3 . Recent advancements in PP-copolymers and BOPP micro and nanocomposites have further enhanced the dielectric strength, permittivity and loss levels of polypropylene film for their application in High Voltage. The characteristic properties of bi-axially oriented polypropylene (BOPP) film under consideration (Tervakoski RER film) have been stated in the table 3.2. [12] [23]. The thickness of the film as reported by manufacturer is 14.4µm which has also been verified by cutting a cross section of film in nitrogen and taking its SEM image as shown in the figure 3.7.

Table 3.2. Properties of capacitor grade BOPP Tervakoski RER film[26].

Dielectric Constant (at 25°C, 50Hz-1MHz)	2.2
Dissipation Factor (at 25°C, 50Hz-1MHz)	≤1.8x10^{-4} Ωm
Resistivity	>1x10^{15} Ωm
Tensile Strength	≥180 MN/m^2
Density	0.905-0.910 g/cm^3
Melting Point	165-170 °C
Softening Point	140°C
Water absorption	<0.01%
Shrinkage	≤4%

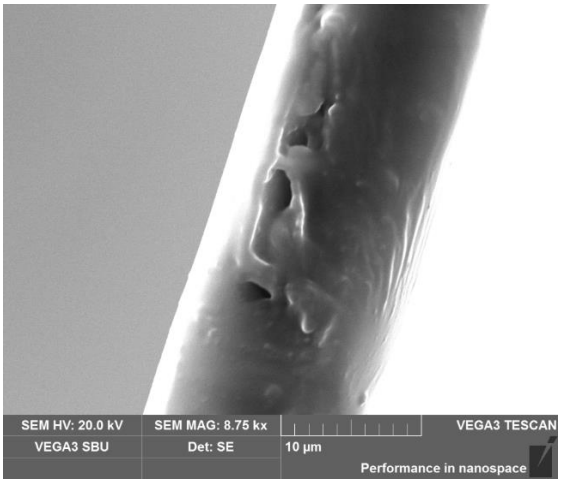

Figure 3.7. SEM cross sectional image of Tervakoski RER BOPP film.

The commercial grade PP film manufacturing process starts with the polymerization process where raw polypropylene is formed. This polypropylene is then fed into an extruder with additives, stabilizers and agents. This extruder is equipped with various melting and mixing stages with molding dies and finally it cools down and cut into pallets of polypropylene. These pallets are then fed into second processing stage to stretch into thin films. This can be done using two methods. One is known as blown or bubble method in which a thick walled tube using a tubular die is extruded. The tube is then quenched in water. After this it is flattened passing through rollers. This film is then reheated and inflated by air pressure and forms a bubble which is then stretched in both machine and transverse direction and then air ring cools down the film. The other process of film formation is tenter process in which the film is not stretched in both directions at the same time rather it is two step stretching but in new technology simultaneous stretching during tenter process is also possible. This process involves the formation of thick cast film which then passed through rollers to be stretched first in machine direction to the ratio of about 4:5:1. The film is then passed through a regulated tunnel where its edged are gripped in tension clips. The film is stretched in transverse direction to a ratio of 8:1.[27][11]

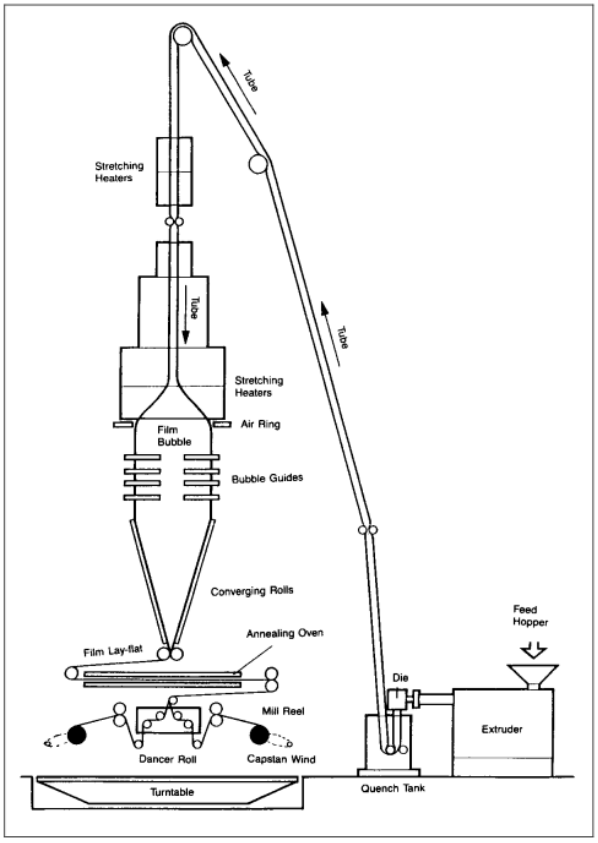

Figure 3.8. Blown process or bubble process for BOPP film[27].

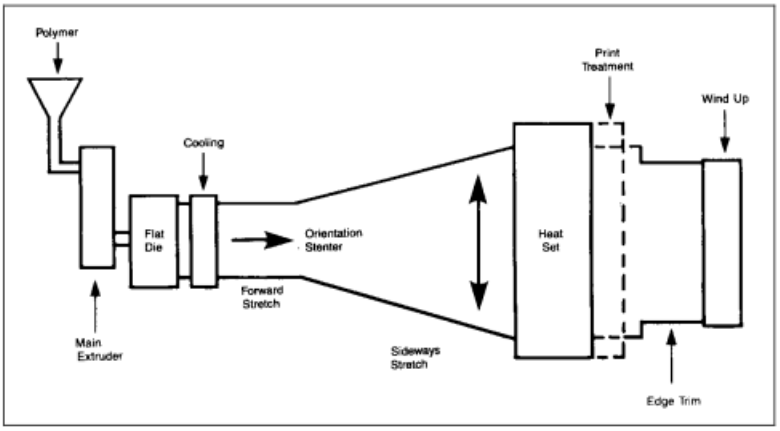

Figure 3.9. Tenter process for BOPP film[27].

3.6 Capacitor fundamentals

Capacitors (also known as condensers) are basic building block of almost every electronic device ever made. They are available in many variants according to their applications. Capacitors differ in their shapes, sizes and electrical characteristics. The right type can be selected based on desired application. Capacitor simply consists of 2 parallel plates called electrodes separated by a dielectric material. Capacitors can be divided into 2 broad categories based on their electrical applications which are:

1. Direct Voltage
2. Alternating Voltage

Capacitors can be further divided into sub categories. AC capacitors are further divided into 2 categories based on their frequency response:

1. Line Frequency
2. High Frequency

[11][28]

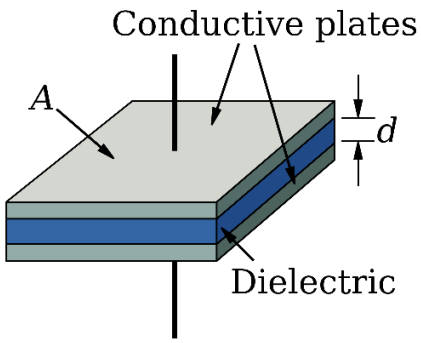

Figure 3.11. Model of capacitor[28].

The permittivity of capacitor, denoted by symbol ε, depends upon the dielectric material.

If we apply a potential 'V' across the plates of capacitor, then the capacitors accumulate charge. The ability of a capacitor to store charge is called 'Capacitance of capacitor' which is given by a relation:

$$C = \frac{Q}{V} \tag{3.27}$$

For idealized capacitor, the capacitance can also be given by:

$$C = \varepsilon \frac{A}{d} \tag{3.28}$$

The S.I unit of capacitance is "Farad" which is defined as the capacitance required storing a charge of 1C which produces 1-volt potential difference across the plates of capacitor.

Now let's derive the formula for Work/Energy stored in capacitor.

Consider that the plates of capacitor are initially uncharged. Now start charging the plates by transferring Q charge from one plate to another. This will increase the charge on one plate by +Q and reduce the charge on other plate by –Q. Now an Electric field is established between the plates. It will require work by external battery to transfer any further charge. This work is same as the energy stored in the capacitor in the form of Electric field. Let's calculate this Energy:

$$W = \frac{1}{2} C V^2 \tag{3.29}$$

The work done in transferring an infinitely small charge dq is given by:

$$dW = V dq \tag{3.30}$$

Work done in transferring a complete charge Q is given by integrating a work required to transfer small charge dq.

We also know that V=Q/C

So,

$$dW = \frac{q\, dq}{C} \tag{3.31}$$

$$W(Q) = \int_0^Q \frac{q\, dq}{C} = \frac{Q^2}{2C} \tag{3.32}$$

This energy is stored in the electric field of capacitor. The energy density is given by:

$$\omega = \frac{\varepsilon E^2}{2} \tag{3.33}$$

The above formula shows that energy density is only dependent upon Electric Field, Voltage between plates and dielectric material. The energy density of a capacitor can be increased by increasing voltage between plates or by using dielectric with high relative permittivity. [28]

In real capacitor, the energy density is lower as compared to that given by the above formula due to the packaging of capacitor. The space occupied by connections and insulations account for this loss.

The real capacitor can be modeled by using other components in combination with ideal capacitor. The electrical connections can be modeled by an inductor and resistor in series with the ideal capacitor. The dielectric of capacitor can be modeled by a resistor in parallel with ideal capacitor as no dielectric is absolute insulator and allows flow of current.

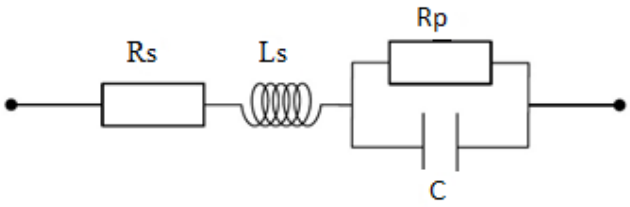

Figure: 3.12. Equivalent circuit of capacitor with series and parallel components [9].

If we know the operating frequency, then we can calculate the combined equivalent resistance of Rp and Rs which is called Equivalent Series Resistance (ESR). The series inductance is called Equivalent Series Inductance (ESL). ESL is usually constant over the range of frequencies and voltage.

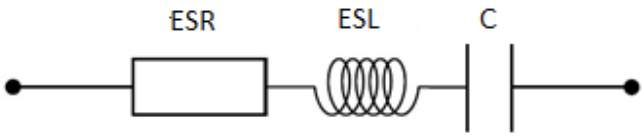

Figure: 3.13. Equivalent circuit of capacitor with series components [9].

The power loss in real capacitor can be given by:

$$P_{loss} = I_{rms^2} R_{ESR} \tag{3.33}$$

Dissipation factor is an indicator of power loss in capacitors;

$$\text{Tan}\delta = \frac{R_{ESR}}{X_c} \tag{3.34}$$

4. POLYMER NANOTECHNOLOGY

4.1 Polymer Composites

In order to alter the properties of dielectric materials or polymer materials, certain fillers are homogenously dispersed in a small amount resulting in polymer composites. Thus the amount of filler added to about 50 to 60wt-% of the total material is known as micro filler and the polymer is known as micro composite. It was observed that the addition of micro fillers helps in increasing the thermal, mechanical and tensile strength but at the same time there was degradation observed in the electrical properties including; reduced dielectric strength, increased permittivity etc. Thus, the experimental research revealed the idea of adding nanofillers up to (1 to 10wt-%) in the matrix which resulted in enhancing the thermal, electrical and mechanical properties at the same time and consequently became a new field of research for high voltage insulating industry[29][30].

4.2 Nanocomposites Science

Polymer nanocomposites are basically the polymer composites with homogenous dispersion of nano sized fillers of small weight percentage (normally 1 to 10wt-%). Some of the examples of nanocomposites are BOPP (Bi-axially Oriented Polypropylene), polyethylene (PE), PEEK, Polyamide (PA) and so on with the addition of fillers like silica (SiO_2), Alumina (Al_2O_3), Magnesium Oxide (MgO) etc. The advancement of the composites from micro to nanocomposites can be differentiated on the basis of three main factors including [31], [32];

- Size and shape of the fillers
- Specific surface area of the fillers
- Type of the filler

Since the nanofillers are in very small quantity in comparison to the base polymer molecules thus the actual polymer does not lose its inherent properties. Some of the properties remain the same in nanocomposites as that of unfilled polymers like density of the material[31]. The scientific reason behind the improved insulating and mechanical properties of the nanofiller is the large interfacial area and the interaction zone between the base polymer and the filler. K.Y. Lau et al. [29] described in his article that as the size of the filler is very small, thus the specific surface area increases. Therefore, the interfacial region between the nano particles and the polymer matrix has higher fraction of volume because of higher surface to volume ratio of the fillers. This basically alters the properties of the base polymer.[1]

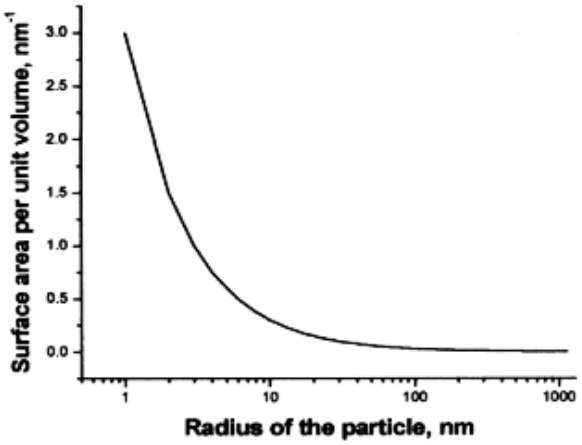

Figure 4.1. Surface area/volume of nanocomposites w.r.t nanofiller size [1]

Thus, the latest increasing demands of voltages in HVAC and HVDC transmission systems can be fulfilled economically by using different types and proportions of nanofillers according to the insulation needs based on application without degrading the other mechanical and electrical properties.

4.3 Structure of Nanocomposites

There are three main structural constituents of nanocomposites including;

- **Polymer Matrix**: consists of different types including thermoplastics, thermosets and elastomers. Thermoplastic materials are those that tend to get softened if heat is applied to them. Thermoset materials are those which form cross linked chains and turn the polymer chains in a desired shape on the application of heat. Elastomers are those which on the application of force change their shape temporarily and then revert to their original form when the force is released.

- **Nanofillers**: are also of three types. One dimensional, two dimensional and three dimensional. One dimensional is also known as platelet, two dimensional includes nanotubes and nanowires and three dimensional includes inorganic substances. The most commonly used in high voltage studies are one dimensional including layered silicates and three dimensional including silica (SiO_2), alumina (Al_2O_3) and Magnesium Oxide (MgO).

- **Nanofiller-Polymer Interface**: Tanaka et al. [32]explains in his findings that there are three layers in the interfacial zone of polymer and nanofiller including the First layer that is the bounded layer which is the transitional layer and it tightly bound the organic and inorganic substances using the coupling agents. Bounded layer has approximately 1nm thickness. The second layer is the bound layer in which the inorganic particles are bound with the second layer and it is made up of several nanometers of polymer chains. The third layer is the loose layer which has

tens of nanometer thickness and is loosely bounded to the second layer. There exists also an electric double layer or columbic layer which positively and negatively charges the nanoparticles. [31]

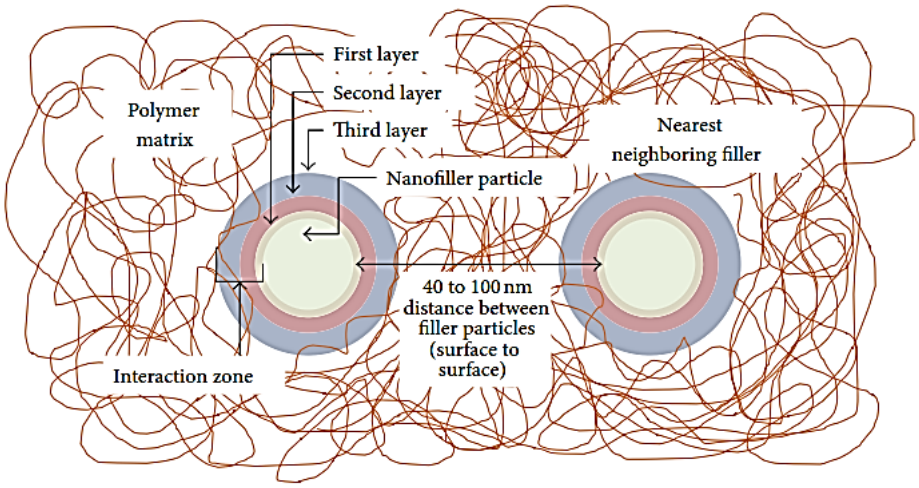

Figure 4.2. Structural constituents of Polymer Nanocomposites[29].

4.4 Nanofiller- Polymer Interfaces

As we have already discussed about the distinctive properties of nanocomposites which are different as compared to respective microcomposites and base polymers, we reached to a conclusion that the main cause of these favorable electrical, thermal and chemical characteristics of nanocomposites is basically the introduction of interfacial region. In literature there are different models of interfacial regions and their basic model contains three structural components including; nanofiller, interface and polymer matrix [33].

4.4.1 Diffuse Double Layer Model

This model is also called Lewis Model and it consists of Stern layer and Gouy Chapman diffuse double layer which exists at the interfacial region. Stern layer is an ionic layer that is strongly bonded to the nanofiller surface by the attractive forces attracting the diffuse layer and is much stronger than the electrostatic forces. The diffuse has both repulsions from the similar ions and attraction from the counter ions towards the nanoparticles. The nanoparticle gets charged when it is introduced in the dielectric material. Thus, the matrix of the base polymer tries to react to that and this can be balanced either by reorganization of polarization around the particle or with the formation of layers as discussed by Lewis. The stern layer and diffuse layers are having moving ions and when the no. of nanofiller particles which are positively charged, these layers start overlapping and conductive path appears to exist. Thus, this process improves the dielectric strength. Lewis also explains this conduction as electron hole pair recombination and consequently this

internal recombination reduces the chances of electron to conduct through the electrodes and improves dielectric strength as shown in the figure 4.3.[30][33]

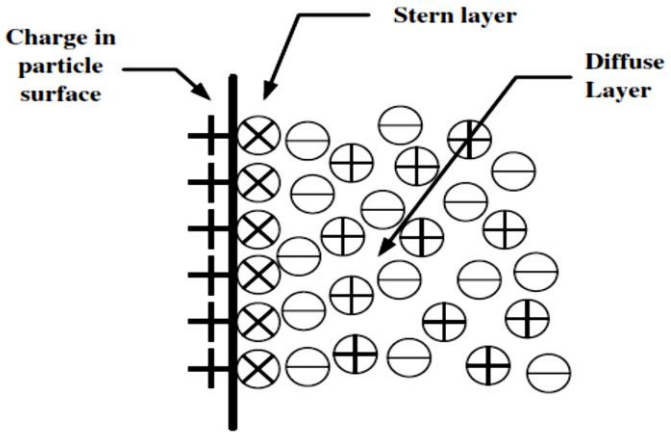

Figure 4.3. The Stern layer and diffuse layer formed around positive charge[34].

4.4.2 Multicore Model

The multicore model or Tanaka model consists of multiple layers including the bounded layer, bound layer, loose layer and Guoy Chapman diffuse layer. The bounded layer is a transitional layer and is strongly bonded through different agents to polymer and nano-filler. The second layer is the bound layer or actually interfacial layer which has polymer chains bound with the first layer and the nanofiller particle. The third layer is the loose layer which loosely interacts with the second layer and different arrangements of chain, dynamics and free volumes. The fourth layer is the diffuse layer which overlaps the entire first, second and third layers. Also, it helps in charge decaying effect due to distance and thus gives the idea that interfacial regions of different nano particles overlap and cooperates with each other resulting in the improved electrical properties.

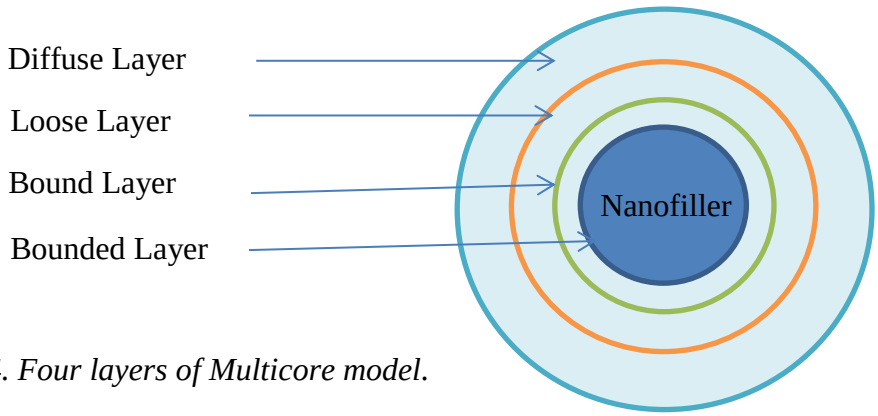

Figure 4.4. Four layers of Multicore model.

4.4.3 Multiregion Model

S.Li et al. [35] have proposed this model which consists of bounded region, a transitional region and a normal region that is the polymer matrix. The bounded region is strongly bonded to the particle and the highest bonding strength in the interfacial region because of hydrogen and silane bonds at the surface of the nanofiller. Such unsaturated bonds and silane coupling give strength. The other layer is the transitional layer which is mainly consists of molecular chains of ordered polymers and its characteristics are dictated by cohesive energy forces. The more the energy density of the cohesive forces, the more the flexibility of the polymer chain and thus it increases the failure strength of the polymer as more force is needed to break the chain. These layers collectively help in reducing the failure probability of the polymer.[33][34]

4.4.4 Tsagarapoulos' Model

This model has its central idea around glass transition temperature and it consists of a tightly bound region and a loosely bound region. Loosely bound region contributes in glass transition unlike tightly bound region. Many researches have shown that polymer silica nanocomposites have two peaks in the curve of tanδ. Out of these two peaks one is because of loosely bound layer and the other one is the usual one. It is also described that as the nanoparticles loading increase the reduced mobility polymers decrease and immobilized region increase and the loosely bound region starts overlapping and the glass transition temperature tends to decrease.[34]

4.4.5 Double layer Model

This model has been proposed by Singha and Thomas and based on Tsagarapoulos' model. It consists of two layers the inner most strongly bonded layer with the nano particle surface and is very immobile and the outer layer is the loosely bonded layer. If the inner most layer dominates then the glass transition temperature increase and the permittivity and conductivity decreases whereas the loose layer domination decreases the glass transition temperature and charge movement enhances which increases the permittivity and breakdown strength can be decreased.[33][34]

4.4.6 Other Models

There are few other models which are not directly based on interfacial layers. One of such models is ***3D Electrostatic Model***. This model has been proposed to check the electrostatic field inside, outside and around the nanofiller particle. Moreover, it also helps to figure out the diameter of the nanoparticle, thickness of interfacial layers, concentration of the nanoparticles, permittivity etc.[34]

One other model is ***Interphase Volume Model*** which helps in explaining different phases of interfacial layers based on different structure as compared to the base polymer structure. The interphase structure is the result of influence of the base polymer matrix, the type of nanoparticles and their surface modification. It further calculates the fractional volume, diameter and thickness of interphase. This model helps in identifying the effect of interphase on loss tangent, electrical, mechanical and thermal properties, delay in material degradation etc.[34]

There exists one model which is based on some old theory but still a better choice for understanding the basics that is ***Water Shell Model*** which explains the effect of water absorption by epoxy nanocomposites. It describes two layers; one is strongly bonded layer to the surface of the polymer and the other one is the conductive layer that has loosely bonded water molecules by Van der Waals forces. The high concentrated regions around nanoparticles with water have percolated path that adversely affect the dielectric properties of the polymer. It is mentioned that the epoxy nanocomposites degrade more than pure epoxy due to the presence of water layers overlapping and a percolated path forms for electrical conduction that helps in electrical breakdown strength reduction, more dielectric losses and increase conductivity.[34]

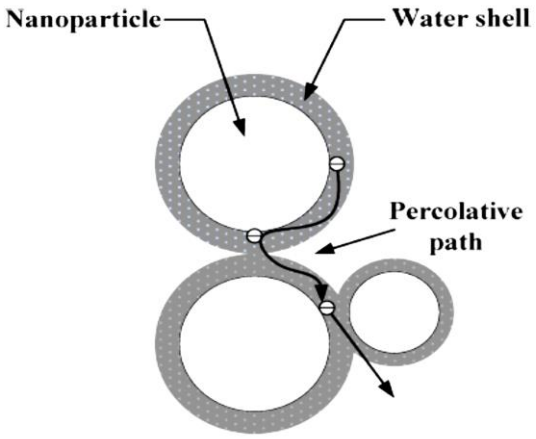

Figure 4.5. Water shell model [34].

4.5 Some Electrical Properties of Nanocomposites

4.5.1 Dielectric Breakdown Strength

The dielectric breakdown strength of nanocomposites is much better than their respective microcomposites. This is mainly because of the mitigation of space charge accumulation in nanocomposites and improved charge decay whereas in microcomposites there is a huge accumulation of space charge. Therefore the dielectric strength is higher in nano-

composites[33]. Montanari et al. [36] has discussed about nanosilicate filled polypropylene and mentioned a relaxation process for charge trapping in the interfacial region between base polymer and nanofiller. The magnitude of the space charge is smaller whereas the kinetics of the charge mitigation is higher for the nanocomposites. Thus, nanocomposites enhance the dielectric breakdown strength.

Some of the articles claims that the interaction zone or interfacial area acts as a quasi-conductive region [37] which has overlapping with the interfacial region and this overlapping consequently helps dissipating the charge and improves breakdown strength and endurance capability of high voltage.

F. Fujita et al. [38] explains that the interfacial region improves the breakdown strength by scattering mechanism which means the increase in path length of the charge carriers and change in distribution of space charge is responsible for this improvement. The size of the filler if becomes comparable to the chain spatial arrangement then they cooperate with the base polymer and helps suppressing the Maxwell-Wagner polarization peak. Tanaka et al. [32] found working on polyamide that Maxwell-Wagner polarization peak is much larger around 1kHz for the microcomposite with 3µm filler loading whereas the pure Polyamide has no peak around 1 kHz. This peak was found to be suppressed if the filler size is reduced to 40nm. Thus, the interfacial polarization reduces due to space charge mitigation with the decrement in filler loading. But the frequency at which Tanaka et al. [32] describes the interfacial polarization peak at 1kHz and above whereas the interfacial polarization effect exists at lower frequencies. At higher frequency, the chances of space charges drift and accumulation after the application of electric field is low. Moreover there is higher time lags to move and drift under such high frequency[39].

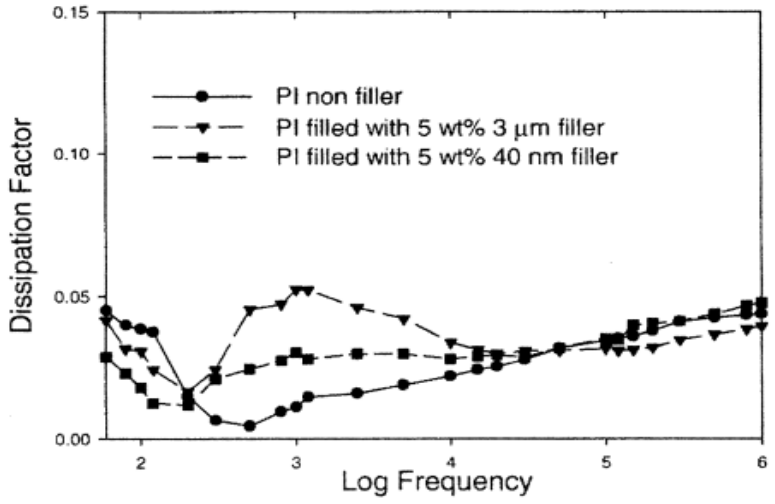

Figure 4.6. Dissipation and Polarization peak for polyamide with 3µm and 40nm filler loading w.r.t Frequency[32].

The morphological changes in the polymers due to nanofiller addition can lead to the improvements in the breakdown strength as well. The intra-spherical regions have more breakdown strength than the inter-spherical regions[5].

S. Li et al. [35] describes that AC and DC breakdown strength of the nanocomposites is higher as compared to microcomposites and the effect of nanofiller towards higher breakdown strength is evident for smaller nanofillers. The improvement reduces with the increase in the nanofiller loading after the threshold filler loading. It was observed that polypropylene nanocomposites have reduced accumulation of charge as compared to un-filled polypropylene.

The polymer films under observation in this thesis are Bi-axially oriented polypropylene (BOPP) films. The studied samples NPO49 (unfilled BOPP) and NPO30 (4.5wt-% BOPP nanosilica) were tested for breakdown strength behavior of polypropylene and its nano-composites by Rytöluoto et al. [7] in High Voltage laboratory of Tampere University of Technology. It was found that with the increase in the nanosilica loading in pure BOPP, the overall breakdown strength behavior declines as compared to pure BOPP. But at the same time the breakdown homogeneity is increased and breakdown variance is reduced as shown in the figure 4.7. [40] Lu et al. also explains the overall breakdown strength reduction for epoxy-alumina nanocomposites for both lower and higher breakdown probability regions of epoxy-Al.

Moreover, it was found that the lower silica loadings in BOPP help in shifting the higher probability breakdown points towards the higher values of dielectric strength. Higher loadings of silica as shown in the figure 4.7. for NPO30 (4.5wt-%) shifts the breakdown region with lower breakdown probability towards the higher dielectric strength as compared to pure BOPP. NPO30 has more homogeneity and less dispersion which is of extreme importance in real applications. More over the lower filler loadings of less than 1wt-% can be interesting to use in future. Rytöluoto et al. [7] further explain that only the filler loading is not responsible for the changes in the breakdown performance. Certain other parameters e.g. manual mixing of raw materials can lead to agglomerations and increased risk of low probability breakdowns whereas automatic mixing has better low probability breakdown performance. Similarly, the amount of co-stabilizer also affects the breakdown strength as for BOPP decreasing the amount of antioxidant Irgafos 168 improves the breakdown strength. Further the increase in the orientation temperature from 157 °C to 165 °C can also improves the surface morphology of the polymer film and ultimately improving the breakdown performance.

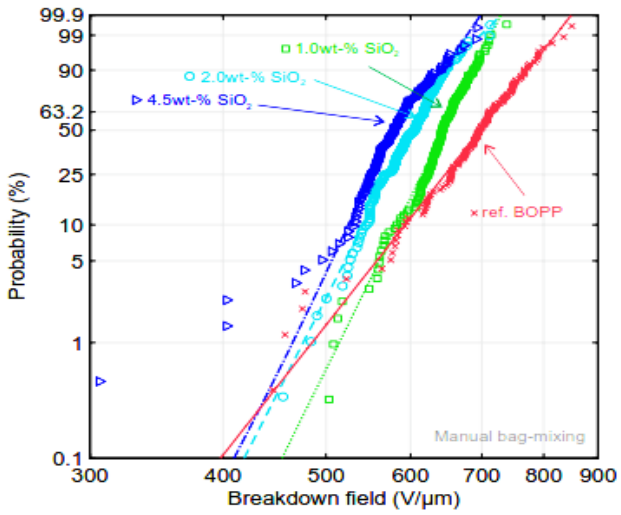

Figure 4.7. Breakdown Performance of pure BOPP and BOPP-Silica w.r.t nanofiller loading. [7]

After referring to various articles and experiments it is evident that breakdown performance is dependent also on various factors else than the filler loading and it cannot be simply explained by considering a single factor. Moreover, the optimum weight-percentage of filler w.r.t the other affecting parameters are required to be considered.

4.5.2 Resistance to Partial Discharge activity

Partial discharge is a localized electrical discharge which can occur in various insulations. The weak spots in insulation like a gas bubble or voids accompany partial discharging as sparking occurs at those points under high voltage stress. A localized breakdown is possible at these weak spots and thus erodes the insulating material. Partial discharges are of the following types:

- Internal discharge: This kind of discharge can occur in the materials with lower dielectric strength and its effects are quite detrimental. A series of internal discharges result in treeing
- Surface discharge: This kind of discharge can occur in the presence of stress component which must be strong enough to cause the discharges. It is less harmful as compared to internal discharge.
- Corona: occurs when the air gets ionized under high voltage and creates a glow outside the conductor in a section like sharp corner where electric field locally exceeds the breakdown strength of air. Corona discharge is normally acidic.

Tanaka et al. [32] and many other authors concluded that with the addition of small amount of nanofillers, partial discharge decreases and Kozako et al. [41] mentions that only 2wt-% addition of nanofiller polyamide layered silicate improves the resistance to partial discharge. Tanaka et al. [32] explains that the partial discharge follows a haphazard

path and thus avoids the nanofiller region and consequently increases the partial discharge resistance. Maity et al. [42] also explain the degradation due to partial discharges on an addition of metal oxides like nano-alumina and nano-titania to epoxy.

K.Y.Lau et al. [33] says that most of the experimental results about partial discharge addresses the surface discharge whereas internal discharge effect is more detrimental and needs to be explored. Henk [38] has published that nanosilica has major effect on the internal discharge resistance of thermosets but no effect on thermoplastics.

4.5.3 Tracking Resistance

The formation of conducting film on the surface of the insulator under high voltage which results in erosion of the surface is called tracking. All the polymeric insulators which are installed outside can get coated with moisture, dust and other foreign particles and thus a conducting path becomes on the surface. Under high voltage this path conducts and get more brittle thus the insulation surface gets damaged. This can result in sparking and continuous sparking can result in permanent damage to insulation. Thus, to mitigate this issue there is a need to increase the tracking resistance of the insulation material. Therefore inorganic fillers are being tried to add in the polymers and thus there are some observations which gives the evidence of improvement in tracking resistance in the polymer nanocomposites[33].

El-Hag et al. [43] explains that nanosilica filled silicon rubber has much better erosion resistance as compared to its respective microcomposite. But at the same time during one experimental test it was found that 5wt-% nanosilica addition has much better tracking resistance as compared to 30wt-% but at the same time it was found that 10wt-% nanosilica addition has much better erosion resistance than 5 or 30wt-% whereas the other properties were found to be degraded. Thus, the optimum filler percentage for nanofiller addition needs to be selected. There is still further need of research in this field as it is complicated to increase the filler percentage to higher percentages as it results in agglomeration and degradation of other properties.

M. Thomas et al. [44] describe in his article that for improving the tracking resistance of silicon rubber usually the microcomposites around 30 to 60% by weight were being used which tends to reduce the flexibility of the material and also creates many processing problems. Thus, they moved to nanocomposites and found the optimum percentage of nanofiller to achieve the better erosion or tracking resistance with no degradation of other properties. It was observed that 4wt-% of nanoalumina SR has almost the same improved tracking resistance as 30wt-% of SR microcomposite. Moreover, it was found that there is a gradual increase in the erosion resistance in microcomposites with the increase in percentage loading. Because of the better thermal stability and other interfacial properties discussed earlier nanocomposites with lower filler concentration has comparable tracking resistance as microcomposites show at higher concentration. Guastavino et al. [13] found

in his tracking experiments that average tracking time of epoxy nanoccomposites (3.2h) is more than the tracking time of microcomposite (1.7h). At the same time the nanostructured composite shows no tracks even for tracking time of 6h.

4.5.4 Dielectric Permittivity

Different researches show different behavior of permittivity in nanocomposites. Some give evidence of increment in effective permittivity and some literature reviews show a decreasing trend. P. Zhang [45] shows that the permittivity is low for Polyamide nanosilica for frequencies in the range 100Hz to 1MHz. Also Toshiba et al. [37] explain the reduction in permittivity and tanδ for layered silicate epoxy nanocomposite than base epoxy polymer.

Polarization process is responsible for the changes in the permittivity and can explain its different behaviors. Polymers can have different types of polarization mechanism including;

- Electronic Polarization
- Ionic Polarization
- Hopping Charge and Interfacial Polarization
- Dipolar Polarization

All the above polarization mechanisms have a relaxation frequency. The dielectric permittivity shows an increasing trend with the increase in the nanofiller loading but at the same time the decreasing trend is also observed with less loading percentage in some samples as compared to the corresponding unfilled polymer of the nanocomposite.

Figure 4.8. shows the permittivity of BOPP commercial film, NPO49 (Pilot scale unfilled BOPP film made by VTT/Tampere University of Technology) and NPO30 (4.5wt-% BOPP/SiO_2 nanocomposite). The films were treated in vacuum under the set temperature of 35°C and measured in Novocontrol device after sputtering the gold electrodes with 75nm thickness. It can be observed that the commercial BOPP film shows the permittivity value rated according to the manufacturer that is around 2.22. NPO49 (unfilled BOPP) film shows 2.17 and NPO30 (4.5wt-% SiO_2) film shows permittivity around 2.05 which is slightly less than the permittivity of commercial and pilot scale unfilled BOPP films. There is around 7 to 8% reduction in the overall permittivity of nanocomposite. The decrease in dielectric permittivity is an effect of the change in polarization mechanism. Relative permittivity of SiO_2 is around 2.5 to 3.9 that are slightly higher than the permittivity of the base BOPP film. Thus, there might be some other reason (could be possibly hidden in the interfacial properties) of the reduction of the permittivity than that of the inclusion of the nanofiller.

Interfacial polarization is negligible above 1 kHz and its effect is prominent under lower frequency range and here we can see an overall decrease in the permittivity thus undermining the effect of interfacial polarization [39]. The reduction in the mobility of the polymer chain due to the formation of the bounded layer as was discussed by Tanaka et al. [32]. These bounded layers around nanosilica and BOPP interface in the whole polymer helps in restricting the movement of the BOPP chain and consequently reduces the effective permittivity of NPO30. Moreover, when the nanosilica layers reaches the length of the polymer chain then the entanglement of the secondary chain further reduces the mobility. This immobility of nanosilica must be dependent on nanosilica dispersion and concentration. The similar decrease in permittivity has been explained by Takala et al. [30] for glycidyl POSS-EP nanocomposite and by Wang et al. [46] for epoxy/Al_2O_3 nanocomposite.

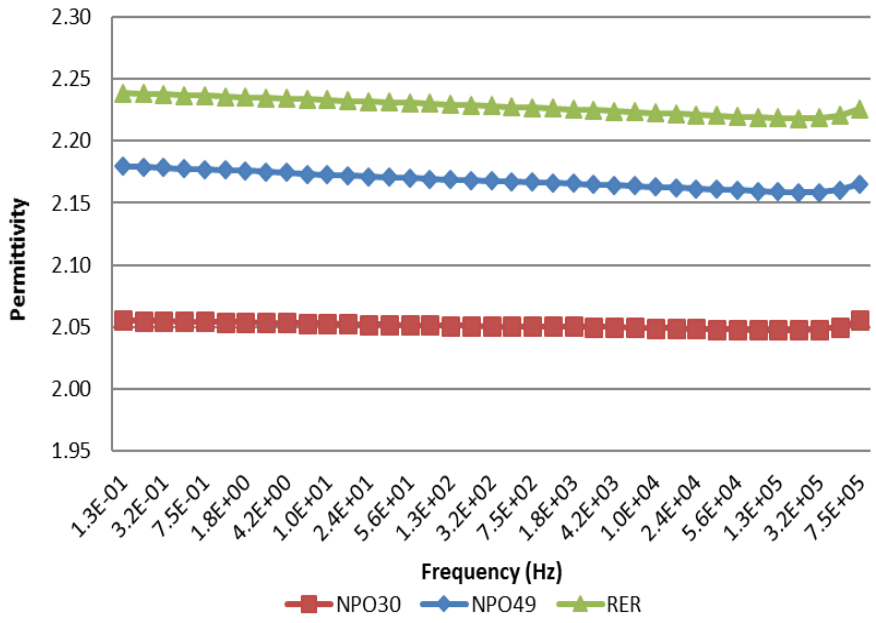

Figure 4.8. Relative permittivity of NPO30 (4.5wt-%.), NPO49 and RER w.r.t frequency.

The filler concentration has different effect on permittivity. Low concentration of filler has lower effect of the nanofiller permittivity on the nanocomposite whereas in case of higher concentration of filler, the filler inherent individual permittivity affects the permittivity of the resultant polymer with association of permittivity of base polymer. The mixing rule exists for microcomposites, which directly gives the resultant permittivity of the microcomposite but for nanocomposite the mixing rule does not work as it is rather complicated scenario in nanocomposites. The mixing formula for microcomposite can be written as;[46]

$$\text{Log}\varepsilon^{c} = \text{a Log}\varepsilon^{nf} + \text{b Log}\varepsilon^{bp} \tag{4.1}$$

Where, ε^c is the composite permittivity ε^{nf} is the nanofiller permittivity, ε^{bp} is the base polymer permittivity, a & b are concentration variables.

Wang et al. [46] shows that in epoxy silica nanocomposite the permittivity decreases as the silica loading increases from 0.1 to 3 wt-% of silica filler and then after 3% the permittivity starts to increase. This is because as the filler percentage increases more and more it can form agglomerates and can have dominant effect on the permittivity value. Also, the density of nanofiller affects the permittivity. Three factors; nanofiller density, immobilization and entangling are responsible of the permittivity changes. There exists a threshold of nanofiller concentration where the unfilled and the nanocomposite has the same permittivity e.g., in the figure 4.9. it is 0.1 wt-% and here the all the three factors have the similar effect on permittivity[30].

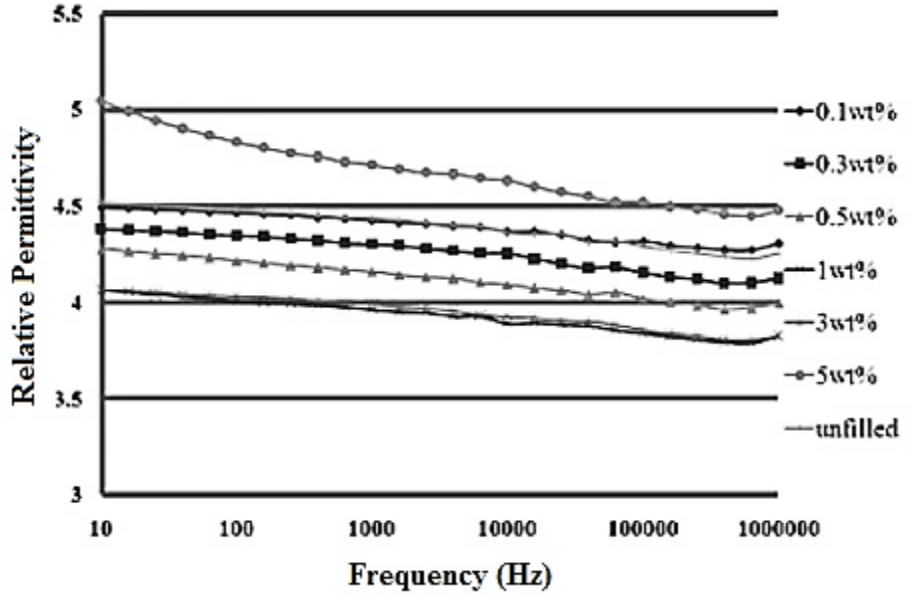

Figure 4.9. Relative permittivity w.r.t frequency of epoxy-SiO_2 nanocomposite for different percentage of nanocomposite[46].

It can be observed from the figure that all three samples which are considered for analysis show a decrement in permittivity as the frequency increases. This is because the permittivity is related to the polarization effect. Under low frequency, the effect of all types of polarizations become more prominent and consequently the effect of polarization on permittivity reduces as frequency increases and thus the permittivity decreases as the frequency goes higher. Wang et al. [46] describes for epoxy- SiO_2 that with the increase in frequency the intrinsic relative permittivity of the nanocomposite filler also decreases that is SiO_2. So, the combined effect is a decrement in effective permittivity.

One more aspect can be figured out that the percentage decrease in permittivity with the increase in frequency is more in case of pure BOPP (NPO49) and commercial BOPP (RER) as compared to BOPP nanosilica (NPO30). Therefore, the average permittivity of

low frequency, high frequency and mid frequency dispersion are calculated for all three samples and then the percentage decrease of permittivity in case of high frequency range (above 10^4Hz)w.r.t medium frequency range ($10^4 to 10^1$)Hz and also the percentage decrease of permittivity in case of medium frequency range w.r.t low frequency range (below 10^1Hz) is plotted in the figure 4.10. It is clear that the percentage decrease in permittivity in both cases is lower in case of NPO30. This could be explained in relation to the interfacial layers that the strongest bounded layer restricts the mobility of the dipoles even at lower frequency dispersion where the interfacial effect is more pronounced and therefore the overall difference in permittivity is lower w.r.t the frequency change. This gives stable permittivity values with very small difference and proves the BOPP nanosilica as a better insulator than unfilled BOPP. Moreover, there is another observation that the decreasing effect of permittivity is more between medium to high frequency range than lower to medium frequency range.

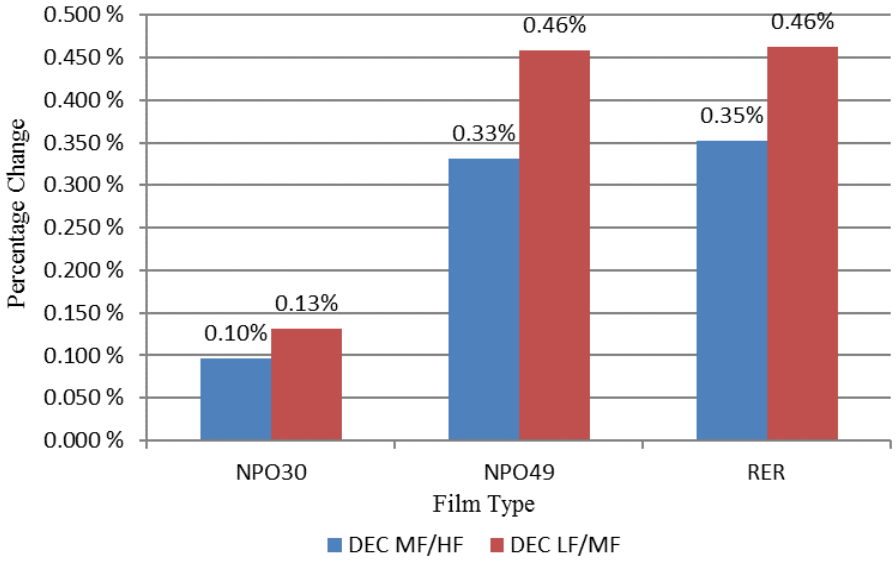

Figure 4.10. Percentage change of NPO30, NPO49, RER's average permittivity w.r.t to high, medium and low frequency dispersion.

4.6 Dielectric Loss

The dielectric loss in nanocomposites is the dissipation of energy as heat and is dependent on frequency, capacitance and resistance. It can be further break into conduction and polarization losses. Conduction loss is related to the actual travel of charges through insulating material whereas polarization loss is related to the friction that a dipole faces during its orientation when an electrical field is applied. Conduction and polarization loss is related to the changes in temperature, voltage and frequency. The effect of different types of polarizations is frequency related as shown in the figure 4.11. At lower frequency range all kinds the polarization effect could be possible.

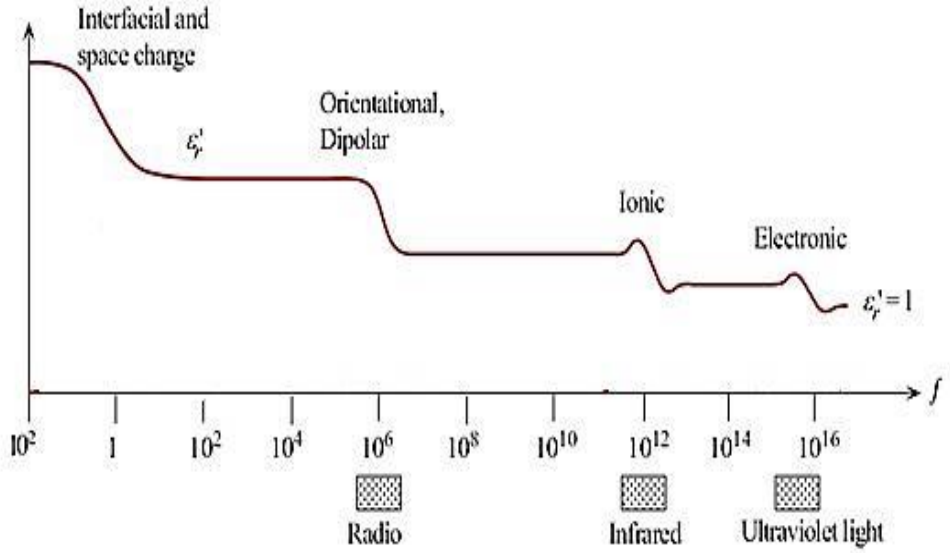

Figure 4.11. Polarization effect w.r.t frequency range[47].

In the figure 4.12., it can be observed that BOPP nanosilica (NPO30) has lower dielectric loss as compared to its unfilled BOPP (NPO49 and RER). This is due to lower electrical conductivity in nanocomposites. The nanoparticles make a barrier to the charge transport and decrease the mobility of the charges. Moreover, the entanglements further cause hindrance in charge movement. This reduced mobility of the charges reducing the electrical conductivity and consequently also the dielectric loss. This is true for lower nanofiller concentration with homogenous dispersion because if the nanofiller concentration exceeds the threshold level then the overlapping of interfacial layers is possible which increase the charge mobility and thus can increase the dielectric loss[30],[39].

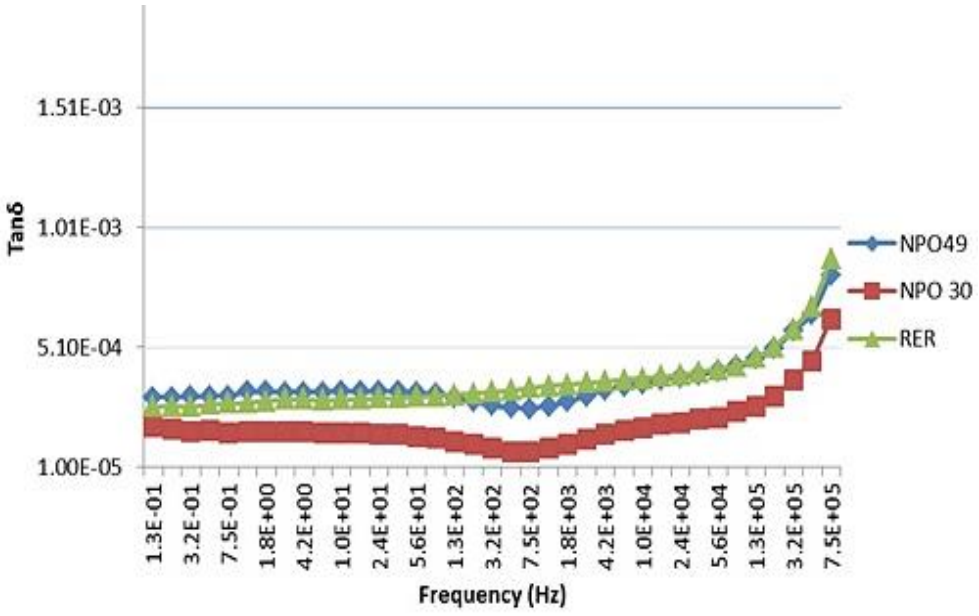

Figure 4.12. Loss factor of NPO30 (4.5wt-%.), NPO49 and RER w.r.t frequency.

5. TEST ARRANGEMENT AND PROCEDURES

Before starting the actual spectroscopy measurements, the first and foremost important issue is to define the best and optimum test procedures to get the desired accurate optimal and repeatable results with precision. These issues start from defining the sample preparation methods, pre-sample cleaning, electrode formation, procedures involving electrode formation. It has been observed that by altering various parameters during the sample preparation and testing, the results of dielectric spectroscopy change especially the value or curve of loss tangent. Therefore, different parameters were changed and tested many times to establish the optimum testing procedures to get the precise and repeatable results. There could be two main procedures or ways to fabricate electrodes on the polymer samples that are sputter coating or evaporation method. We have extensively used sputtering method in this thesis for electrode formation which is discussed in the section 5.2 of this chapter 5. Gold has been chosen as a metal to make the electrodes because of its better conducting properties and resistance to corrosion or oxidation.

Novocontrol device has been used for dielectric spectroscopy throughout the thesis and various loss factor and permittivity curves have been analyzed through this device. It has been found out that all the loss factor curves show high loss factor as a peak at very high frequency irrespective of the type of the sample and testing parameters. This could be because of some of the hidden errors in the testing equipment or calibration which need to be identified in future. The results of dielectric loss factor are mentioned even for higher frequency and high loss region to show the changes in the loss curves in that region as well. Kahouli et al. [48] has described in his article for metallized thin PP film that annealing flattens this high frequency high loss peak whereas without annealing there is slope of 1 in the loss factor curve. Annealing helps in reducing the defects and improve the crystalline ratio and reduces the glassy phase. S. Kume et al. [49] and Chun et al.[50] described that annealing helps in reducing the loss factor and increases the conductivity. Dielectric loss depends on intrinsic and extrinsic losses and need to be analyzed in future. The experiments performed in this thesis are without annealing.

5.1 Sample preparation and vacuum treatment

In order to prepare the samples, the film of the desired polymer is cut from the polymer thin film roll into squares of 40mm×40mm. Thickness of these samples are then measured by taking the mean of 5 different point of the area where the electrodes are to be prepared.

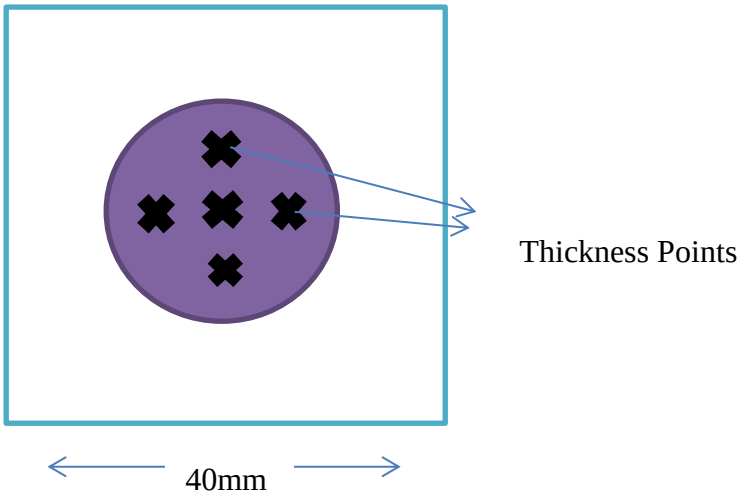

Figure 5.1. Model of thin film electrode.

These samples are then cleaned with isopropanol for any dust particles, grease and then every sample is placed in a paper envelop. These covered samples are then placed in a vacuum maintained jar at room temperature for a suitable duration. The samples are then sputtered with gold electrodes using SC7620 mini sputter coater. The masks used to hold the samples during sputtering process were made from Folex imaging BG-72 polyester based crystal clear film of 0.125mm thickness. In order to figure out the effect of pre-vacuum treatment, a comparison of the loss factor values of pre-vacuumed and no vacuumed samples has been made in figure 5.2. There is a clear hump in the middle frequency for no vacuumed sample. These humps and irregularities in the loss factor curve give a hint of the presence of moisture in the BOPP film. Several tests were made with and without vacuum treatment and the loss factor was found higher in magnitude with peaks in case with no vacuum treatment. The results were repeatable but the peaks found in no vacuumed case were not always same as the moisture content differs but pre-vacuumed samples have shown the repeatable same curve almost every time. Therefore, it was decided to first pre-vacuum the film samples before sputtering the electrodes to avoid trapping of moisture. In figure 5.2., the curve of loss factor in case of vacuum treatment is smooth with no humps and overall loss level is also low that is 9.42×10^{-5} at 50Hz as compared to the loss level of the sample without vacuum pretreatment that is 1.92×10^{-3} at 50Hz.

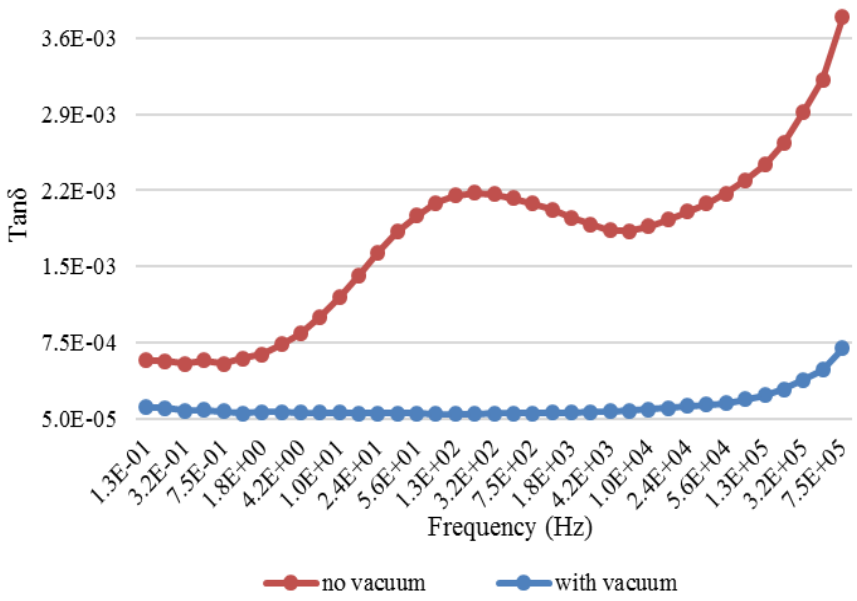

Figure 5.2. Loss factor curve without any vacuum treatment and with vacuum treatment for Tervakoski RER (BOPP) film.

The next task was to study the duration of pre-vacuum treatment required for the optimum results. Therefore, several samples were prepared with electrodes using same sputtering level that is 6*30s*30s*25mA (76.5mm thickness) and then subjected to vacuum treatment for 16h, 20h, 24h and 48h respectively under 35°C. It was found that the loss factor curve decreases as the vacuum timing increased from 16h to 20h to 24h as shown in figure 5.3. But there is no further significant difference observed between the 24h and 48h curves. Thus, the vacuum treatment reaches its saturation point at 24h and no further vacuuming is required. Next question arises that whether the heat treatment with vacuum treatment would affect the results or not. It was observed in figure 5.4. that as the temperature is increased from room temperature to 30°C, the loss level decreases but as the temperature further increases, the loss level starts to increase and at 60 to 70°C, there is huge increment in loss factor value which shows that vacuuming at higher temperatures for longer duration can age the sample due to thermal stress. As already discussed in the beginning of this chapter that higher loss peak at high frequency region might have some reasons hidden in the testing equipment calibration. This region has been considered just to view even the small differences in the behavior of loss factor. All the vacuum related tests were performed twice and repeatable behavior has been found out with no significant difference.

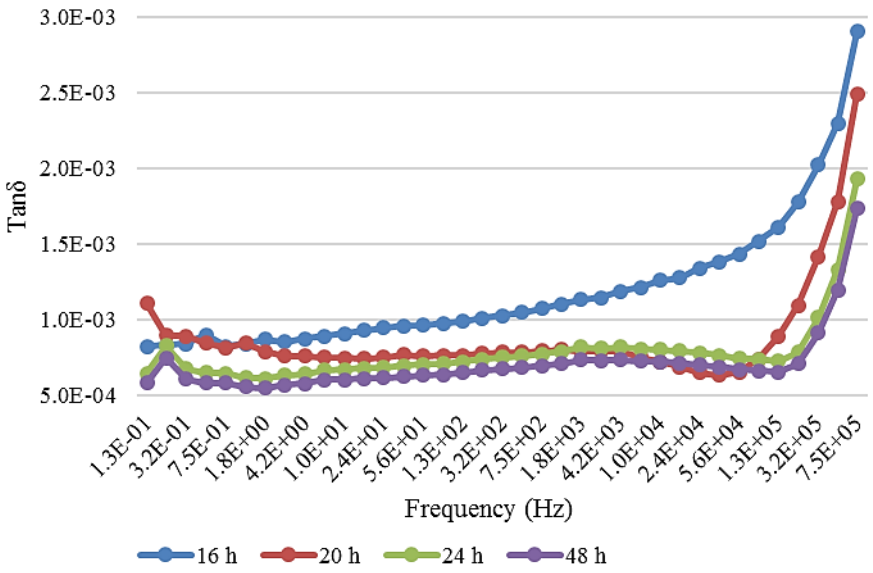

Figure 5.3. Effect of changing pre-vacuum duration on the loss factor value.

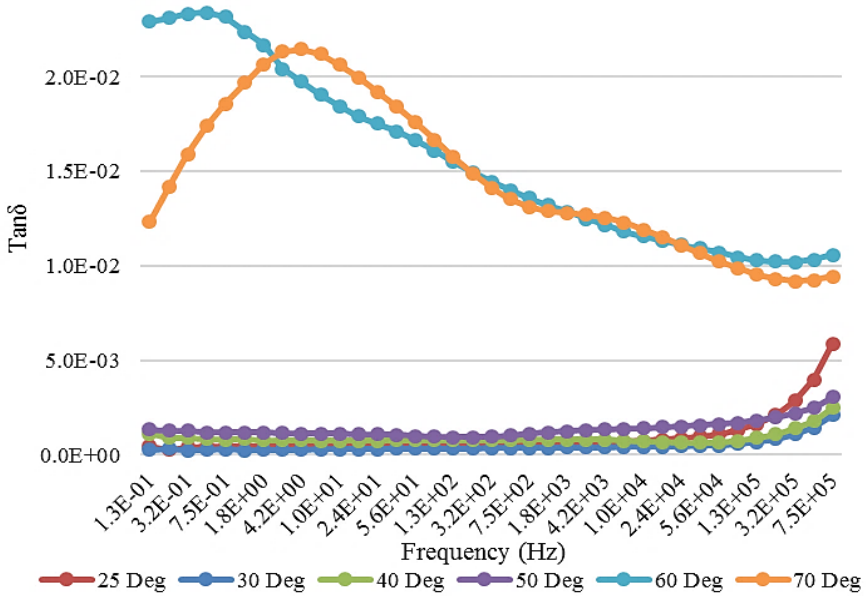

Figure 5.4. Effect of changing pre-vacuuming temperature on loss tangent.

After analyzing the effect of vacuuming before sputtering electrodes, post vacuuming after making electrodes has also been studied at 35°C. Figure 5.5. shows the pre-post vacuuming effect on the loss factor curve which shows that there is no distinguishable positive effect of post vacuuming even with different durations though there is a slight increment with post vacuuming at 48h. Thus, pre-vacuuming is more important because after making electrodes it would be difficult to remove the moisture from dielectric as the metal electrodes shield or cover the dielectric and moisture traps inside the material. It has also been studied that post vacuuming sometimes slightly increases the loss factor value as shown in figure 5.6 for post vacuuming for 20h at 35°C and in figure 5.5. for

post vacuuming for 24h and 48h at 35°C. Also, post vacuuming was studied by changing temperatures during vacuuming but still no effect of post vacuuming was found as shown in the figure 5.7.

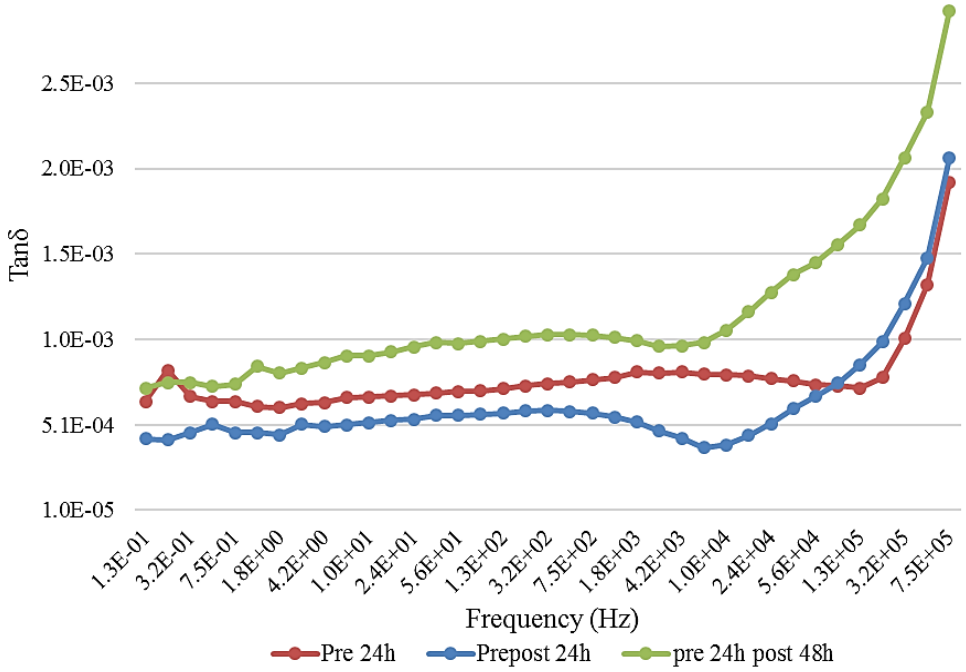

Figure 5.5. Effect of changing vacuum duration and order on the loss factor value.

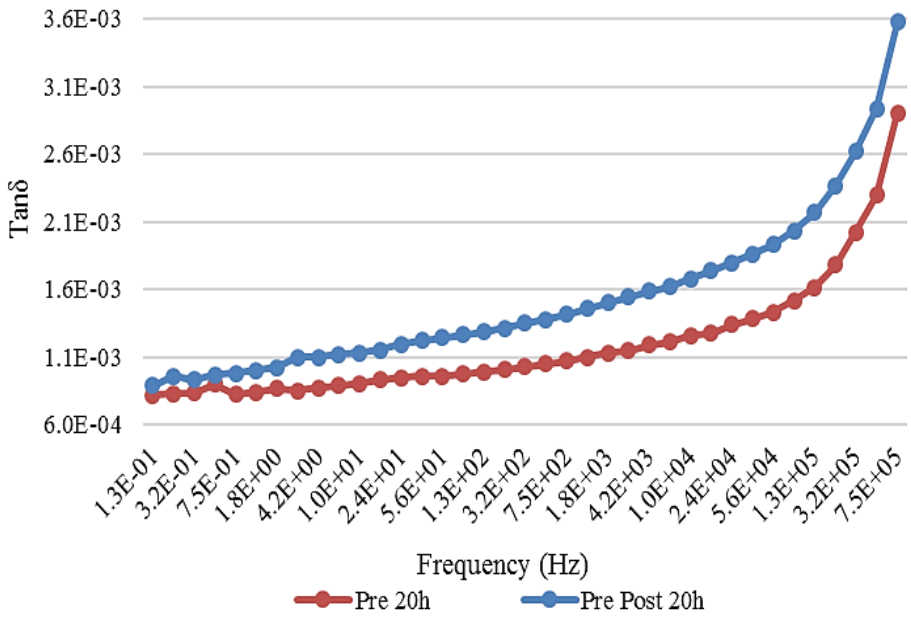

Figure 5.6. Difference of pre and post vacuuming for 20h on loss tangent.

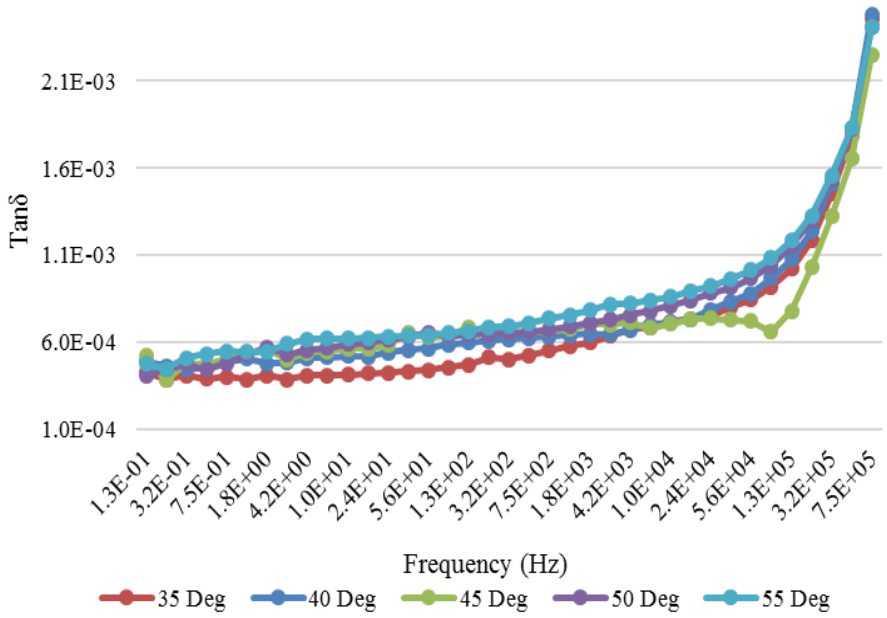

Figure 5.7. Post vacuuming effect on loss factor with varying temperature.

5.2 Fabrication of electrodes

Electrodes can be fabricated either by using evaporation method or sputter coating method. These processes of making an electrode is also known as physical vapor deposition (PVD) and are commonly used for making thin film electrodes.

Evaporation is based on the concept that there exists a vapor pressure over the material and the material can either sublime (transition from solid to vapor directly) or evaporates (transition from solid to liquid to vapor). The vapor pressure is given by the equation;[51]

$$P_{evap} = 3\times10^{12}\ \sigma^{3/2}\ T^{-1/2} e^{\frac{\Delta H}{N_A kT}} \approx P_0 e^{(\frac{E_a}{kT})} \tag{5.1}$$

where N_A is the Avogadro's number, ∇H is the enthalpy change and σ gives the surface tension. In evaporation process the metal can be deposited by evaporating through heating or electron beam bombardment. In evaporation, the chamber is fitted with a pump (turbo or diffusion) which helps in evacuating the evaporation chamber. In the chamber, high vacuum should be maintained to reduce the impact between the left-over gases and the evaporated metal particles. The source of metal evaporation is the electron beam which evaporated the target metal and these metal particles then get deposited on the surface of the substrate forming a thin film. The number of molecules or particles leaving the target to the substrate is;[52][51]

$$J = \sqrt{\frac{P^2}{2\pi kTm}} \tag{5.2}$$

Where k is the Boltzmann's constant, p is the pressure with unit Pascal's, T is the temperature in Kelvins and m is the molecular mass.

The thickness of film, metal deposition growth and rate of evaporation is controlled by quartz crystal which is mounted under the substrate holder. High vacuum maintained in the chamber helps the metal particles to easily travel to the substrate. For a uniform and flat coating on the film, the distance and angle between the target and the substrate is very important.

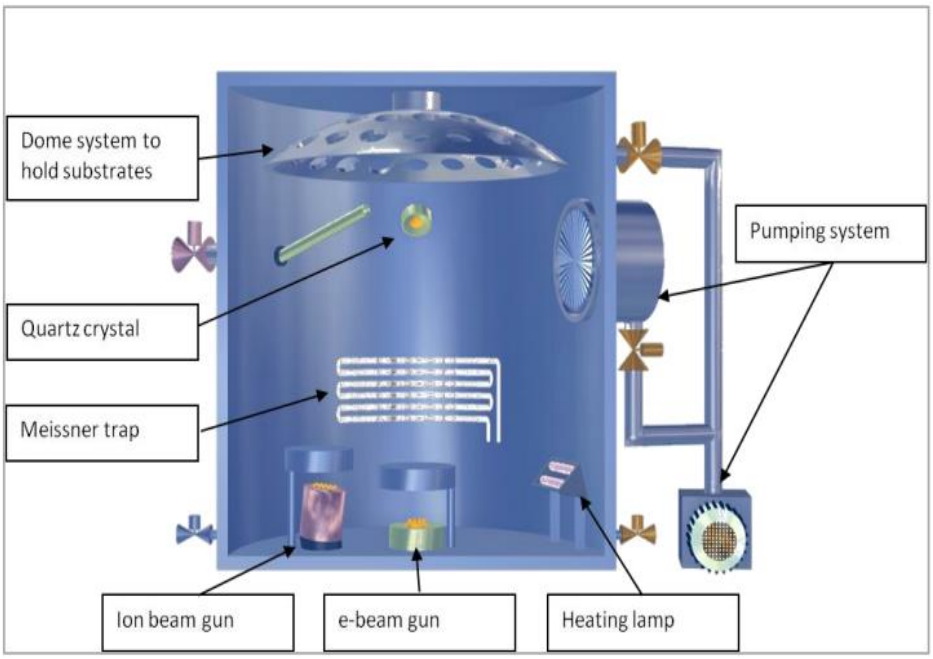

Figure 5.8. chamber of evaporation process[51].

Sputter coating is the method which has been extensively used and studied during this thesis. It is also known as cathodic sputtering. In this method first the gaseous plasma is established. The ions from this plasma have possessed energy to displace the metal particles, molecules, clusters etc. to sputter it on the substrate or the film. The target is at negative voltage and an inert gas e.g. argon is used as the working gas which gets ionized under electric field. Thus, these positive argon ions move towards the negative target and sputter the metal particles on the film or substrate. To sputter the metal threshold energy is needed and sputter efficiency is the sputtered metal per argon ion. The threshold energy required to emit particles from the target;[51]

$$E_{threshold} = \frac{Vaporization\ Heat}{\gamma(1-\gamma)} \tag{5.3}$$

Where $\gamma = \frac{4M_1M_2}{(M_1+M_2)^2}$ and M_1, M_2 are the masses of targeted atom and ion.

The device used in thesis is magnetron sputtering which has magnets placed over the target area which is sputtered. These magnets help in increasing the density of the sputtering and increase the rate of sputtering.

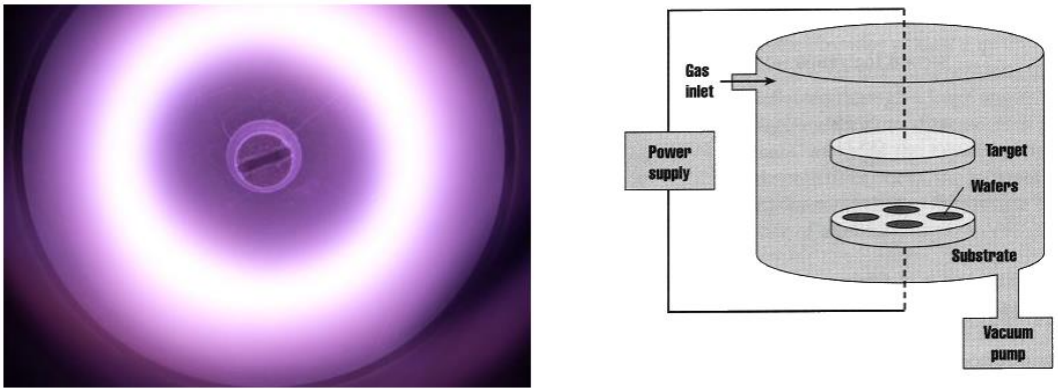

Figure 5.9. (a) showing plasma glow (b) showing chamber of sputtering device[51].

A factor which can help in analyzing uniformity of deposited metal is step coverage. If the targeted metal deposits on the material in one direction more than the deposited material will have poor step coverage. More uniformity of metal thickness means more step coverage. The step coverage in sputtering is better than in evaporation process where as the evaporation results in highest purity of film coating because of low pressure and vacuum. The density of the sputter coating is higher whereas to increase the density in evaporation an ion beam gun is used. Moreover, some thermal stress and other plasma stresses are possible in sputtered films if the cooling system is not present during sputtering. The device used in thesis for sputtering has no cooling system whereas some samples that have been evaporated have been maintained at room temperature throughout the process. Due to these stresses the sputtered film can cause bowing or cracking. These stresses can be extrinsic or intrinsic.[51]

Extrinsic stresses are those forces that act on the deposited film from external sources e.g. thermal stress as we already discussed.

$$Stress_{thermal} = \frac{Young\ mod.of\ Film}{1-(Poisson'sRatio)} \int_{T\ room}^{T\ depos.} (\alpha_{deposited\ film} - \alpha_{sputter\ material}) \quad (5.4)$$

where α represents the coefficient of thermal expansion.

Intrinsic stresses are those forces that are internal to the deposited films. e.g., atomic mass variation, orientation, impurities etc. and can be given by the equation;

$$\text{Stress} = \frac{\delta \mathrm{Y} d^2}{t(1-v)3R^2} \quad (5.5)$$

where Y is the Young's modulus, R and d represents the radius and thickness of sputtered material respectively, t and y represents the thickness and poison ratio of film.[52]

Figure 5.10. Effect of stress on the sputtered sample[52].

During the thesis Bi-axially Oriented Polypropylene film (Tervakoski RER) was sputtered using SC7620 Mini sputter coater. Different experiments were made using different parameters. One of these sputtered films with gold electrode thickness of 55nm was observed using a profilometer. Figure 5.11. (left hand side) and (right hand side) shows the 3D image of thickness profile of the observed film. It can be observed from both the figures that the electrode thickness is more at the edges as compared to the center and there is a bulging trend around the edge area which can be related to the tensile stress discussed above. Moreover, it can also be observed from 3D plot in figure 5.12 (left hand side) that the edge maximum thickness is around 130 nm whereas in figure 5.12 (right hand side) the maximum thickness away from the edge is 92 nm. Therefore, it was not possible to verify the sputtered thickness value because of thickness variations due to stresses and thus the nominal thickness value (100nm) used is an approximate value. Apart from stress analyses it was found during dielectric spectroscopy of BOPP sputtered and BOPP evaporated samples of 100nm thickness that there is a slight decrease in the loss level of evaporated samples as compared to the sputtered samples as shown in figure 5.13. This could be because of the heat stress due to the absence of cooling circuit in mini sputter coater used.

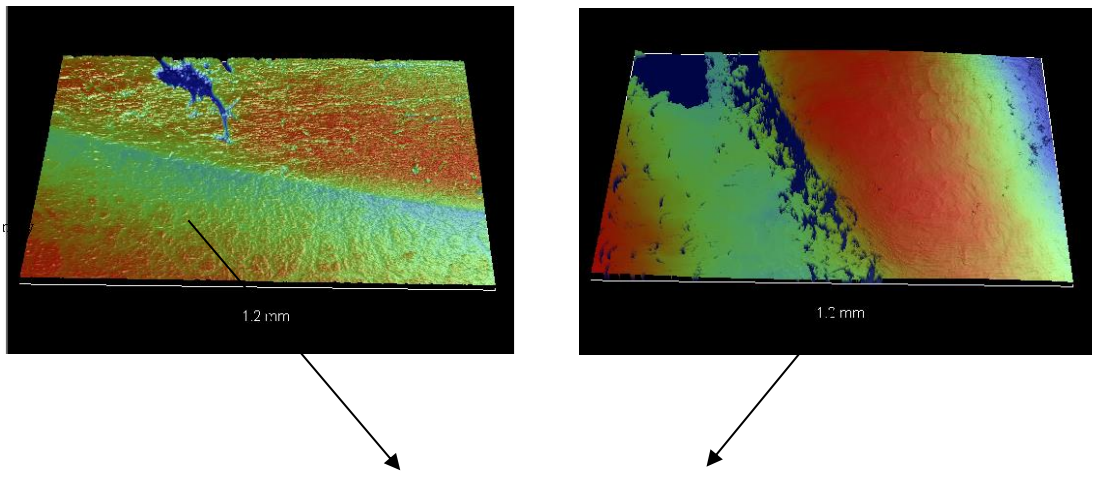

Figure 5.11. Profilometer 3D thickness profiles of BOPP sputtered film.

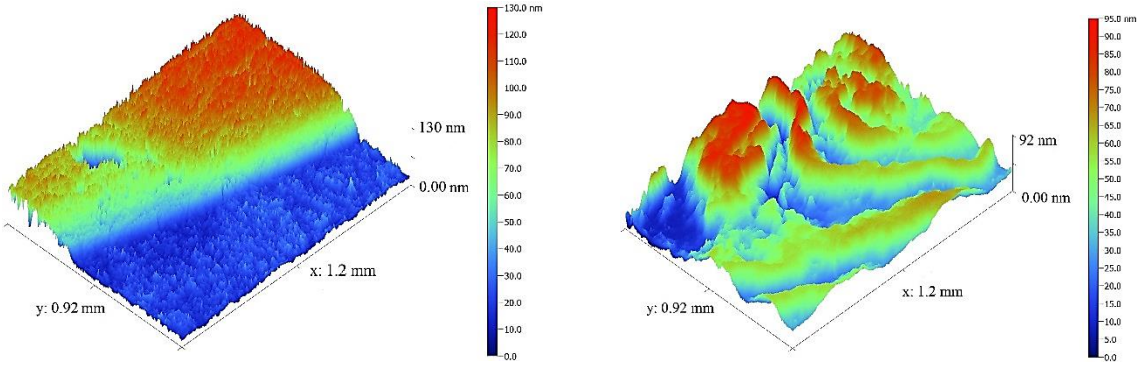

Figure 5.12. Profilometer 3D plots of thickness profile of BOPP film (left hand side) from the edge and (right hand side) from the middle portion.

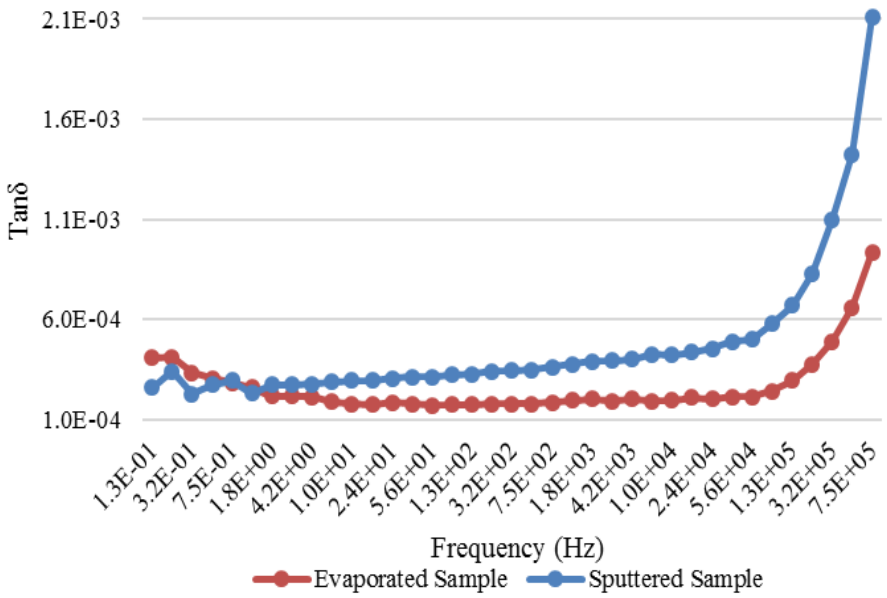

Figure 5.13. Loss factor w.r.t frequency for evaporated and sputtered samples.

Another issue was found out during sputtering process which is the use of mask for holding the sample during the process. At first the stainless-steel masks were used which resulted in wrinkled sample after sputtering. This might be possibly because metal transfers heat (plasma heat) more. Moreover, the magnets used in the sputtering device further determines that the use the magnetic material or metal is not appropriate. Thus, the masks were made up of Folex imaging BG-72 crystal clear film of 0.125mm thickness. This film is highly heat resistant and its base material is polyester. The masks made with this material helped in relatively more uniform sputtering with no wrinkles in the sample film.

5.3 Effect of different sputtering combinations on loss level

In order to figure out the optimum sputtering procedure, some of the experiments were performed by varying distance of the sample from the target. Three samples for each experiment were sputtered with the same routine of 6*30s*30s*25 mA to achieve the electrode thickness of 76.5nm and their distance of the sample from target was varied as 35mm, 45mm and 55mm. It can be observed from figure 5.14. that the loss factor value increases as the distance decreases from target to the sample. This could be most probably because of the plasma and heating stress effects the sample as the energy which displaces the target ions and particles produces heat and less distance means more heat stress on the sample.

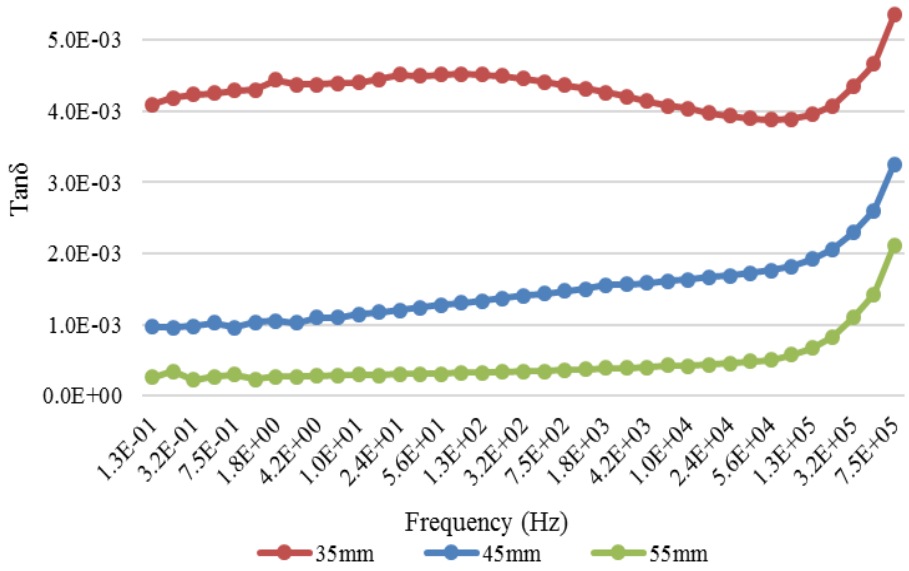

Figure 5.14. Effect of distance of the sample from the target on the loss tangent.

Next task came forward to establish the optimum sputtering intervals. 4 samples were sputtered each side using 3*60s*60s*25mA, 6*30s*30s*25mA, 1*180s*25mA and 2*90s*90s*25mA to make 18mm diameter electrodes using 55mm distance from the target. All the samples were sputtered for 180s in total but having different intervals. The sputtering which has the shortest interval of 30s with 30s of alternate rest intervals has the lowest loss factor value whereas the sputtering which has no rest interval and sputtered for 180s has the maximum loss factor value with a hump as shown in figure 5.15. This proves that sputtering process generates heat and it can be controlled by sputtering in short intervals which reduces the chance of thermal stress build up. One of the important testing factors i.e. thickness of metallization of electrode was also varied by varying the plasma current. The samples were sputtered 3 times each side for 60s of sputtering and 60s of rest with different current levels including 18mA, 20mA, 25mA and 40mA in order to make 18mm diameter electrode with the sputter distance 55mm from the target. The figure 5.16. shows that higher the current lower will be the loss level which is mainly

because of the fact that high current increases metallization thus making better electrodes. But increasing the current level also increases the heating effect to the sample which increases the loss level, thus 25mA is an optimum current level to be used for sputtering as inferred from the tests. According to the formula;

$$d=KIVT \tag{5.6}$$

d is the nominal thickness of the electrode (Å) though in practice thickness found to vary along the electrode, K is the constant according to the metal; for gold, it is 0.17, I is the plasma current (mA), V is the working voltage i.e. 1kV and T is the sputtering time (s)

By changing time or current, the metallization or the thickness of the electrode can be changed. The metallization above 100nm does not make major decrease in loss level. Thus, the optimum thickness value is between 75nm to 100nm. 40mA is not used because the sputtering device doesn't support this current level and needs some special tricks to do sputtering at this level in order to avoid heating and automatic disconnection. Moreover, the sputtering device manufacturer's allowed highest current level is 25mA. The thickness value of 76.5nm is optimum as the difference in the loss level between 76.5nm, 100nm and 122nm is very small and it can be concluded that the saturation level has been reached and further increment in thickness of electrode does not have major impact on the loss level.

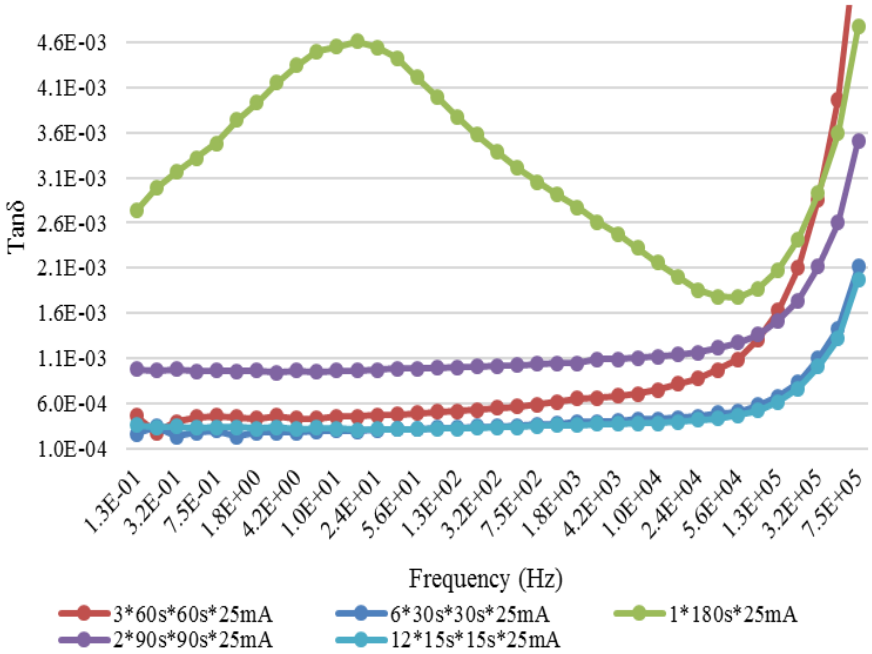

Figure 5.15. Effect of different sputtering intervals on loss level.

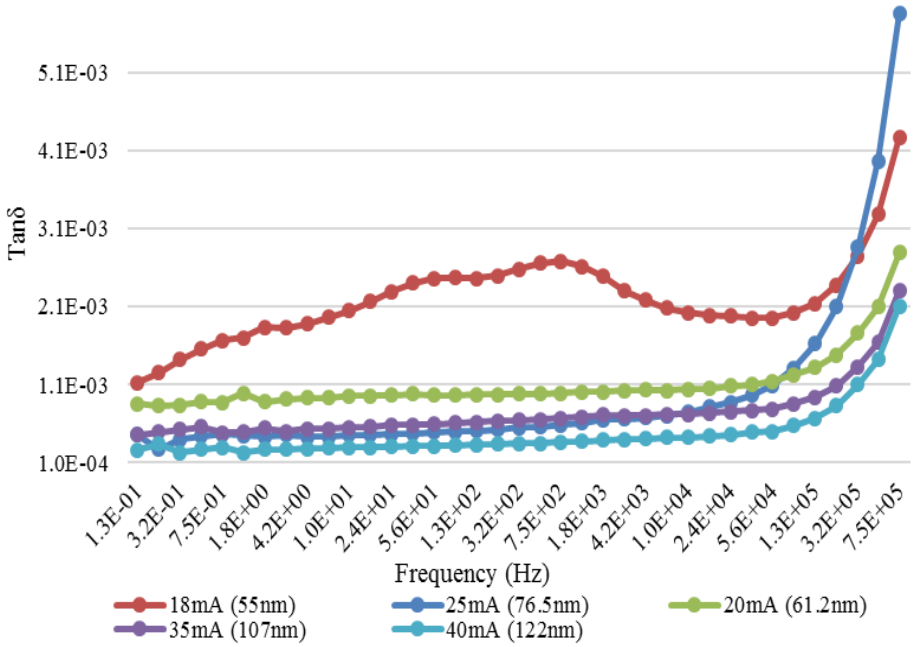

Figure 5.16. Effect of metallization thickness on the loss factor w.r.t frequency.

After all the experiments and results found during experiments it has been finalized that the electrode material used would be 'gold' as gold is the most inert metal and it does not get oxidized and it also sputter maximum number of atoms per ion during sputtering as compared to other metals. Thus evaporation energy required would be minimum[52]. Each sample would be pretreated under vacuum for 24h at 30 to 35°C and then sputtered using the routine of 6×30s×30s×25mA (number of sputtering×sputter time×rest time×current in Amps) with 55mm of sputtering distance. These samples are then used for dielectric spectroscopy through novo control device.

5.4 Reliability Analysis

Every research project needs to establish the validity of its results and experiments, for which reliability analysis is a useful tool for evaluation. Reliability analysis gives a measurement of consistency for a method or procedure applied. However alone reliability analysis cannot give an assurance of valid results. There could be a possibility of getting similar results repeatedly which might deviate from the expected results. Thus, uncertainty should be taken into consideration to analyze this deviation of a measurement or result. This deviation is identified as standard deviation or standard error. Different aspects of statistical reliability have been studied during this thesis using SPSS (Statistical Package for the Social Sciences) software. The samples used for the measurements are pre-vacuumed for 24h at 30°C and sputtered using the sputtering routine of 6*30s*30s*25 mA. The diameter of the sputtered electrode is 18mm with 100nm thickness. The selected material for reliability test is commercial Tervakoski RER film of 14.4µm average thickness. Each measurement set comprised of the loss factor values from 1×10^{-1} Hz to 1×10^{5} Hz.

It has been reported in literature that inherently it is difficult to comment on exact measure of reliability, it can be estimated using four main estimators of reliability analysis which are under consideration during this thesis;

- Test-retest reliability: This form of reliability estimation involves multiple sets of measurements performed by the same rater using the same sample and same instrument. In this thesis, 3 measurements have been taken by one rater using the same sputtered sample.
- Interrater reliability: This form of reliability estimation is done using the same sample and same instrument but different raters. It helps in making a judgement about the capability of raters to make reliable measurements and it also helps in identifying the variance among measurements of different raters. In this thesis, three different raters have made single measurement of the same BOPP sample using Novocontrol device.
- Parallel forms reliability: In this form of reliability estimation, different measurements can be made using different raters or same raters at different times. It helps in analyzing the reliability of measurement or testing procedure over a period. In this thesis, four BOPP samples have been sputtered using the same configuration and measured carefully by one rater in the same way through Novocontrol device. All four measurements in this case were made at different times.
- Internal consistency reliability: This form of reliability estimation can be made using one sample and one measurement set. It measures that how consistent are the results within a test and is termed as Cronbach's alpha. [53], [54]

Table 5.1. gives a summary of all the statistical findings extracted by analyzing the four estimators of reliability through SPSS software. To observe the correlation between different measurements and items of measurements, intraclass correlation (ICC) method has been chosen. This is because if we want to assess interrater reliability of more than two raters ICC makes better reliability estimation because of its flexibility. Pearson correlation on the other hand is valid for an analysis between measurement set of two raters only. In each of the estimations, 3 or more tests are made so ICC is appropriate to be considered. [55], [56]

Starting with interrater reliability, table shows that the mean value (loss factor value) of rater 1 and rater 3 are same whereas the mean value of rater 2 is comparatively low. For interrater reliability, the main concentration should be on single measurement statistics rather than average of all the measurement sets. The mean or average value of rater 1's measurement and rater 3's measurement is higher with higher standard deviation which shows that rater 1 and rater 3 have more variance and dispersion in their measured results as compared to rater 2. Thus, rater 2 has measured the results with more reliability. The average value of ICC is 0.94 with 95% confidence interval of 0.89-0.97 which is under reasonably acceptable limits. Value of ICC above 0.9 is exceptionally desirable as it shows that the selected raters can reproduce similar results. Though the slight difference in variance and inter item correlation among the raters is due to the difference in handling the sample, difference in applied pressure while mounting the sample in Novocontrol

device, difference in measurement of average thickness of the BOPP insulation film etc. Apart from these factors, calibration of Novocontrol device was only done once before the start of this reliability estimation test and not done before every rater's measurement. Moreover, the sample which has been subjected to repeated measurements can possibly have some invisibly small changes in the surface due to its exposure to different hands and environments.

Next reliability estimation is test-retest reliability which is also generally known as intrarater reliability or repeatability. This estimation has been made by one rater using same sample at three different times during the day. Novocontrol device has been calibrated each time before each measurement. Table 5.1. shows the mean value of all three cases, which are approximately the same with case 1, having slightly higher standard deviation and case2 bearing relatively low standard deviation. This shows that case 1 shows more variance in results as compared to case 2 and 3. The average value of ICC is 0.92 with 95% confidence interval of 0.85-0.96 which is under reasonably acceptable limits. Looking at the inter item correlation matrix, the best correlation is between case 1 and case3 whereas the least correlation is between case1 and case2. Despite this difference, all correlations are above 0.7 and are acceptable. Test-retest reliability has been qualified and it identifies that one rater using the same device and sample can reproduce similar results.

Next reliability estimator is parallel forms reliability in which four similar samples were made using the same sputtering routines but during different days. Case 1,2,3 and 4 have been performed on 13/11/2015, 27/11/2015, 31/12/2015 and 19/3/2016 respectively. As a matter of fact, if there is a long interval between two measurements there is always a probability of higher variance in results. Unlike other two reliability estimations, table 5.1. shows that there is higher difference in the mean or average values of all the cases in parallel forms reliability test. Consequently, it also results in highest range among all the tests. Case 1 shows highest mean with highest standard deviation whereas case 3 appears with lowest of all the mean values with relatively smaller deviation which implies that case 1 has more variance in its results as compared to case 3. This reliability estimation came across the maximum and minimum variant results among all the estimations which are not unexpected since all the samples were prepared at different times having different physical conditions. Though careful measures were taken to minimize the effect of physical factors e.g. change in relative humidity (from 80% to 98%), ambient temperatures (0°C to 5°C), different effects of plasma heat on samples, difference in the average thickness values of BOPP film samples, difference in sample mounting pressure, difference in handling the sample with the passage of time, inherent uncertainty in the performance of sputtering device to make electrode and so on. Technically it is impossible to replicate the entire procedure with same precision. Therefore, having a close look on ICC and inter item correlation reveals the extent of reliability. The average value of ICC is 0.96 with confidence interval of 0.93 to 0.98 which is exceptionally good. The intraclass correlation is maximum between case 1 and case 2 and correlation between all items are above 0.8

which clarifies that parallel forms reliability exist in procedure being followed throughout the thesis.

Fourth estimation of reliability can be performed using one test and one sample. It identifies the level of internal consistency between the items of one measurement set. Therefore, internal consistency reliability has been calculated for all the measurement sets used in the other three reliability estimation. It is normally extracted from Cronbach's alpha or coefficient alpha. Cronbach's alpha specifically measures internal consistency of continuously measured variable[55]. The method does not give interpretation of homogeneity but only comments on internal consistency of measurements being made by an instrument. Table 5.1. shows that Cronbach's alpha values for three estimation tests are 0.92, 0.94 and 0.96 which guarantees that measurements made through Novocontrol device are internally consistent using the defined procedure in thesis. Any value of Cronbach's alpha above 0.7 is statistically acceptable.

Table 5.1. Statistics of reliability estimators as extracted from SPSS software.

Statistical Characteristic	Test-retest reliability	Interrater reliability	Parallel forms reliability
Cronbach's Alpha	0.92	0.94	0.96
Cronbach's Alpha (Standardized Items)	0.92	0.98	0.96
Mean of Case 1	5.3E-04	4.7E-04	6.1E-04
Mean of Case 2	5.4E-04	3.9E-04	4.9E-04
Mean of Case 3	5.6E-04	4.7E-04	3.7E-04
Mean of Case 4	N/A	N/A	5.4E-04
Mean of all items	5.4E-04	4.4E-04	5.0E-04
Range of all items	2.1E-05	8.3E-05	1.6E-04
Inter-Item Correlation Mean	0.80	0.94	0.87
ICC (Single Measures)	0.78	0.84	0.85
ICC (Average Measures)	0.92	0.94	0.96
Lower Bound ICC (95% CI)	0.85	0.89	0.93
Upper Bound ICC (95% CI)	0.96	0.97	0.98
Standard Deviation of Case1	8.65E-05	1.01E-04	6.49E-05
Standard Deviation of Case2	5.12E-05	8.36E-05	5.11E-05
Standard Deviation of Case3	6.75E-05	1.55E-04	4.62E-05
Standard Deviation of Case 4	N/A	N/A	4.31E-05
Standard Error Case 1	3.06E-05	1.77E-05	1.13E-05
Standard Error Case 2	1.81E-05	1.46E-05	8.90E-06
Standard Error Case 3	2.39E-05	2.70E-05	8.04E-06
Standard Error Case 4	N/A	N/A	7.50E-06

Table 5.2. Matrices of inter item correlation.

Test-retest reliability

	Case 1	Case 2	Case 3
Case 1	1.000	0.765	0.832
Case 2	0.765	1.000	0.812
Case 3	0.832	0.812	1.000

Interrater reliability

	Rater1	Rater2	Rater3
Rater1	1.000	0.977	0.923
Rater2	0.977	1.000	0.916
Rater3	0.923	0.916	1.000

Parallel forms reliability

	Case 1	Case 2	Case3	Case4
Case 1	1.000	0.999	0.836	0.821
Case 2	0.999	1.000	0.834	0.820
Case3	0.836	0.834	1.000	0.917
Case4	0.821	0.820	0.917	1.000

As discussed before reliability doesn't give an assurance of producing the required results. For example, in this thesis the mean value of loss tangent stays around 5×10^{-5} which is expected to be 1.8×10^{-5} as per the manufacturer's rating. Here comes the concept of uncertainty or standard uncertainty that measures the doubts in a measurement. All uncertainty contributors are standardized at the same confidence intervals and are termed as standard uncertainty. Standard deviation of mean is known as standard uncertainty of mean or standard error. The exact value of standard deviation needs many measurements therefore the estimation of standard deviation has been used. Standard uncertainty can be evaluated as a function of multiple factors for example as a function of temperature, non-ideal repeatability, humidity, calibration etc. This is often termed as combined uncertainty. Some of the possible sources of uncertainty in this thesis could arise from the fact that reliability of sputtering device has not been calculated. Moreover, the reliability of thickness measuring instrument and other small scales used in this entire process of making dielectric measurements has not been reported. Ideally combined reliability of a process should consider the reliability of all the instruments being used. The standard error can be analyzed from table 5.1. which ranges from 1.3×10^{-6} to 7.5×10^{-5} .[57]

5.5 Novocontrol device set up for dielectric spectroscopy

The dielectric samples were subjected to dielectric spectroscopy using Novocontrol Alpha analyzer. The operating principle of measurement can be seen in the figure 5.19.

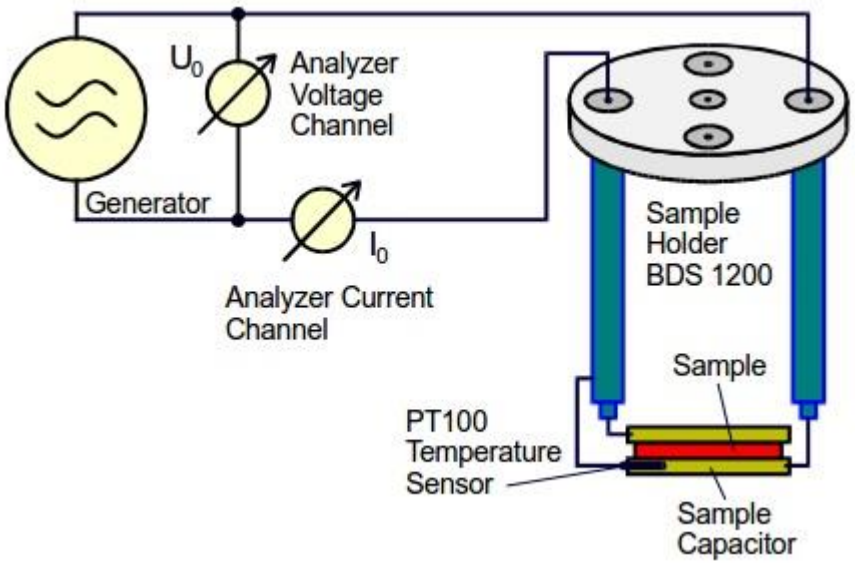

Figure 5.19. Sample arrangement for dielectric spectroscopy[58].

The dielectric film sample is placed in between two gold plated electrodes. A voltage V_0 is applied to the sample which generates the current I_0 with a phase shift θ due to capacitance. The phasor relationships between current and voltage can be represented as follows;

$$V(t) = V_0 \sin(\omega t) = \mathrm{Re}(V^* e^{i\omega t}) \tag{5.7}$$

$$I(t) = I_0 \sin(\omega t + \theta) = \mathrm{Re}(I^* e^{i\omega t}) \tag{5.8}$$

$$V^* = V_0 \tag{5.9}$$

$$I^* = I' + iI'' \tag{5.10}$$

The impedance of the sample dielectric can be written as;

$$Z^* = Z' + iZ'' = \frac{V^*}{I^*} \tag{5.12}$$

The permittivity can be calculated as;

$$\varepsilon^* = \varepsilon' - i\varepsilon'' = \frac{-i}{\omega Z^* C_0} \tag{5.13}$$

Equation are referred from Novocontrol manual [58]

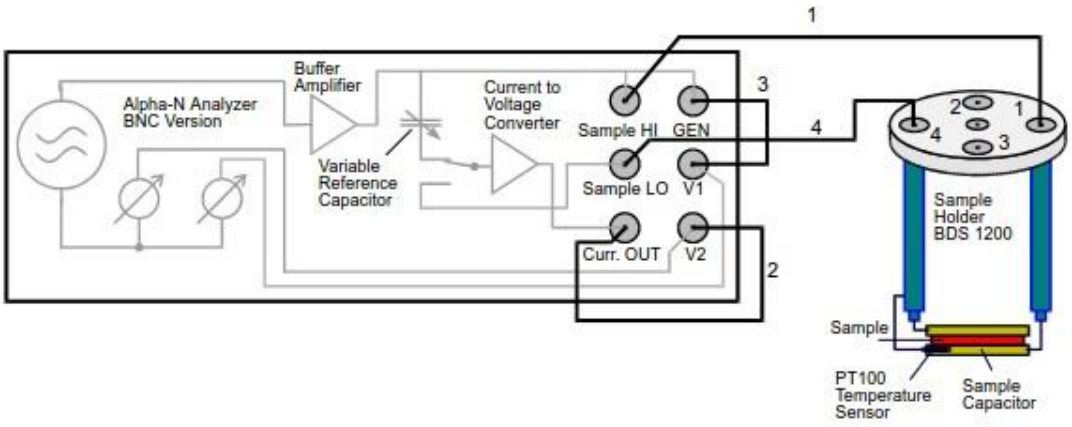

Figure 5.20. Setup for measurement of dielectric material with alpha analyzer[58].

The sample cell consists of two parallel electrodes. This setup is calibrated by using calibrate all option every time before measurement. Capacitance, dielectric loss tangent, permittivity and impedance measurements can be made using this setup. The alpha analyzer can be made up of two sections one is the frequency analyzer with dc biased generator and the other one is an impedance converter. There could be two configurations e.g., two wire and 4 wire set up. The alpha analyzer is used to measure conductivity, impedance, loss factor and permittivity of low loss capacitors with high precision and better optimization. The frequency range it supports is 3µHz to 20MHz and tanδ range is from 10^{-5} to 10^{4}. A temperature sensor Pt100 is used when making measurements between -100°C to 250°C. Temperature measurements are made with using a special temperature cell with nitrogen tank. The nitrogen is heated from the liquid form using a heater in order to maintain the temperature of the experiment. The dewar pressure controller helps in maintain the pressure near the set point[59]. For high field measurements the alpha analyzer is used with high voltage amplifier Vp= ±2000V.[58]

6. INTERPRETATION OF EXPERIMENTS

The polypropylene materials used in this research are commercial BOPP Tervakoski RER film, BOPP pilot scale nanocomposite (NPO30) and its unfilled reference BOPP film (NPO49). The comparison of nanocomposite and its base polymer has been made for different physical properties. The pilot scale film is prepared using materials polypropylene HC318BF. Irganox 1010 is used as a process stabilizer together with Irgafos 168 as a co-stabilizer to the ratio of 0.47% to 0.35% by weight. These stabilizers act as antioxidants and protect the polypropylene from oxidative degradation. The filler used in the compounds to make nanocomposite is Aerosil R812S. The filler percentage added to the base polymer to produce NPO30 nanocomposite film is 4.5wt-% but there is some loss of silica during process and the actual silica percentage found to be 3.56wt-%. Silica and polypropylene powders are mixed in a drum mixer using a plastic bag for 4mins. To avoid clusters of large particles, the silica powder is pre-heated in oven at 70˚C for 30mins to remove any moisture from hydrophobic silica and the mixture of silica and polypropylene is also dried under vacuum. The compounder used in the mixing process is the high speed screw compounder (Berstorff). The compound is then bi-axially stretched at 155˚C into thin film. The film thickness is between 14 to 17µm.

Each of the considered film are then prepared as samples for dielectric spectroscopy. Film samples of RER, NPO30 and NPO49 are cleaned with isopropanol and then measured for their thickness values. The average thickness of RER, RERT, NPO30 and NPO49 film samples are found to be approximately 14.4µm, 10µm, 14.7µm and 15µm respectively. All the samples are then dried under vacuum for 24h at 30˚C. These film samples are then sputtered using SC7620 mini sputter coater to make gold electrodes of 100nm thickness. The diameter of electrodes for water immersion tests is 18mm whereas the diameter of electrodes for temperature and field related tests is 10mm. The dielectric response is recorded using novocontrol device by placing the film electrodes between two gold plated electrodes of sample container with upper electrode of 10mm diameter and base electrode of 30mm. The reason of using smaller diameter of sputtered electrode for temperature and field related tests is to avoid any stray capacitance and field stress on the edges of electrodes. An ac voltage of 1V is applied and the frequency range of 10^{5}Hz to 10^{-1}Hz is used to analyze dielectric behavior.

In this chapter, first the effect of water immersion and ambient humidity are studied. For this test the samples are immersed in distilled water for immersion test whereas in the ambient humidity test the film samples are placed in a container for a certain defined time. Each of the dielectric spectroscopy session takes around 12min to measure loss factor and relative permittivity w.r.t frequency from 10^{6}Hz to 10^{-1}Hz. The next section of this chapter involves the study of dielectric behavior as a function of temperature. In this test,

thin film samples are placed in a sample cell attached with a nitrogen tank utilized to maintain certain temperature during spectroscopy. The temperatures are applied from -60°C to 130°C in steps of +10°C. Each spectroscopy session during the temperature test takes around 48min to measure loss factor and relative permittivity w.r.t frequency from 10^6Hz to 10^{-2}Hz. The last section of this chapter is related to the study of dielectric behavior as a function of applied field. The spectroscopy tests are made at different field strengths that are 98 MV/m, 77 MV/m, 56 MV/m, 35 MV/m, 14 MV/m, 7 MV/m, 3.5 MV/m and 0.7 MV/m. Each spectroscopy session lasts for 12min approx. for the frequency range of 10^6 Hz to 10^{-1} Hz.

6.1 Water absorption in water immersion

Recent advancement has proved that nanocomposites have made many potential improvements in the field of electrical insulation as well as developed optimum mechanical and chemical properties including improved dielectric breakdown, improved partial discharge resistance, decrease space charge formation, reduced dielectric loss etc. as discussed in chapter 4. But still there are many uncertainties that need to be clarified and strictly observed. It has also been observed that nanocomposites can absorb more moisture as compared to unfilled polymer or its microcomposite when exposed to humid environment. This is because of the formation of nanofiller/matrix interface which act as a host in accumulation of water molecules. Water absorption deteriorates the electrical and mechanical properties of dielectric nanocomposites. Zhao et al. [60] has observed that in epoxy nanosilica composite the dielectric constant increases and the overall mechanical and electrical properties degrade. The percentage of nanofiller clearly affects the water absorption behavior of the nanocomposites.

Certain physical conditions also enhance the adverse effects of water absorption on nanocomposites. Rowe et al. [3] describes for silica filled epoxy nanocomposites that nanocomposites have irreversible detrimental effects on exposure to humid environment at elevated temperatures. It results in chemical degradation and expansion of void and cracks formation in the polymer matrix. The absorption of water has already been described using the basic water shell model in chapter 4 which discusses that water molecules form a strongly bounded layer with nanofiller, and a second loosely bounded layer based on Van der Waals forces and third layer is the dispersion of water in the polymer matrix. The distance between nanoparticles is around few nanometers and thus with the absorption of water the water layers of neighboring nanoparticles may overlap and provide a path for charges and thus QDC behavior occurs at low frequency region.

K Y Lau et al. [33] found while working on polyethylene silica nanocomposite that addition of untreated nanofiller has higher water absorption as compared to the addition of treated nanofiller in the hydrophobic base polymer. Both loss factor and dielectric constant has higher values for untreated nanosilica. Untreated nanosilica surface has hydroxyl

groups which on treatment with silane coupling agent hydrolyze to –OH group forming silanol. In this thesis treated hydrophobic silica is used as nanofiller.

In order to figure out the behavior of BOPP and its nanocomposites, the film samples are immersed in distilled water for different time durations and then subjected to two different types of immersion tests. These are pre and post immersion tests. In pre immersion test the electrodes are made after immersing the polymer samples in distilled water for a certain defined time and in post immersion test the electrodes are made before immersing the samples in distilled water. The reason of using these two different ways of immersion test is to check the effect and validity of immersion test.

The dielectric spectroscopy results during this thesis have revealed that pure BOPP is hydrophobic in nature and it will not adsorb moisture or high amounts of water during water immersion. No major increase in the loss factor and permittivity was seen during the water immersion experiment as shown in figure 6.1. (a) & (b) and 6.2 (a) & (b). The increase in loss factor at 50Hz from day 0 to day 21 of immersion in case of pure BOPP is 5.46 times and 3.48 times for NPO49 and RER samples respectively whereas the percentage increase in permittivity is 8% and 5% respectively. The loss factor values are still in an acceptable range even after the slight increments. The loss factor in case of BOPP nanocomposite NPO30 is almost in the same range as that of pure BOPP but there is a movement of relaxation peaks from medium frequency towards higher frequency with the increase in water absorption as shown in the figure 6.3. (a). Moreover, there is a slight increase in the loss level in lower frequency range. The average increase in loss factor at 50Hz from day 0 to day 21 is 1.94times for NPO30 which is also slightly less than that of the increase in pure BOPP. The overall loss level on day 21 is still in the acceptable range but with a relaxation peak between 1Hz to 1kHz where the loss level is relatively very high that is 3.11×10^{-4}. The reason of higher loss level at very high frequencies in all the experiments have already been discussed in the beginning of chapter5.

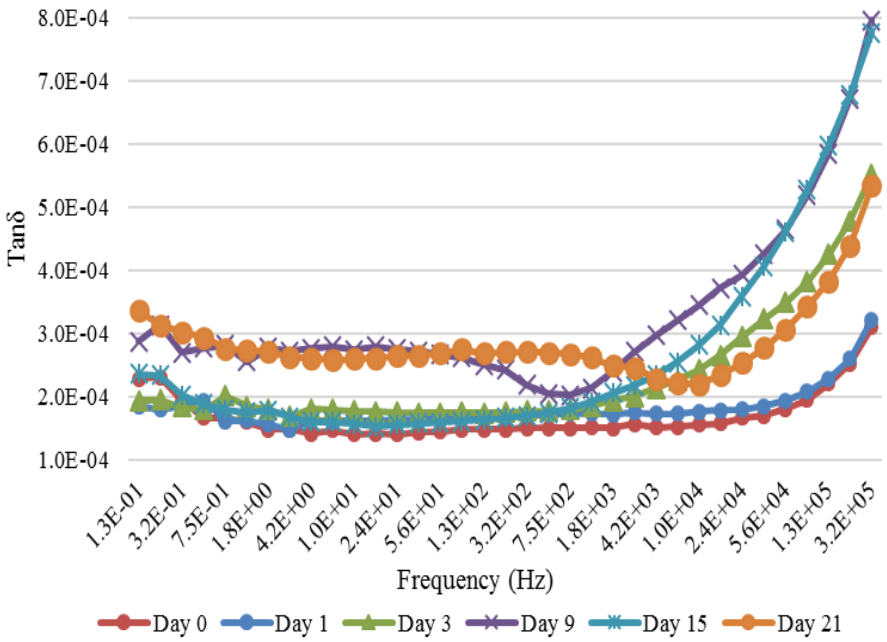

Figure 6.1. (a) loss factor of reference unfilled BOPP film, NPO49

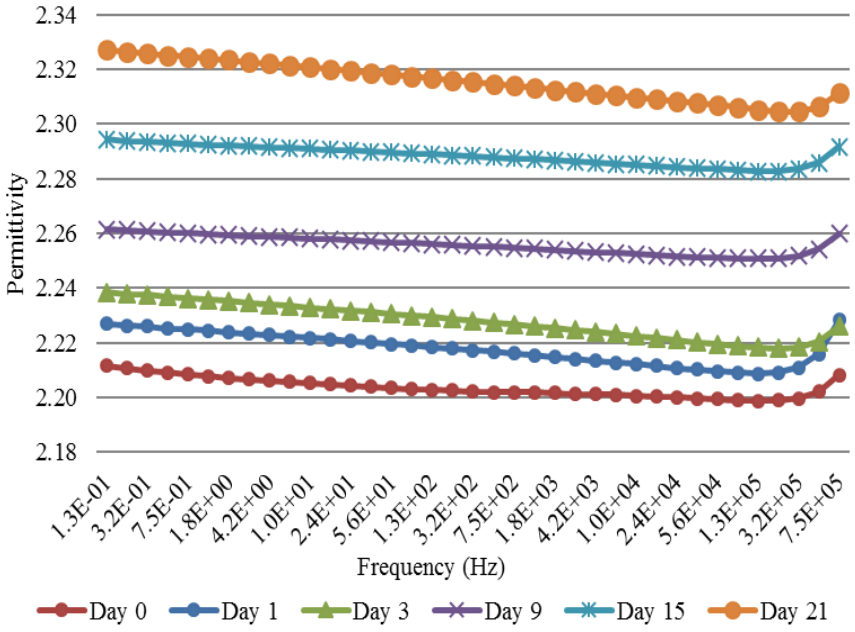

Figure 6.1. (b) permittivity of reference unfilled BOPP film, NPO49

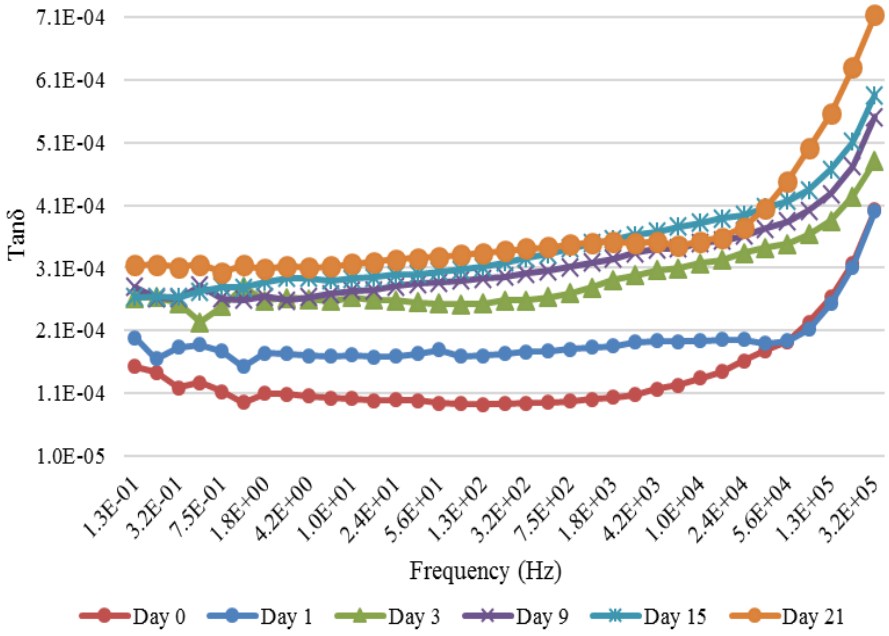

Figure 6.2. (a) loss factor w.r.t frequency of commercial unfilled BOPP film, RER.

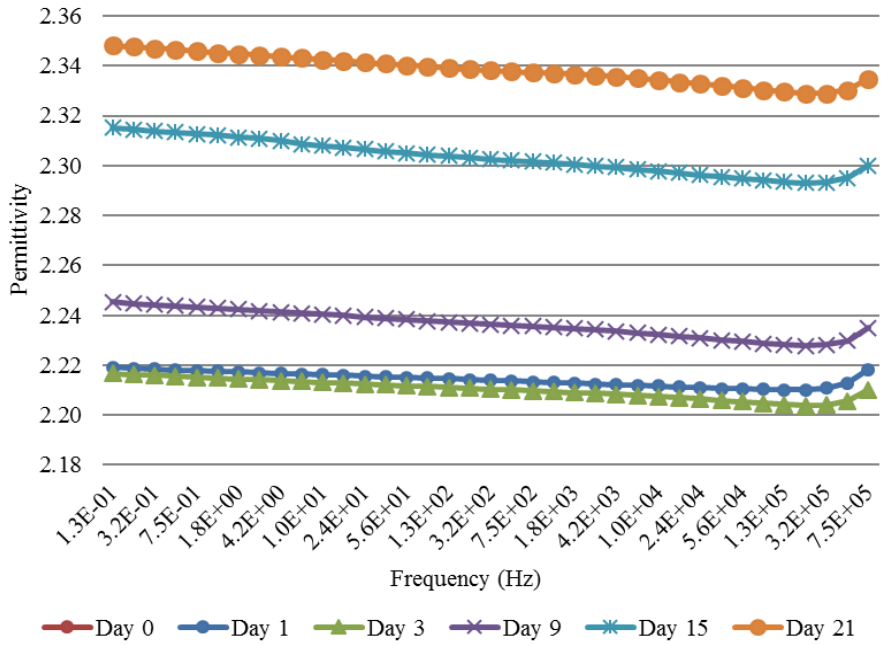

Figure 6.2. (b) relative permittivity w.r.t frequency of commercial unfilled BOPP film, RER.

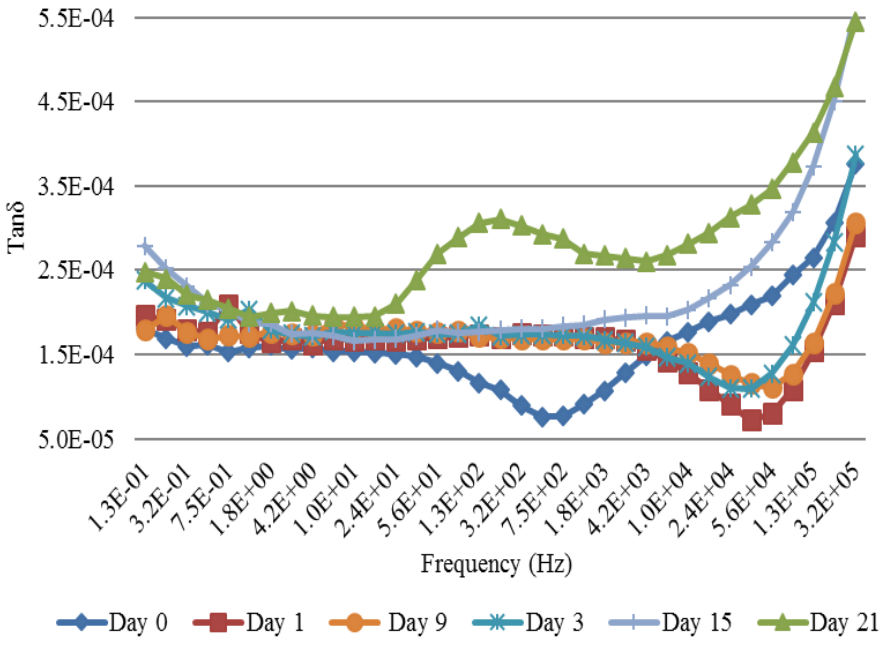

Figure 6.3. (a) loss factor w.r.t frequency of BOPP nanocomposite film, NPO30.

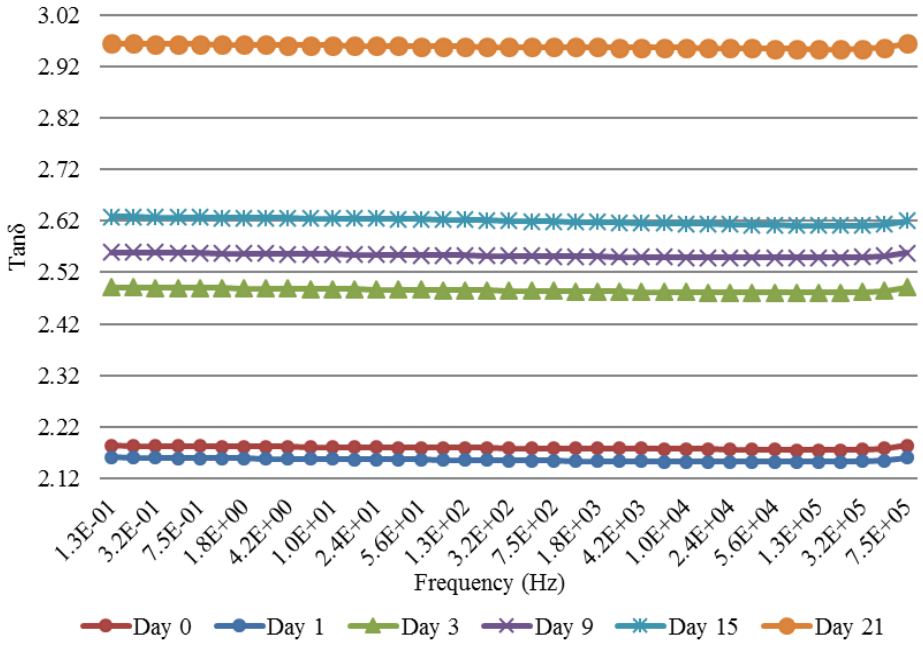

Figure 6.3. (b)relative permittivity w.r.t frequency of BOPP nanocomposite film, NPO30.

The water shell model discussed earlier is good to explain QDC behavior at lower frequency range which corresponds to the increase in loss level under low frequency in case of NPO30 nanocomposite. Since the nanocomposite particles surrounded by some water molecule layers which overlap with the neighboring particle layer and thus provides a

channel for charge carriers. But this model is no more popular but still explains the basic concepts. The movement of dip in case of NPO30 from medium frequency to the higher frequency is due to the presence of multiple layers of water. Figure 6.3 (a) shows that there is a dip in the medium frequency range at day 0 which moves towards higher frequency gradually with the increase in the number of days of immersion whereas on day 15, the curve has no more dips or peaks as it has moved to very high frequency which is not under observation due to equipment limitations. On day 21 a second peak appears the medium frequency range. These movements of peaks and dips is because of different layers of water. Rowe et al. [3] and K Y Lau et al. [33] have mentioned primary, secondary and tertiary layers of water. Primary layer is a strongly bonded layer of water molecules with the nanoparticle because of strong bonding with the hydroxyl ion. This layer exists in untreated nanosilica composites and corresponds to increase in very high loss level. But in this thesis treated hydrophobic nanosilica has been used and this is the reason of overall similar loss range for pure BOPP and its nanocomposite. Secondary layer is the loosely bounded layer because of Van der Waal forces which is mainly related to the peak or dip in the medium frequency range whereas the tertiary layer of water is bonded loosely with secondary layer and is responsible for the movement of dip towards the higher frequency. The extent of the formation of primary secondary and tertiary layers are dependent on the duration of immersion, surface treatment and also temperature. The nanofiller-matrix interface is the potential area of water absorption therefore the surface treatment of nanofillers significantly affect the water absorption. K Y Lau et al. [33] reported a great increase in overall loss level for untreated nanosilica with wider peaks which we did not observe in our NPO30. Moreover, Lau has mentioned a second loss peak on day 14 whereas the secondary peak appeared in NPO30 after day 21. The surface treatment improves the dispersion of silica in a polymer matrix and alters the absorption process. The increase in the permittivity is due to the –OH (hydroxyl groups) or dipoles which conducts readily when an electric field is applied. Though the silica used in BOPP is hydrophobic but still the presence of some hydroxyl ions in the functional groups couples with water molecules resulting in hydrogen bonding and causes affinity of the nanocomposite towards water absorption. The introduction of polar water molecules in non-polar polymer matrix may lead to the increment in permittivity as water molecules can conduct on the application of field[61]. The increase in permittivity though does not show a linear increment with water absorption.

6.1.1 Immersion after sputtering the electrodes

Since the sputtering process introduces extended heat and plasma treatment on the samples which may affect the moisture content of samples, some further tests were made in order to evaluate this effect. Therefore, each sample is sputtered after vacuum treatment with 18mm diameter gold electrode on both sides and then immersed in deionized water for 21 days. These samples are removed from water and left in air for 4h to get dried and then blow dried with nitrogen gas before spectroscopy. Figure 6.6. represents the results

of no immersion, pre immersion (immersion before sputtering) for 21 days and post immersion for 21 days' tests of NPO30. It can be observed that NPO30 has a peak in the middle frequency for pre immersion test as discussed before in section 6.2 which is an evidence of formation of loosely bound water layer around polymer molecule. But the loss factor curve for post immersion for NPO30 nanocomposite is very high in magnitude at frequency below 1kHz with the same curve shape as in case of no immersion. In other words, this increase in loss level might not be because of water absorption inside the polymer as there is no shift in the peaks and dips in the loss factor curve. Rather this could be a resultant of water or moisture layer forming a local conducting path over and under the electrode and there probably exists some interfacial polarization with corresponding losses. In addition, even some dc current flowing through the outer layer or surface of the dielectric sample may exist. Thus, post immersion probably is not the right way to do immersion test as the already sputtered electrode metal shields the moisture from absorbing inside the polymer and the reason of higher loss factor might be because of the before mentioned reasons. Therefore, we performed the humidity and moisture test by immersing the samples before sputtering the electrode. Though there could be a factor of escape of some absorbed moisture due to plasma heat during sputtering but we tried our best to reduce that factor by using the best possible sputtering routine.

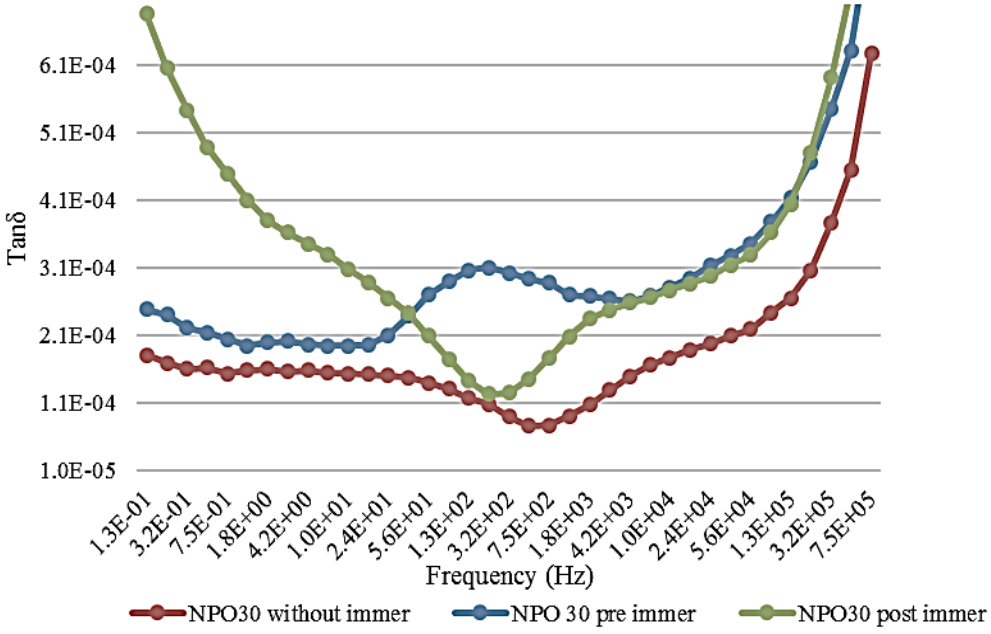

Figure 6.6. Loss factor w.r.t frequency of NPO30 without immersion, with pre immersion and with post immersion.

6.2 Effect of different ambient humidity levels on dielectric response

In order to check the behavior of BOPP and its nanocomposites under humid conditions, absolute humidity test in water immersion is not enough. Thus, different ambient humidity conditions were provided in which the materials were tested for dielectric permittivity and loss tangent. The materials were tested in the following ambient conditions:

- 0% RH: Samples were cleaned with isopropanol and then placed in a vacuum container for 24h under the maintained temperature of 30˚C.
- 33% RH: Samples were cleaned with isopropanol and then placed in a vacuum container for 24h under the maintained temperature of 30˚C. These samples were then placed in a container maintained with 33% RH using saturated $MgCl_2$ solution at room temperature for 2 months.
- 75% RH: Samples were cleaned with isopropanol and then placed in a vacuum container for 24h under the maintained temperature of 30˚C. These samples were then placed in a container maintained with 75% RH using saturated *NaCl* solution at room temperature for 2 months.
- 100% RH: Samples were cleaned with isopropanol and then placed in a vacuum container for 24h under the maintained temperature of 30˚C. These samples were placed in a container filled with deionized water for 30 days at room temperature.

The results from dielectric spectroscopy reveal that as the level of relative humidity increases, the loss factor varies and show a different behavior whereas the overall relative permittivity also increases with the increase in humidity as shown in the figure 6.5. Moreover, the increase in permittivity in case nanocomposite NPO30 is greater as compared to unfilled BOPP, NPO49. The reason behind theses dielectric changes might exist in the fact that water molecules help in forming more dipole moments which react to the applied field and increase permittivity. Figure 6.4. (b) shows that pure BOPP has no big variation in loss factor with the increase in humidity. The 33% RH curve shows a dip in the middle frequency. Also 75% RH curve has the same loss level in middle and low frequency region but high in high frequency region. 100% RH curve has an overall increase in the loss level with a dip. Now in comparison to pure BOPP, NPO30 has a dip at 0% RH as shown in the figure 6.4. (a) which moves towards higher frequency at 75% RH. This is due to the water absorption to make a loosely bound layer which moves the dip or peak towards the higher frequency. Since the nanosilica is surface treated and there are very few hydroxyl groups and thus the effect of water absorption is very marginal. The loss factor curve at 33% RH shows higher loss in the low frequency region which corresponds to Quasi (QDC) current. Since 33% RH can only lead to the formation bound layer as the samples of NPO30 are surface treated and thus the curve shows the QDC current in the low frequency with no peaks due to charges moving through the water layers. 75% RH is high enough to form loosely bound layer as well to generate peaks or dip. A 100% RH,

the loosely bound layers increase and the dip shifts completely towards high frequency resulting in the peak generation in the intermediate frequency. With the increasing humidity level, the activation energy for relaxation decreases and the barrier becomes thinner to let the charges jump over. Free volume for composites are higher and they absorb more water. [62][63][64]

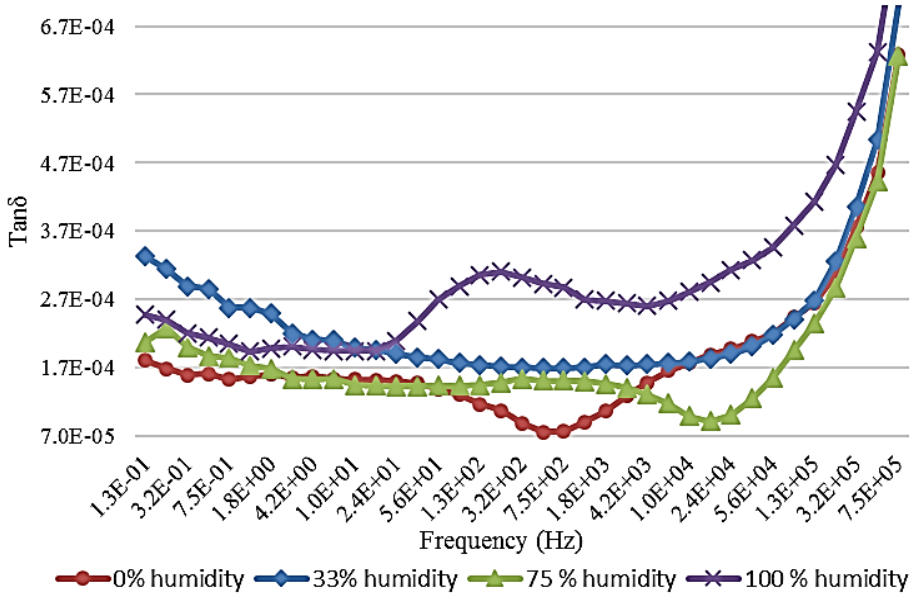

Figure 6.4 (a) loss factor of BOPP nanocomposite NPO30 w.r.t frequency under different humidity conditions.

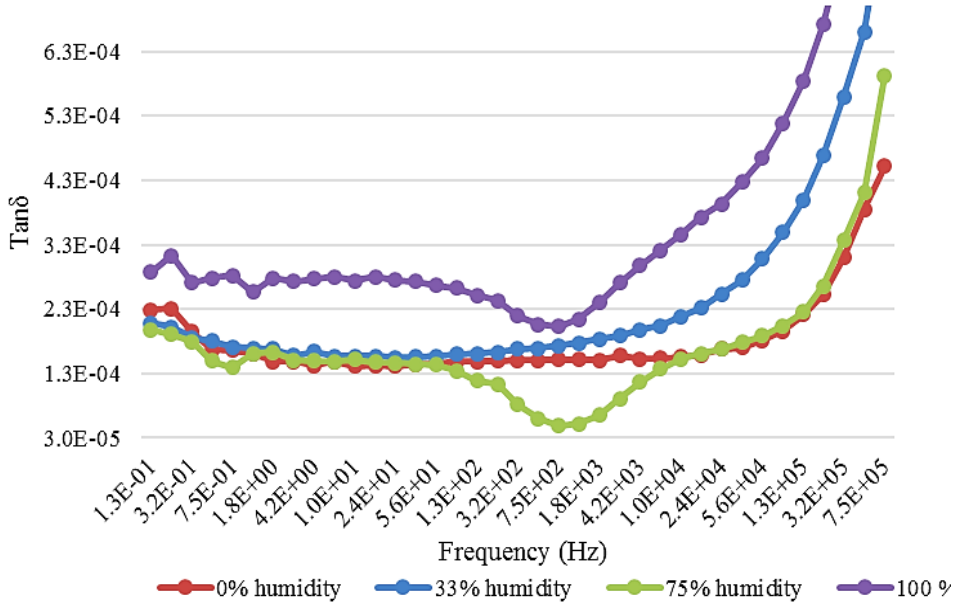

Figure 6.4(b) loss factor of unfilled reference BOPP, NPO49 w.r.t frequency under different humidity conditions.

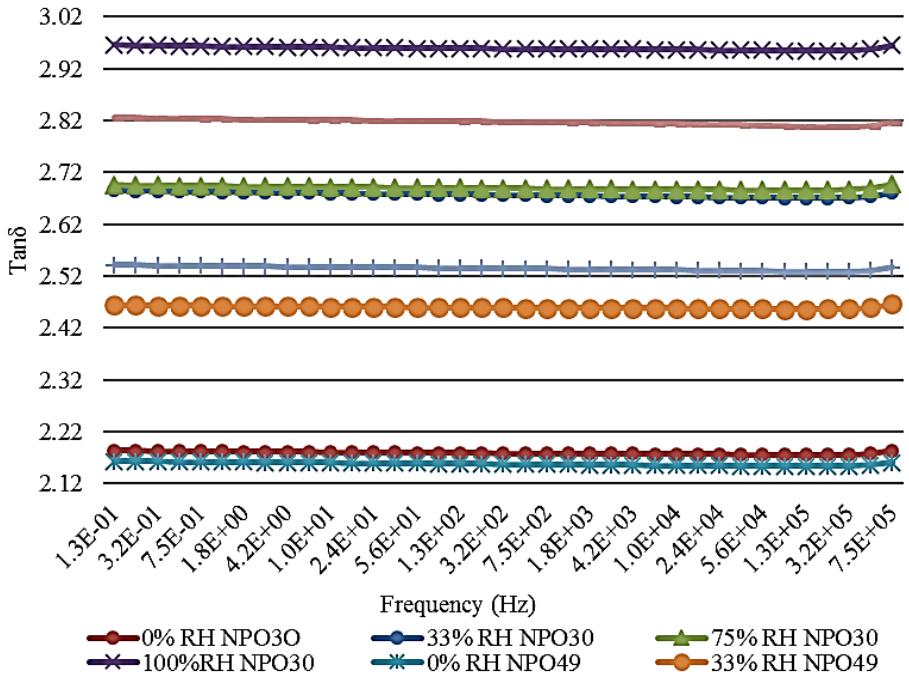

Figure 6.5. Relative permittivity of unfilled reference BOPP, NPO49 and its nanocomposite, NPO30 w.r.t frequency under different humidity conditions.

In order to verify the reliability and repeatability of results, two samples of each material were made and subjected to the similar humidity conditions and then sputtered in the similar routine and carefully tested for dielectric spectroscopy.

6.3 Dielectric behavior of BOPP film at different temperatures as a function of frequency

Since BOPP films are used in capacitors for high voltage applications thus the conduction and dielectric properties of BOPP under high voltage is required to be analyzed both as a function of frequency and temperature. Temperature and frequency has a significant effect on the dielectric behavior of polymers but still there are many ambiguities in defining the exact behavior. In this thesis relaxation mechanism and structural change of polymer will be discussed. Four different films were used in this analysis including Tervakoski RER (14.4µm thickness), RERT (10µm thickness), NPO30 silica filled nanocomposite (14.7µm thickness), NPO49 reference BOPP (15µm thickness). These film samples were sputtered with 100µm thickness and 12mm diameter gold electrodes using SC7620 mini sputter coater. These samples were then subjected to dielectric spectroscopy. In this section the samples are subjected to dielectric spectroscopy using novo control device with temperature control system as discussed in chapter 5. The temperatures are provided from -60° to 130°C. Each of the temperature level applied to the sample had a duration of 36min.

Figure 6.7 (a), (b) and (c) represents the behavior of loss factor w.r.t frequency over a temperature range of -60˚C to 130˚C. It has been observed that the loss level is quite low in overall in the medium and low frequency range at -60˚C but the overall loss factor increases from -60˚C to 50˚C. From 30˚C and above, the loss factor increases more in the low frequency range. Above 50˚C, the loss factor starts decreasing in the mid to high frequency region and thus gives evidence of thermal stability of capacitors under high temperature. But the loss factor increases more and more as the frequency decreases in the low frequency region. At elevated temperatures near and above the maximum possible operating, this might even be because of some ionic conduction. Further the loss factor increases exponentially more above 90˚C w.r.t the temperature which shows the phase change and polarization effect. At higher frequencies, the loss factor of NPO30 at 130˚C is below the loss factor at -60˚C till 50Hz but below 50Hz it increases exponentially but this is not the operating temperature of BOPP. The maximum allowed operating temperature in case of BOPP is 105°C which can be verified also from the dielectric spectroscopy results as in all the figures, the loss factor exponentially increases above approx. 100°C. Whereas the loss factor at 90˚C for 50Hz is approx. the same as that at 20˚C but below 1Hz the loss factor increases gradually to the loss factor of 7×10^{-3}. Thus, the operation of capacitors below 90˚C is thermally stable.

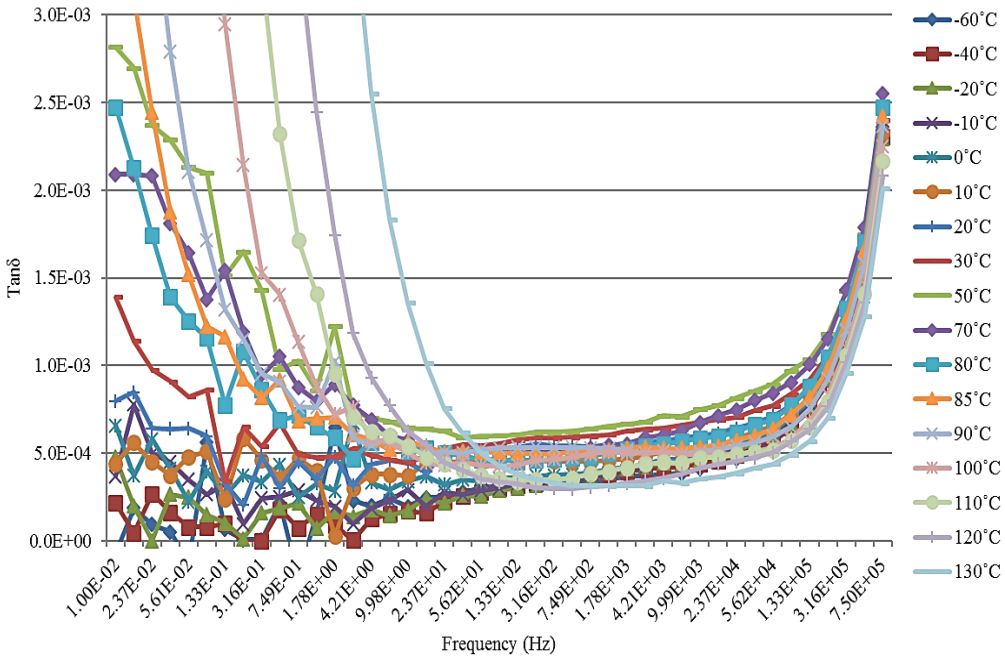

Figure 6.7 (a) Loss factor w.r.t frequency at different temperatures of NPO30 nanocomposite.

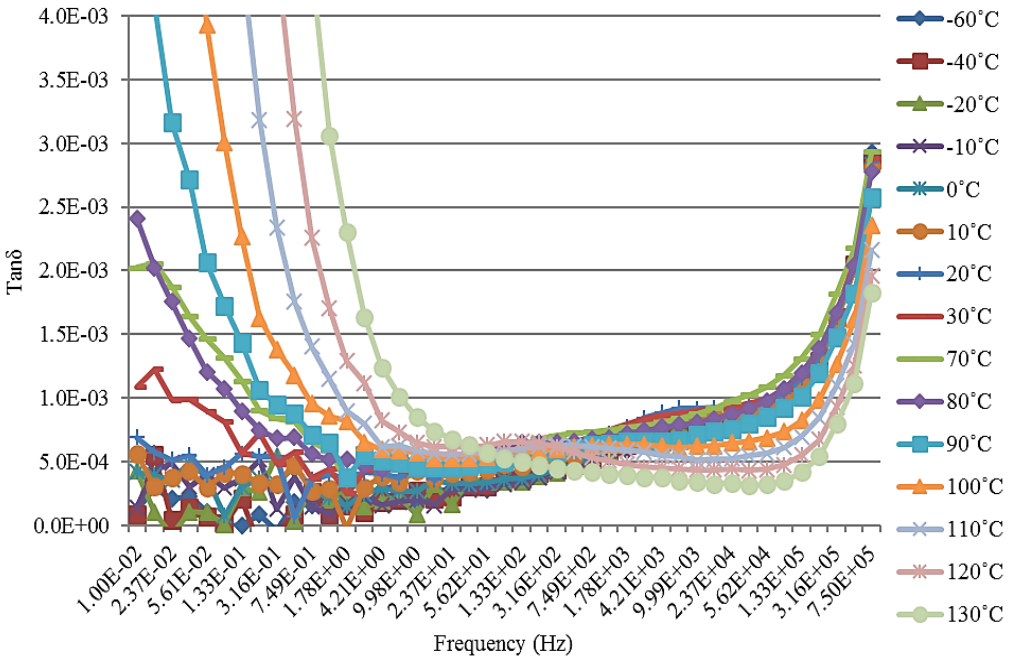

Figure 6.7 (b) Loss factor w.r.t frequency at different temperatures of NPO49 reference BOPP.

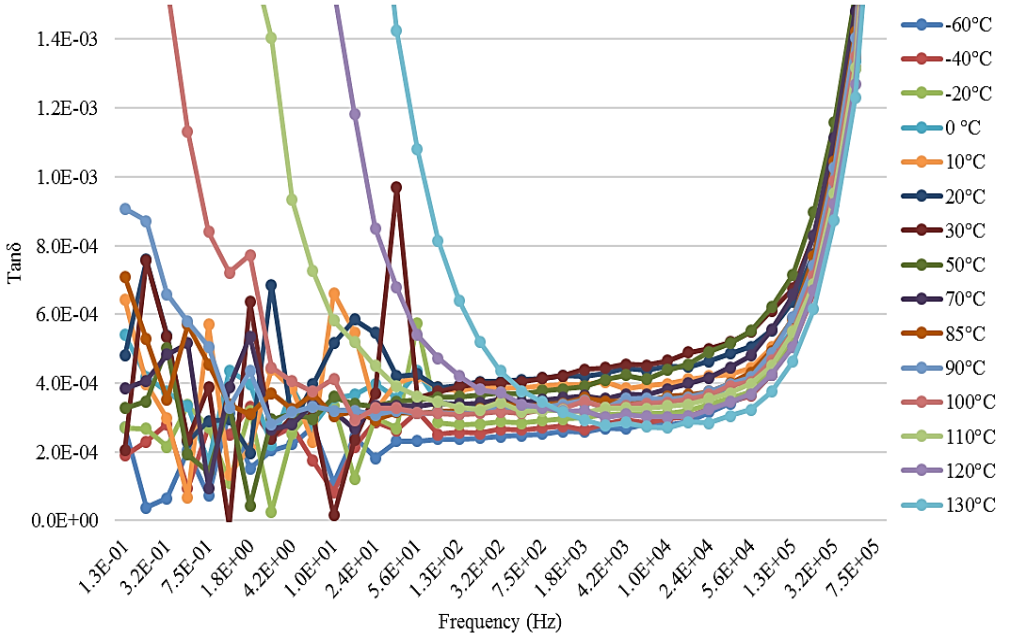

Figure 6.7 (c) Loss factor w.r.t frequency at different temperatures of RER reference BOPP.

Figure 6.8 (a) and (b) shows that permittivity is stable over a wide frequency range till 90˚C and there is a slight decrease of permittivity from -60˚C to 90˚C that is from 2.59 to 2.47. Moreover, there is a gradual overall decrease in permittivity as the temperature increases. This could be because of thermal expansion which could be a source of error to

the expected dielectric behavior. In addition, as the temperature increases it becomes more easy for the different polarization phenomena to occur and thus on the application of electric field permittivity increases.

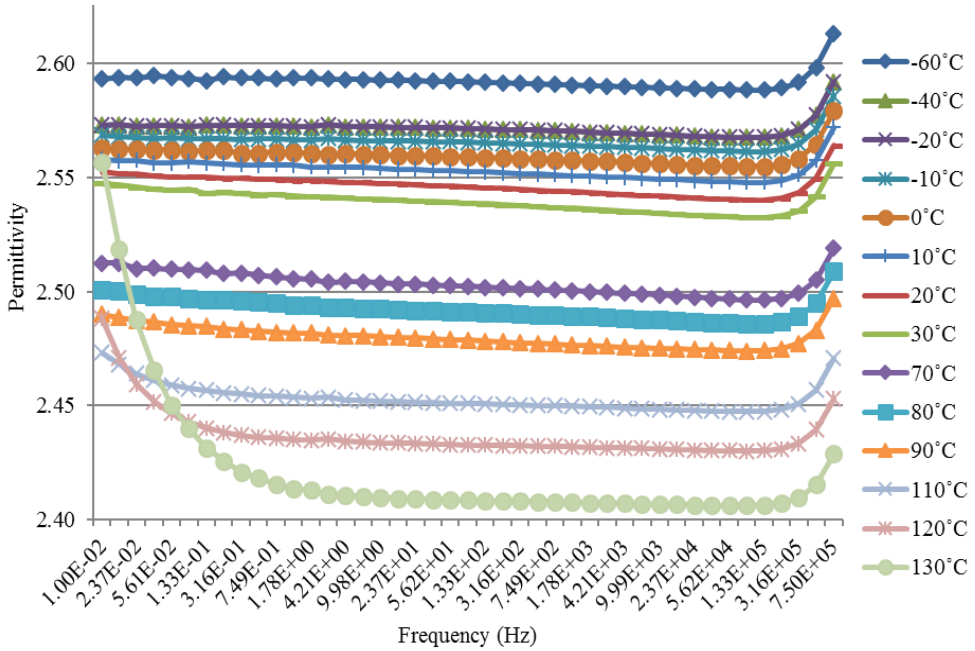

Figure: 6.8 (a) Relative permittivity w.r.t frequency of NPO30 nanocomposite.

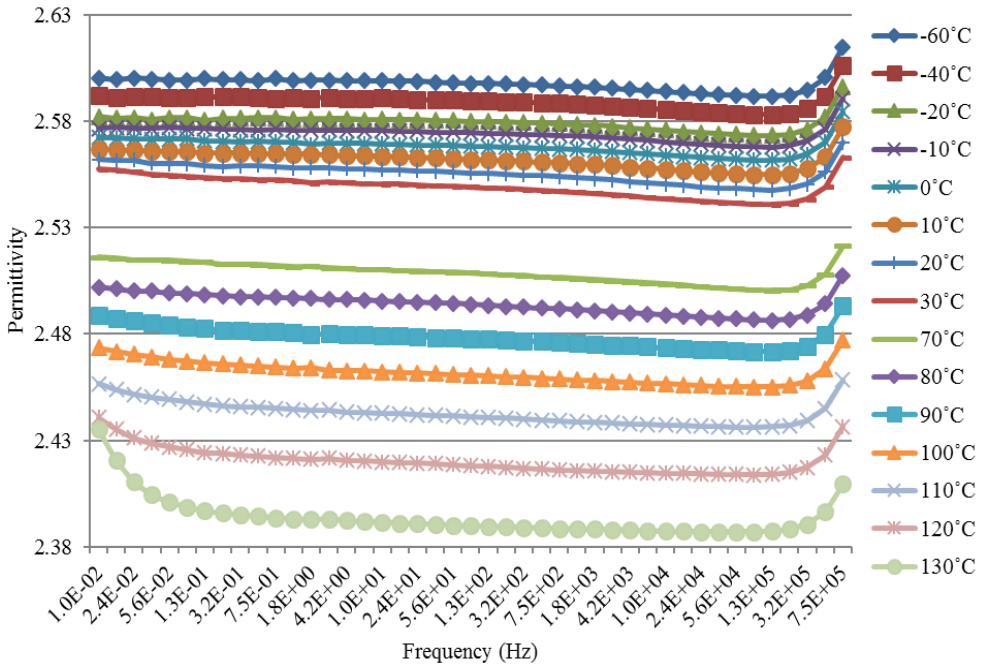

Figure: 6.8 (b) Relative permittivity w.r.t frequency of NPO49 reference BOPP.

6.4 Dielectric behavior of BOPP film as a function of temperature

In this section the samples are subjected to dielectric spectroscopy using novo control device with temperature control system as discussed in chapter 5. The temperatures are provided from -60° to 130°C. The temperature starts from -60°C and gradually increases in steps to 130°C. Figure 6.9. shows dielectric loss as a function of temperature from -60˚C to 130˚C at frequencies of 9992.4 Hz, 1153.6 Hz, 133.19 Hz, 9.9848 Hz, 1.1527 Hz, 0.13309 Hz, and 0.086419 Hz. It has been observed for NPO30 nanocomposite that an α–relaxation appears in high temperature range between -10˚C to 90˚C and the peak appears at 50˚C with the loss factor of 7.5×10^{-4} for 9992.4Hz. As the frequency increases and the magnitude of the peak reduces in the frequency range of 9992.4 Hz to 9.9848Hz and this peak gradually increase in magnitude after this frequency. Moreover, with increase in frequency the peak shifts towards right (Higher temperature) and α-peak breaks into two parts one very small peak at very high temperature and the major portion of big peak but the overall width of the peak remains same till the disappearance α-peak extension. This movement of the peak towards higher temperature is an evidence of higher interaction between the polymer chains [53]. This very small peak disappears below 10Hz and the α-peak's width shrink from 20˚C to 70˚C whereas an ionic conduction probably starts at very high temperatures for frequencies below 1Hz. Whereas figure 6.10 shows that the overall loss level is higher for NPO49 for all frequencies and the peak is not properly defined with a hint of emergence of beta peak. As the frequency increases the peak shrinks for NPO49. Since NPO30 is a nanocomposite and it has different morphology as compared to pure BOPP because of polymer nanocomposite interface. Thus, the alpha peak which is due to the movement of main chain is more prominent but the overall loss level and magnitude of the peak is low due to homogenous charge distribution as discussed in Chapter 4.

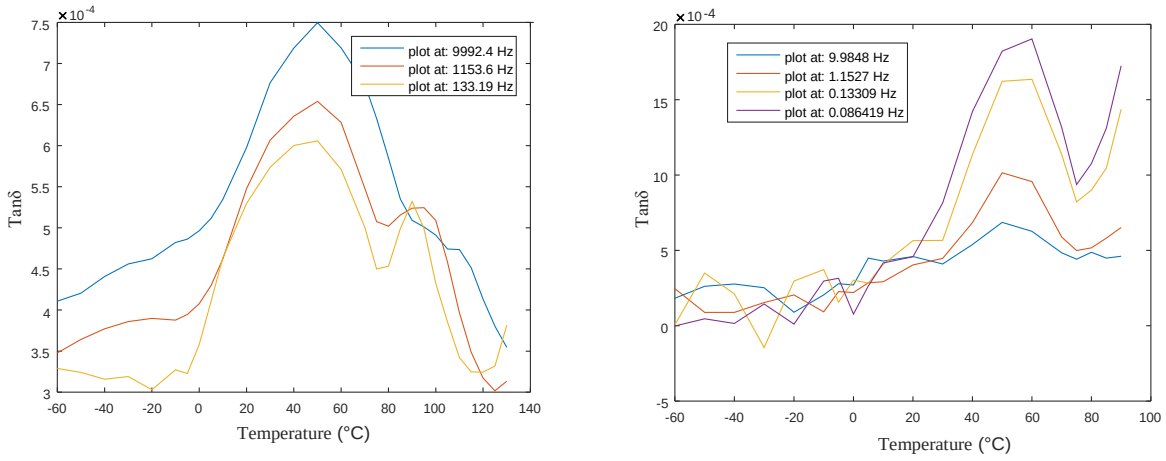

Figure 6.9. Dielectric loss w.r.t temperature at various frequencies; higher frequencies (left) lower frequencies (right) of NPO30.

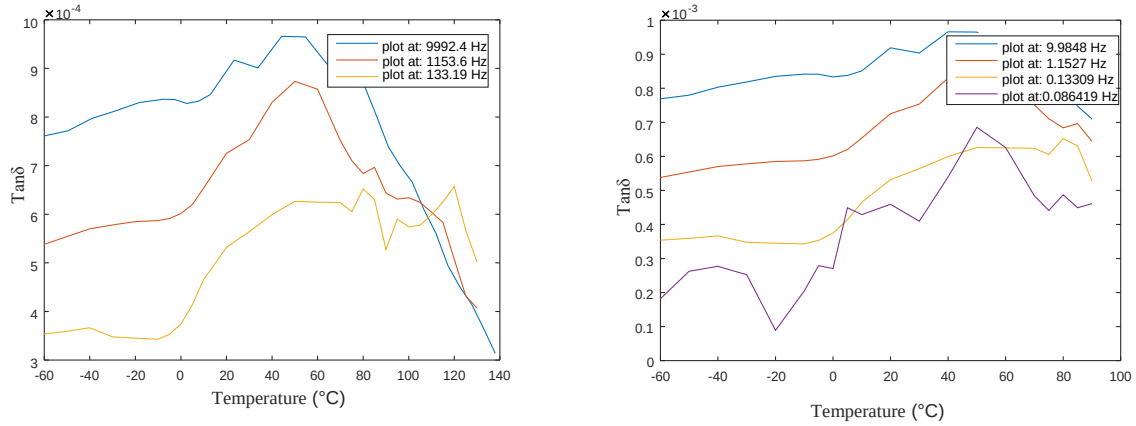

Figure 6.10. Dielectric loss w.r.t temperature at various frequencies; higher frequencies (left) lower frequencies (right) of NPO49.

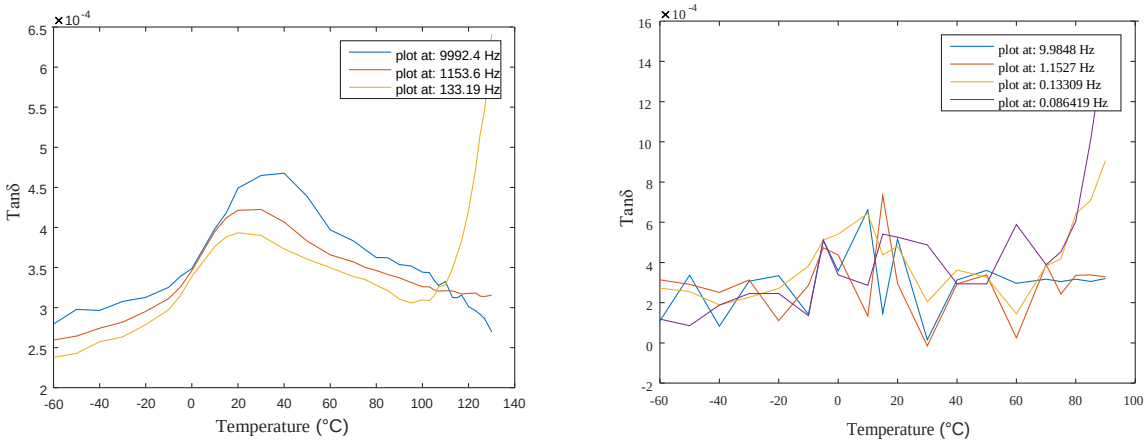

Figure 6.11. Dielectric loss w.r.t temperature at various frequencies; higher frequencies (left) lower frequencies (right) of RER

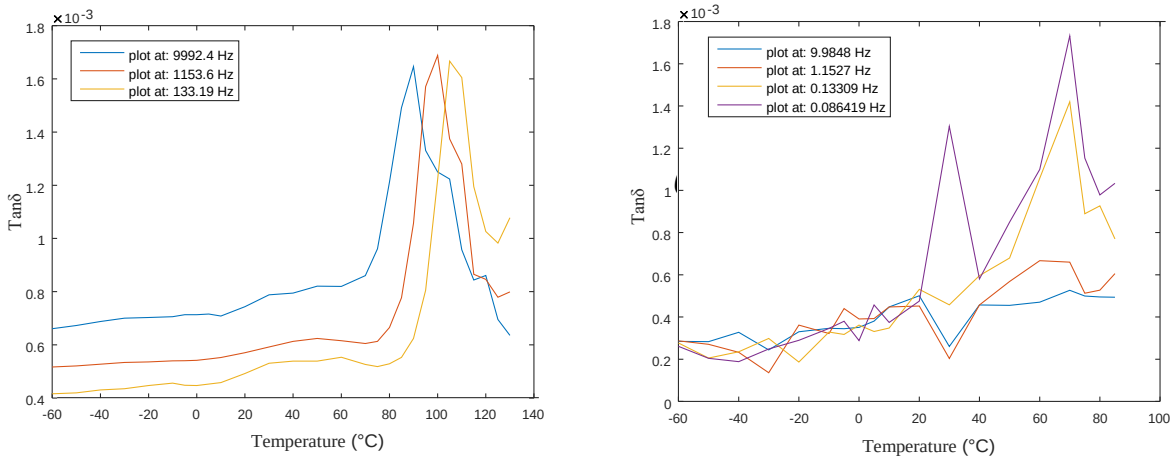

Figure 6.12. Dielectric loss w.r.t temperature at various frequencies; higher frequencies (left) lower frequencies (right) of RERT.

Two samples of Tervakoski RERT and RER films with different thickness (10µm and 14.4µm) values are also tested. In figure 6.11 and 6.12, it was found that RERT film shows well defined sharp and narrow peaks at high temperature between 60˚C to 120˚C for 9992.4Hz and this peak then shrinks and moves towards higher temperature with the increase in frequency and disappears below 10Hz. Whereas in thicker film RER the loss level is very low and the α-peak exists between -20˚C to 60˚C which reduces as the frequency increases and disappears. Narrow sharp peak shows the smaller mobile amorphous phase. There are no distinguishable peaks at lower frequencies. Moreover, RER film also shows probably ionic conduction below 1 kHz at temperatures above the operating temperature of BOPP i.e. 105°. Gallot et al. [48] discuss the opposite of what we found in our tests i.e. we have found a decrease in loss factor for the film with higher thickness value than for the film with lower thickness value. The increase in thickness is supposed to be associated with increase in crystallinity ratio and lower thickness means that the film is stretched more in transverse and machine direction. Apart from the mentioned reasons, thickness of a polymer film is also dependent on certain other factors involved during the process of film production and is not very simple to conclude. Also, the increase in loss level and unlikely result shows that dielectric response is also dependent on certain other factors like the catalyst used and surface treatment etc.

Figure 6.13. (a), (b), (c) and (d) shows that the overall permittivity increases as the frequency decreases over the entire temperature range for NPO30, NPO49, RERT and RER films. This is in accordance with the concept that as the frequency decreases it becomes easier for different polarizations phenomenon to occur. Each of the permittivity curves shows that as the temperature increases permittivity decreases but this decrease is rather slight, for NPO30 that is from 2.58 to 2.42. For RER and RERT the permittivity increases drastically after 120˚C at very low frequency below 0.9 Hz.

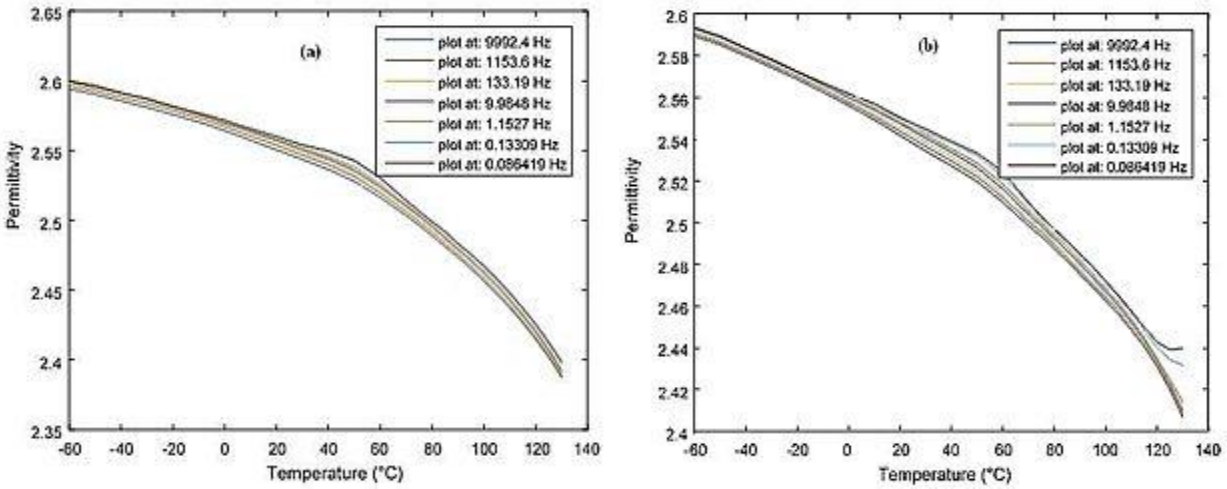

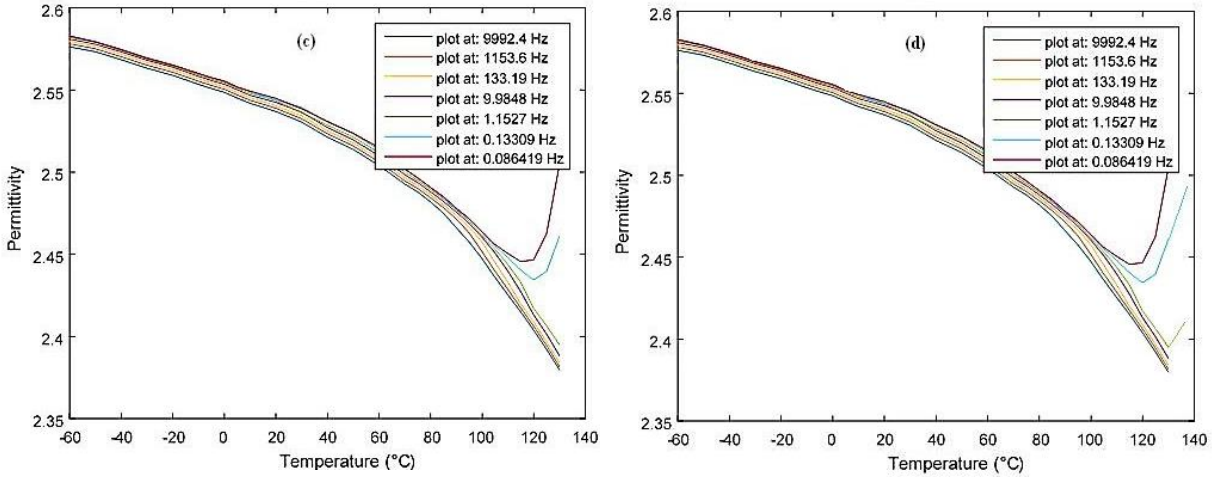

Figure 6.13. Relative permittivity w.r.t temperatures at various frequencies of (a) NPO49 (b) NPO30 (c) RER (d) RERT

The physical aging in a polymer is related to the conformational and segmental motion in the polymer chain. When the temperature decreases from the glass transition temperature, the polymer chain conformational motion decreases to reduce the strain and achieve equilibrium. At elevated temperatures, the dielectric dispersion is the motion of polymer molecules between quasi equilibrium positions around the main chain and causes rearrangement of the main chain. This change in the dielectric response is related to the main chain rearrangement is known as α-relaxation[65]. As the temperature is reduced, the relaxation time increases and the peak appears in the dielectric loss curve as a function of temperature at various frequencies. In the low temperature region, the side chains and intermolecular movement is more prominent and thus causes the second peak known as β-relaxation. BOPP thin film has both amorphous regions and crystalline regions. In the crystalline region the movement of molecules from the folded lamellas is difficult and associated with some potential energy. The main chain shows the movement of molecules with the increase in temperature and becomes maximum at glass transition temperature T_g which is associated with maximum dielectric loss known as α-relaxation. The physical degradation is associated with the reduction in free volume. Below T_g, the free volume is fixed but as the temperature increases and the glass like polymer expands and reduces the intermolecular distances. At T_g, the free volume expands and rubber like polymer expands which allows rotational and linear motion and thus associated with high dielectric loss. The temperature at which the relaxation becomes infinite and frequency approaches to zero is normally represented as T'_g. At this temperature, the relaxation is very slow and segmental motion occurs which can be observed only during a very long time. This phenomenon to achieve the thermal equilibrium is known as aging.[4][11][48]

Apart from the relaxation theory the dipoles possibly attached to the main chain also play greater role as they are strongly bonded by some restoring force. Thus, dipoles in the crystalline region cannot move and their movement is associated with certain temperature

and frequency whereas the movement of dipoles between equilibrium states is very frequent and relatively easier in amorphous region and they are associated with a wide frequency range. The polarization effect plays the main role in the dielectric behavior of a polymer. Electronic polarization occurs fastest in 10ns whereas ionic polarization takes effect in 1 to 10msec. Dipole polarization is the slowest among these three polarization to occur. Interfacial and hopping charge polarization are even more slower. Under high frequency dipoles cannot orient themselves. Also, the low temperature doesn't not provide favorable condition for the dipoles to orient. Thus as the temperature increases the dipoles can orient more easily and thus increases the dielectric constant.[65]

During the spectroscopy measurements carried out for this thesis, it has been found that the samples of the dielectric films get aged because of continuous application of heat over a wide temperature range of -60°C to 130°C. During the whole temperature range the samples face 17h 30min of temperature stress with each temperature level stress of 36min. It was found that if the measurement was carried out for a fresh sample only at a single temperature point thus minimizing the temperature stress, the loss level remains very low. A test was made where fresh film samples were measured only at three temperature points, 0°C, 30°C and 110°C with a total measurement duration of approx. 1h. For RER film (pure BOPP), it can be seen in figure 6.14 (a) that 0°C has higher loss level in the higher frequency range as compared to 0°C age whereas 30°C has a steep increment in loss level below 4.5kHz whereas 30°C age has low loss factor with no sudden increment till 1.5×10^{-2} Hz. Moreover, for 110°C the loss factor shoots up at 1kHz whereas this shoot up shifts to a very low frequency 1.78Hz for 110°C age. For NPO30 nanocomposite this difference in loss factor is smaller as compared to pure BOPP and also the overall loss factor is lower in case of NPO30 nanocomposite as shown in the figure 6.15. Therefore, it shows that the samples also get aged during testing because of physical and thermal stresses.

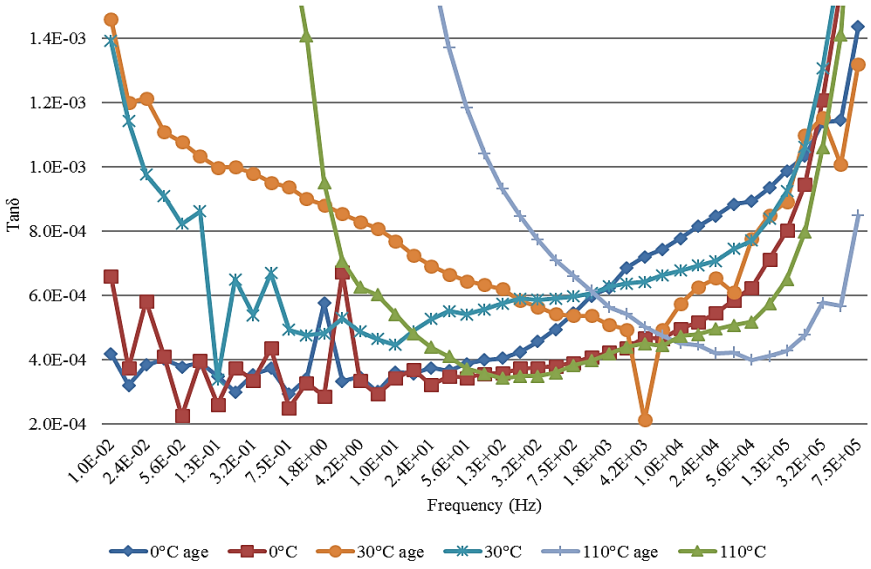

Figure 6.14. (a) Loss factor w.r.t frequency for continuous (°C age in the figure) and point change (°C in the figure) in temperature for RER film.

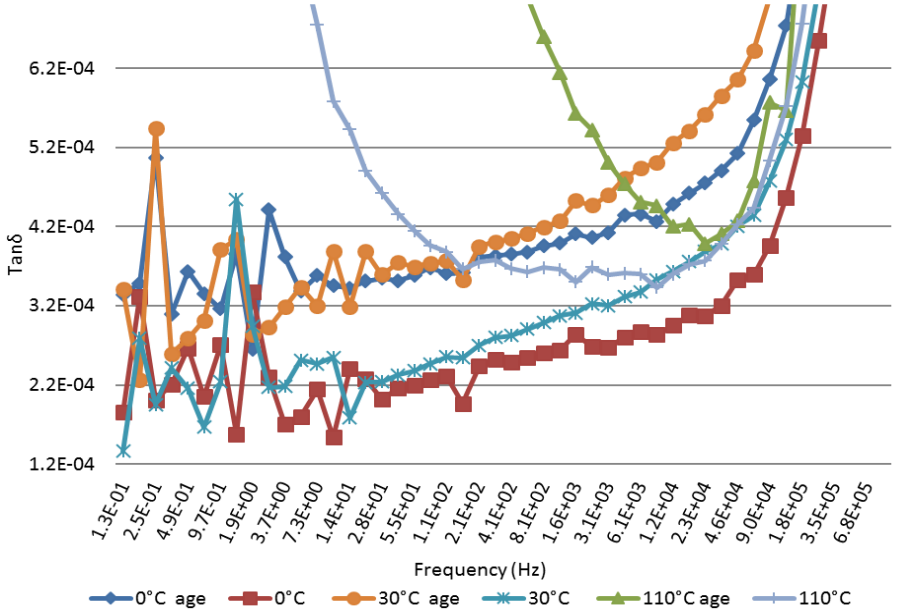

Figure 6.14. (b) Loss factor w.r.t frequency for continuous (°C age in the figure) and point change (°C in the figure) in temperature for NPO30 film

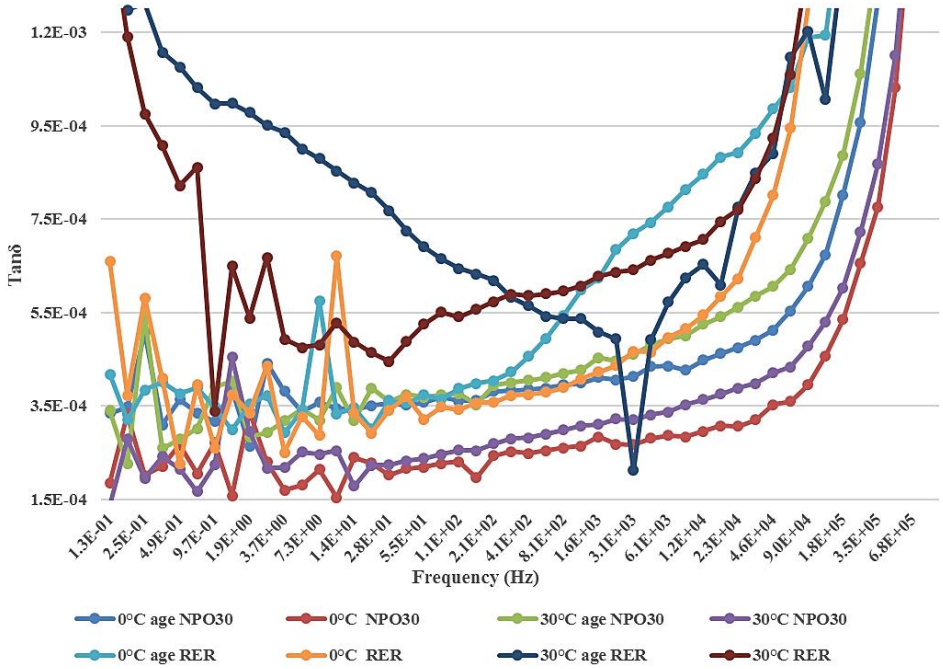

Figure 6.15. Loss factor w.r.t frequency for continuous (°C age in the figure) and point change (°C in the figure) in temperature for NPO30 and RER film.

6.5 Dielectric response of BOPP as a function of applied field

Three different films were used in this analysis including Tervakoski RER (14.4μm thickness), NPO30 silica filled nanocomposite (14.7μm thickness), NPO49 reference BOPP (15μm thickness). These film samples were sputtered with 100nm thickness and 10mm diameter gold electrodes using SC7620 mini sputter coater. These samples were then subjected to dielectric spectroscopy using alpha A analyzer. In this section, we will discuss about the energy density w.r.t electric field, loss factor and permittivity w.r.t applied field. Since the capacitors have high power density and low energy density therefore experiments have been made to increase the energy density. Due to low breakdown strength and low breakdown voltage many capacitors are not able to have sufficient energy storage. But the recent advancement in BOPP (Bi-axially oriented polypropylene) has not only improved the toughness and flexibility in the breakdown conditions but also has developed high energy storage capacity. The metallized thin films or BOPP also possess self-healing property which helps in the operation of capacitor near breakdown voltage thus increasing the operational field strength of capacitors. Energy density can be given by equation 6.1;

$$\text{Energy Density (Joules/cc)} = \frac{1}{2}\varepsilon\varepsilon_0 E^2 = \frac{1}{2}\varepsilon\varepsilon_0\left(\frac{V}{d}\right)^2 \tag{6.1}$$

Where ε is the dielectric constant which is around 2.2 for BOPP (RER film), ε_0 is the permittivity of free space that is 8.85×10^{-12}F/m, V is the applied Vrms voltage, E is the electric field and d is the thickness of the film. Figure 6.16. (a), (b) and (c) shows that as the electric field increases the energy density increases exponentially resulting in a parabolic curve for all the frequency ranges irrespective of the sample type whether it is NPO30, NPO49 or RER. This is in accordance with the energy density equation. Thus, the energy storing capacity is directly proportional to the square of electric field and also to the permittivity. In order to increase the energy density, the polymer should have higher permittivity and low dielectric loss. It should have uniform thickness and moreover, the lower the thickness value the higher will be the energy density as the energy density is inversely proportional to the square of the thickness of the dielectric film. Therefore Bi-axially oriented polypropylene is a better choice for operation of capacitors near breakdown voltage as they are stretched in the form of thin films with better energy density, lower permittivity and lower dielectric loss level.[50][66]

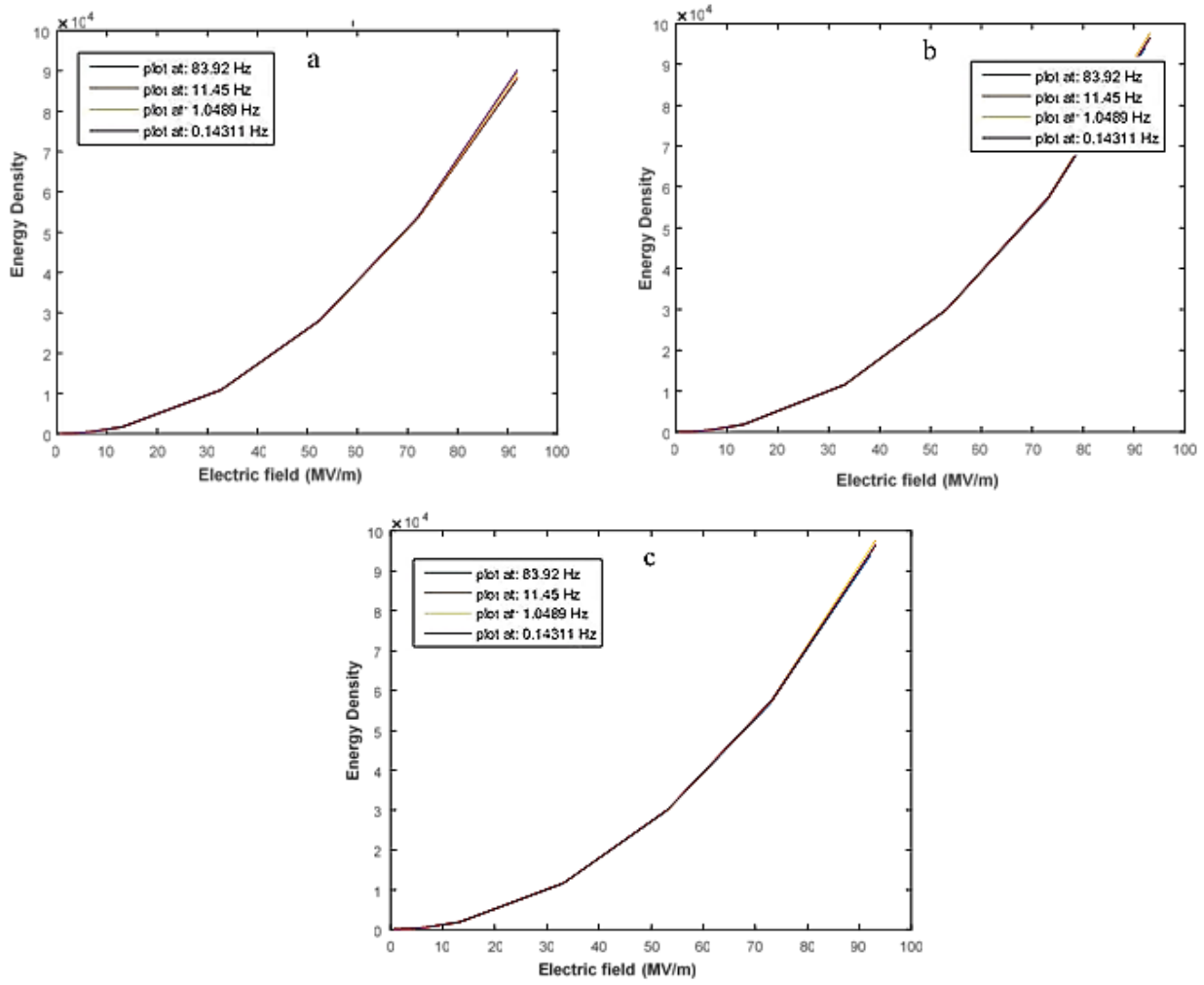

Figure 6.16. Energy Density w.r.t Electric field at different frequency levels of (a) NPO30 (b) NPO49 and (c) RER

During dielectric spectroscopy, the behavior of permittivity and loss factor has been observed w.r.t the applied voltage. Figure: 6.17. (a), (b) and (c) represents the behavior of loss level and permittivity as a function of applied field. As the frequency decreases the loss level decreases and permittivity increases more. This is because at low frequency, different polarization effects can occur resulting in an increase in permittivity. Moreover, there are two different ramps in the loss curve as well as permittivity curve. The increment in the loss level after 30MV/m till 75MV/m is a ramp with comparatively a lesser steep than the increment in loss factor as well as the permittivity after 75MV/m. The slope after 75MV/m is very steep. Thus, it shows that the higher the electric field the higher will be the rate of increment in loss factor and also higher electric field increases the permittivity which corresponds to the idea that energy density increases as the electric field becomes stronger.

(a) NPO30

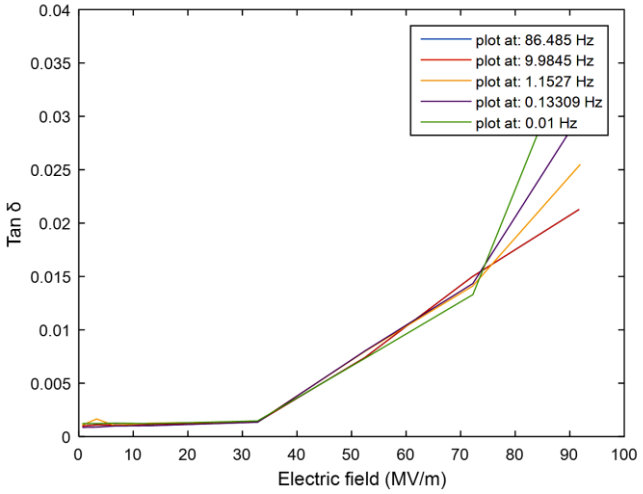

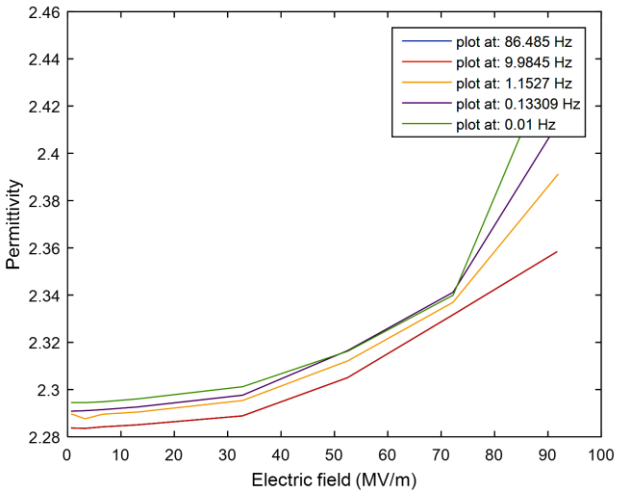

(b) RER

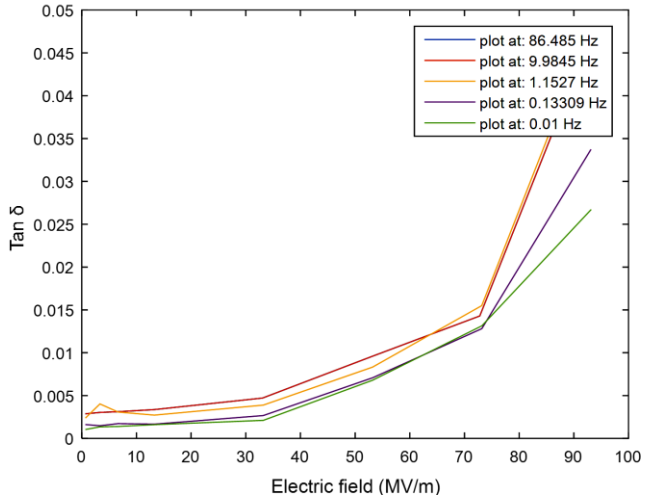

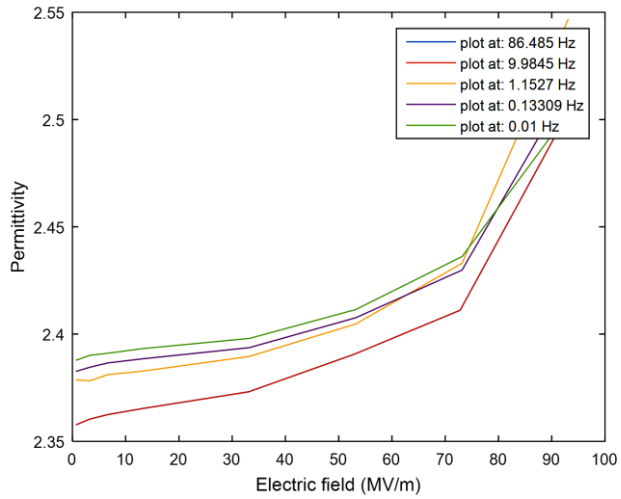

(c) NPO49

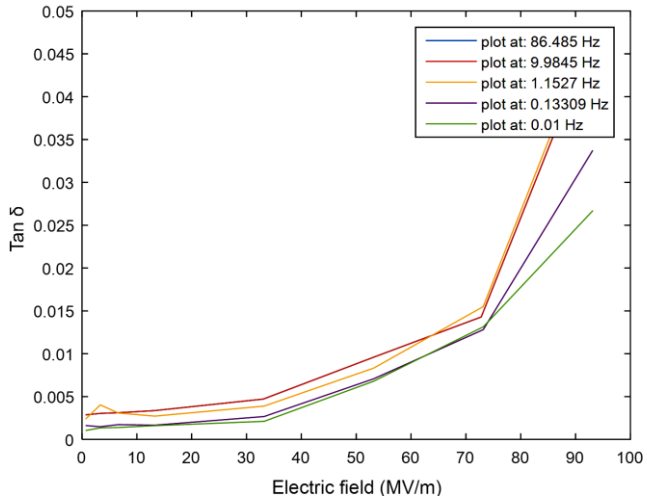

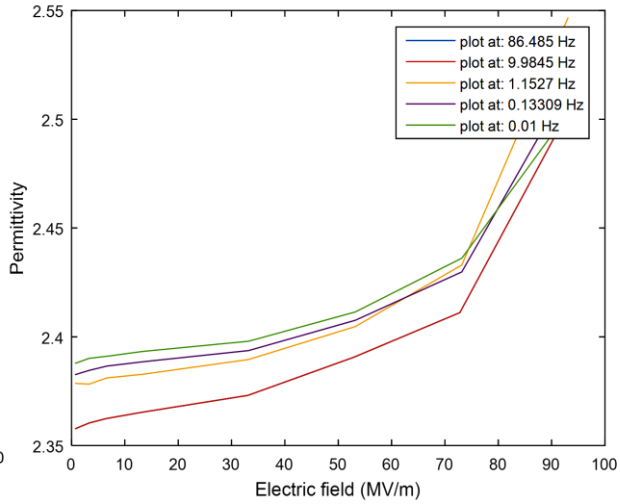

Figure 6.17. Loss factor and permittivity w.r.t Applied field (MV/m) of (a) NPO30 (b) RER and (c) NPO49

The reason of this increment in loss factor with the increase in the applied field might also exist in the concept of high field conduction in BOPP. Nagao et al. [67] describes for nonpolar polymers like polypropylene that at room temperature the dependence of loss factor on electric field is lower and the change in loss factor is smaller at room temperatures whereas if the temperature is increased above 40° C, the loss factor changes more. The dependence of loss factor is also on ac dissipation current waveform. Two component of currents can be used to evaluate the high field ac conduction that is dissipation current I_{xr} and unbalance capacitive current component (ΔI_{xr}) which are shown in the figure 6.18.(a), Ixr increases proportional to the electric field for both up and down of the field but the capacitive current change in unbalanced which could be because of the formation of space charge at higher fields. Fujii et al. [68] has described the distortion in unbalanced component of capacitive current for polypropylene at higher fields as for 150kV/mm as shown in the figure 6.18.(b), the waveform changes from sine wave to distorted wave with a peak and a shift of fundamental wave towards right. this might be because of the formation of space charge at higher fields. Due to ac applied field space charge forms as both homo and hetero space charge. This is because of the polarity reversal in each cycle. At one electrode first the hetero space charge forms and in the other cycle the homocharge appears and the other electrode at the same time extracts the heterocharge which results in peak and distortion in front half of the capacitive current cycle and results in increment in capacitive current.[62][63][67]

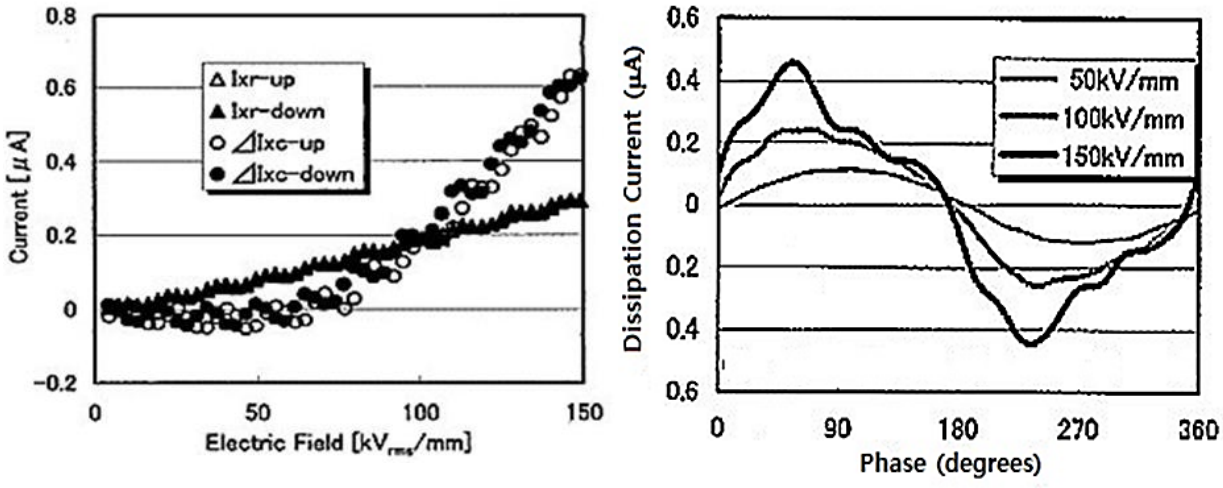

(a) (b)

Figure 6.18. (a) Dissipation current (I_{xr}) and unbalance capacitive current component(ΔI_{xc}) dependence on high field[68]. *(b) Dissipation current dependence on high field at 30°C*[69].

7. DISCUSSION ABOUT THE VALIDITY OF MEASUREMENTS

The focus of this thesis is mainly to comment on the validity of results and measurements especially in the first section of the thesis. The confidence level of measurements set the ground for describing and analyzing the results found in the second major portion of the thesis that is about the dielectric characterization of BOPP insulation. As already described in the section 5.4 that it is inherently impossible to eliminate all sources of errors and uncertainties. Rather it is possible to mention the probable uncertainties which could influence or deviate the measurements or results to some extent from the expected or rated values. Sources of errors and uncertainties exists not only internal to the measurement system but it also exists in the environment, supporting instruments and devices, practices of the operators, morphology of the samples and so on.

Since the Novocontrol device is being used for dielectric spectroscopy in this thesis which requires the optimum sample capacitance for accurate results. The capacitance should lie around 50pF to 200pF or above whereas 100pF is the optimum capacitance to analyze the dielectric behavior at frequencies up to 1MHz [70]. For BOPP, the samples' average capacitance is around 105pF for 10mm diameter samples and around 340pF for 18mm diameter samples. Thus, this aspect is qualified in accordance to the device recommendations. Next comes the other very important aspect to consider which is edge correction. In ideal capacitors, the field exist only inside the electrode area and zero outside the electrode area. But in real capacitors the field is nonuniform at the edges of electrode and it promotes the stray capacitance component in parallel to sample capacitance which is also known as edge capacitance. Novocontrol device contains a feature of using edge compensation to reduce these effects of inhomogeneous field by subtracting the edge capacitance from sample measured capacitance [70] [71]. This feature has been overlooked in this thesis because for edge compensation the top electrodes and sputtered sample electrodes need to be of the same size whereas in this thesis the top electrode in some cases were 2mm bigger in diameter and in some cases 2mm smaller in diameter as compared to the sputtered electrode. The results and measurements made throughout the thesis could possibly have the uncertainty related to edge compensation. To avoid or minimize the edge capacitance, the sample specifications should have smaller ratio of sample thickness /sample electrode diameter. But there are limitations to reduce this ratio as electrode diameter could not exceed the available space of 30mm diameter in the sample holder. Also, increase in diameter after certain limit needs excessive electrode material (gold) which is very expensive. Sample thickness is also limited and could not be reduced after a certain level as it involves technical and manufacturing complications. Thus, to completely avoid this uncertainty of edge capacitance is practically impossible.

With reference to novocontrol device manual, larger electrode diameter results in smaller value of loss factor but there are some complications in increasing the diameter of electrode after certain limits [70]. As already mentioned above the sample holder has limited space for the sample to be placed and the maximum possible sample electrode diameter could be 30mm. It has been found that as the diameter of the sample electrode increases (keeping the top electrode of the same size) to 30mm, the loss factor increases whereas the loss factor for 10mm,18mm and 20mm are relatively smaller as shown in figure 7.1.

The reason of the increase in loss factor with largest possible diameters could be possibly the stray capacitance induced by the metal or steel rods of the sample holder. These steel rods come closer as the diameter of electrode approaches the maximum possible value as shown in figure 5.19. and thus, its effect on capacitance can become prominent. Therefore, in this thesis the diameters of electrodes are either 18mm or 10mm.

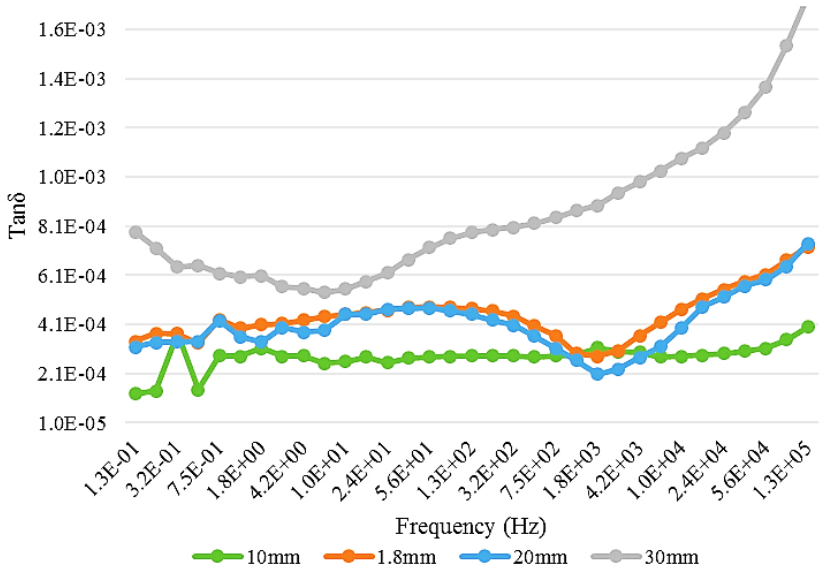

Figure 7.1. Loss factor w.r.t to frequency for different top electrode sizes.

Apart from the electrode diameter, the best possible size of top electrode needs to be selected as compared to the sample electrode. There could be some uncertainties related to the size of top electrode. In some of the experiments 20mm of top electrode has been used for 18mm of sample sputtered electrode. In this case about 19% of the top electrode area is not in contact with the sample electrode and thus could result in certain stray capacitance component in parallel to the sample capacitance. According to the calculation, there could be 23.2% higher value of relative permittivity but when compared with the measurement results of Novocontrol device, the permittivity was found to be 12% higher. This shows that Novocontrol device tries to reduce the error if the correct diameter of sample electrode is entered in the program sample specifications. But still the uncertainty exists in relative permittivity value to some extent. The value of loss factor was found to be same in both cases as loss factor is a relative value and does not depend on this factor directly. The size of top electrode in water absorption test was bigger as compared to sample electrode and can have uncertainty in permittivity value. Moreover, the diameter of top electrode should not be small as compared to the sample electrode. This is because the area of the sample electrode under the smaller top electrode is considered to have low thickness values because of the applied pressure[70]. Thus, it is advised to use same size of top electrode and sample electrode for accurate results. Therefore, in temperature and field related tests, the top electrode and sample electrode size were kept similar that is 10mm. One other reason of using the same size of top electrode rather than using the smaller top electrode was the probability of non-uniform thermal expansion if only a certain portion of sample electrode stays under the pressure of top electrode. Moreover, the area of sample electrode under the top electrode broke down with a hole near the edge of top electrode in field related tests. This might be because of non-uniformity of field and

pressure at the area around the edge and the decision was made to use same size of top electrode as that of sample electrode.

Plasma heat of sputtering process is one of the major issues faced during the thesis. Careful procedures were followed while sputtering the electrode to reduce the effect of plasma heat. But eliminating the effect of plasma heat on molecular scale of polymer film is impossible. There could be possibly some morphological changes which leads to higher loss factor. Plasma heat also creates uncertainty in water absorption test as some moisture content could evaporate during the sputtering process. This source of error could be reduced either by considering a different kind of sputtering device equipped with cooling system or making electrodes by evaporation process. Certain morphological aspects play an important role in introducing uncertainties in measurement results. For example, each of the analysis has also been made for BOPP nanocomposite. Figure 7.2. shows the morphological SEM images of BOPP nanocomposite NPO30 (left hand side) and reference BOPP NPO49 (right hand side). It has been observed that there are wrinkles on the surface of BOPP. Moreover, NPO30 has an observable spread of nanosilica when SEM images are produced. The size of these particles ranges from 75nm,80nm,99nm ,100nm to 200nm. Ideally these particles should have approximately the same size but it is not possible. The natural phenomenon of agglomeration in nanocomposites remain exist even after the surface functionalization. Agglomeration tries to degrade the electrical and dielectric properties [33]. Apart from observing the SEM images of cross section of NPO30 and NPO49 before sputtering, a few SEM images of cross section were also produced after sputtering the electrode on the sample as shown in figure 7.3. The samples were dipped in liquid nitrogen and ripped to get the cross-sectional portion. It has been observed that voids, fractured lines and minute hole appeared and gives a hint of some morphological changes. The point of discussion is that whether these changes are due to plasma heat of sputtering or it has some connection with the ripping of the film to get the cross-sectional portion. It is tricky to figure out the exact reason of this change in appearance but possibly it could have created some uncertainty in the dielectric behavior i.e. loss factor and relative permittivity.

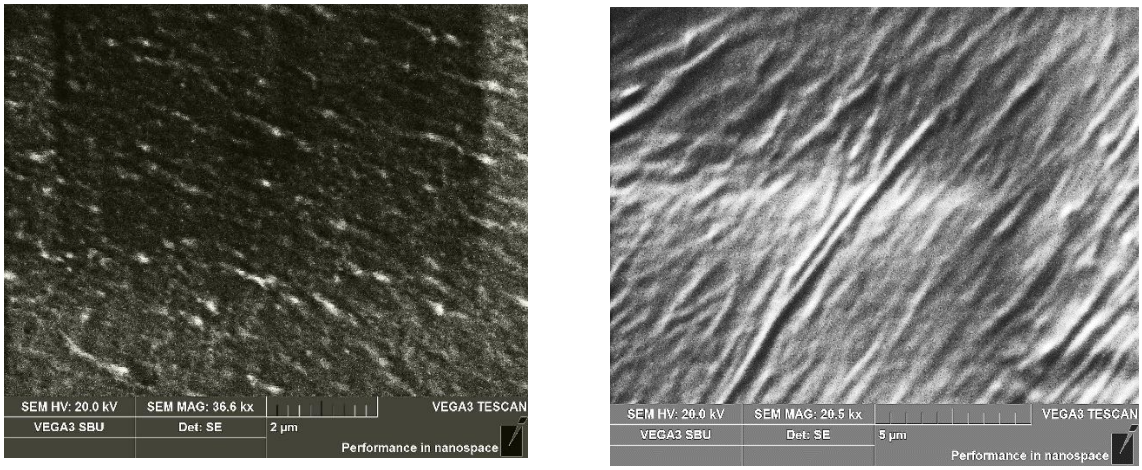

Figure 7.2. SEM image of the cross-sectional portion of NPO30 BOPP nanocomposite (left hand side) and reference BOPP NPO49 (right hand side).

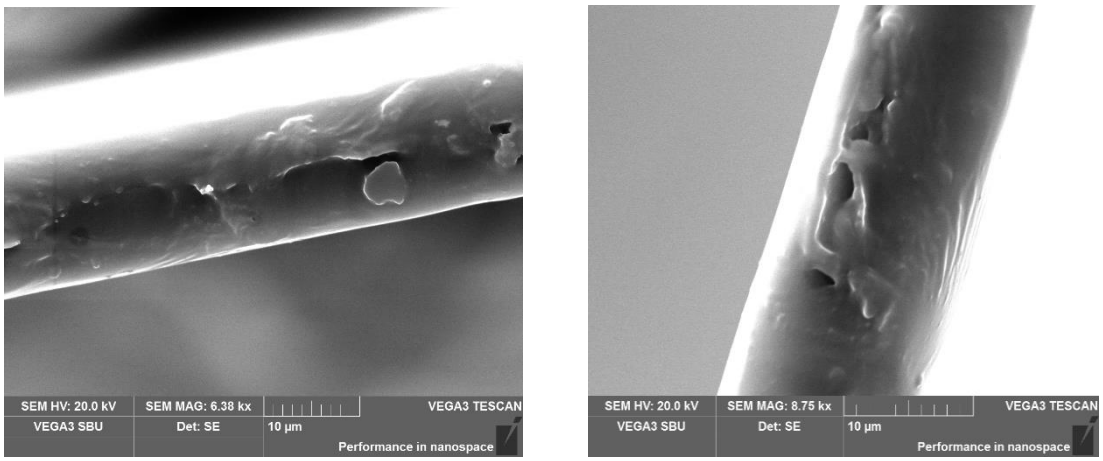

Figure 7.3. SEM images of reference BOPP (NPO49) cross sectional portion with fractured lines, voides and holes.

One of the major issues that has been detected during temperature test was thermal expansion of BOPP film. Apparently the sample and its surrounding area of the film sample looks effected by multiple expansions and contractions as shown in figure 7.4. The diameter of sample elecrode has been changed from 10mm and the sample diamensions have been changed from 40mm×40mm. The samples after undergoing an exposure to different temperatures starting from -60°C to 130°C with 10°C rise in steps must have developed thermal expansion. One possibility to cater with this thermal expansion is to use the calculation based on coefficient of thermal expansion but the weird results of calculations revealed that it is not as straight forward to include this factor of uncertainity by simply calculating thermal expansion. The limitations in making a pre-estimation of possible thermal expansion is that BOPP has two different orientations and the expansion must be different in each direction of orientation. Also, the portion of BOPP under the sputtered electrode bears two thermal expansion effects that is because of BOPP itself and gold. Gold and BOPP has different coefficients of thermal expansion. Moreover, the presuure of top electrode also effects the ease of expansion of BOPP unerneath. One point of discussion can be the fact that BOPP sample has faced many temperatures from -60°C to 130°C and each of the temperatures has impart its own thermal expansion effect. Thus the bottom line is that nullifying the uncertainity due to thermal expansion is very difficult.

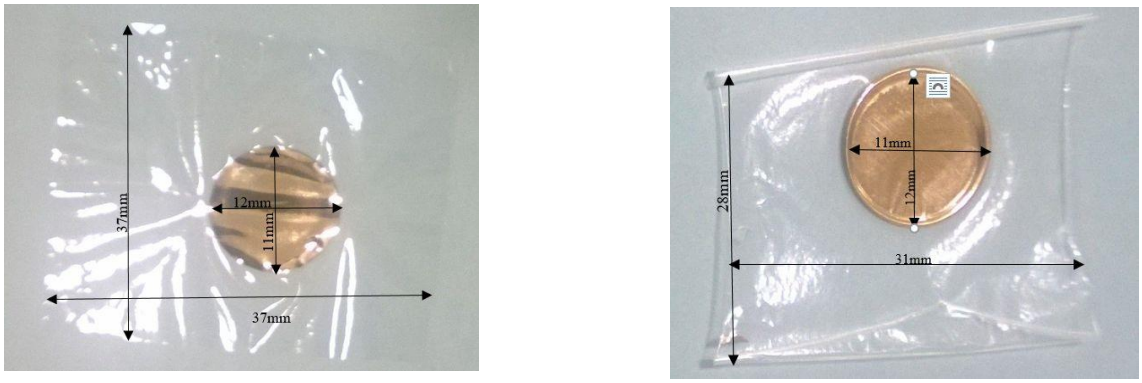

Figure 7.4. Thermal expansion of NPO30 nanocomposite (left hand side) and BOPP RER film (right hand side) during temperature test.

The behavior of antioxidants and additives in certain physical conditions is also not completely known e.g. their behavior in humid conditions or at higher temperatures etc. Handling errors also need to be considered e.g. visually, electrodes on both sides of the sample seem to be exactly overlapped but exact overlapping is sometimes not possible through manual arrangements. Annealing of the sample could also be useful in removing the defects and reducing the loss factor. Moreover, the calibration method that has been used throughout the thesis is same that is calibrate all with low capacity open calibration. Load short and reference calibration methods have not been tried and tested. Ideally all types of calibrations should have been done before making experiments using any device. Reliability and uncertainty issues are directly related to the calibration methods being followed. Therefore, keeping all these sources of uncertainties into consideration, it can be concluded that the measurements made throughout the thesis can have some deviation from the desired loss factor but at the same time the reliability analysis made in section 5.4 reveal that measurements are eligible to be used in making comparative analysis.

8. CONCLUSIONS

The central idea of this thesis revolves around two major tasks; one is the formulation of testing methods and sample preparation for precise results of dielectric spectroscopy using Novocontrol device and second is the dielectric characterization of BOPP (Bi-axially oriented polypropylene) and its nanocomposite. Various experiments have been made by altering different physical condition and parameters which leads us to some important conclusion as discussed in Chapter 5;

- The sample of film is cut into 40mm×40mm squares with thickness measurements made at five point where the electrode is required to be sputtered and cleaned with isopropanol.
- Gold has been chosen to fabricate electrodes as it is the most inert metal. Aluminum if used gets oxidized after some time.
- Pre-vacuuming of the samples before sputtering the electrodes found to be effective in eliminating the moisture peaks and reduction in loss tangent. To make the process of vacuuming more effective, it has been accompanied with heating up to 30 to 35°C with the vacuuming duration of 24h.
- It has been found that the parameters used during sputtering of electrode effect the sample and can degrade the sample under conditions. It was found that increasing the sample distance from the source of sputter coater reduces the thermal stress of plasma heat and thus the optimum distance of 55mm has been agreed to be used. Moreover, the increase in metallization decreases the loss factor because of better electrode formation and thus 75nm to 100nm is the thickness value more than which no reduction in loss is observed. Further findings are related to the time intervals of sputtering and relaxation. Since the plasma current of sputtered device is associated with heat stress thus to remove this stress sputtering was being done for 30s with 30s of rest. The current of plasma also creates heat. Higher the current higher will be the process temperature which degrades the material whereas higher current sputter more metal which reduces the loss tangent. Therefore, a tradeoff is between current and electrode thickness and ultimately 25 mill amperes has considered to be set for sputtering.
- The optimum combination of sputtering the electrode can be represented as; Time of sputtering × time of relaxation × Plasma current × distance from target = 30s×30s×25mA×55mm

A detailed statistical analysis has been made to make estimations of reliability, repeatability and uncertainty. Fortunately, the measurements sets have qualified for all types of reliability estimations. It has been found that the dielectric measurements have internal consistency and these measurements can be reproduced using the defined procedures by different raters at any time. Inspite of qualifying for reliability estimation, there are still

some sources of uncertainties and errors trying to deviate the measured results from the desired or rated values. These aspects have been extensively elaborated in chapter 7. After finalizing the best testing procedures and their validity, the sputtered BOPP samples are then subjected to various experiments involving dielectric spectroscopy to analyze the behavior of dielectric material as a function of frequency, temperature, moisture and voltage. The dielectric properties analyzed were loss factor and relative permittivity. Also, the difference in the behavior of pure BOPP and its nanocomposite has been recorded. The BOPP capacitor films used in this thesis are Tervakoski RER, RERT, NPO30 BOPP silica nanocomposite and its unfilled reference BOPP NPO49.

In Chapter 5 it has been concluded that BOPP nanocomposite has some limitations in establishing electrical properties. BOPP nanocomposites have better charge distribution and space charge accumulation, reduced mobility of space charges and chain entanglements that results in reduction in dielectric loss factor and improved dielectric strength and so on. It was discussed that adding the optimum amount of nanofiller helps in enhancing the electrical properties whereas higher filler concentration sometimes degrades the properties so deciding the right concentration of filler is really important in association with the process of formation of thin films and the added nanofillers' surface treatment.

The thesis includes an extensive study on the behavior of BOPP under ambient humidity and in water immersion. It has been found in Chapter 6 that nanofiller on one hand helps improving the electrical properties but on the other hand enhances the ability of polymer to absorb water in humid conditions. This absorption of water is greater under higher relative humidity which increases the permittivity and dielectric loss tangent. Different humidity percentages were tested (0%RH, 33% RH, 75% RH, and 100% RH). The increase in humidity shifts the peaks and tips further towards to the higher frequencies. This behavior is mild in case of pure BOPP whereas comparatively prominent for nanocomposites. But the surface treatment of nanocomposites helps in reducing the number of hydroxyl groups in the filler surface and reduces the ability of nanocomposites to absorb water.

Beside water absorption analysis, the effect of application of wide range of temperature from -60˚C to 130˚C as a function of frequency has been studied. It has been found that operation of BOPP and its nanocomposite is stable till 90˚C with loss factor and permittivity values under limits. Whereas above 90˚C the loss factor starts increasing in the lower frequency region more and more and the polymer gets aged. The permittivity increases as the frequency decreases because the field gets weaker with reduction in frequency and it becomes easier for the dipoles to orient themselves. Moreover, the dielectric behavior of BOPP and nanocomposites over a range of frequency as a function of temperature has been observed. It was found that for BOPP nanocomposites the α- peak is very sharp and prominent as compared to BOPP and the overall loss factor is low for nanocomposite. This peak hints about the mobile amorphous region. As the temperature

decreases from glass transition temperature, the relaxation time increases and α-peak disappears and no further peak appears in our experiments for BOPP in the low temperature region.

During temperature experiments, it has been found out that continuous application of temperature stress of 17h 30min for a temperature range starting from -60°C and reaching to 130°C in 10°C step increments resulted in higher loss factor whereas the loss factor values found to be lower at the same temperature levels when fresh samples were tested for separate measurements at only those specific temperatures. The last analytical section of Chapter 6 is related to the dielectric behavior of BOPP as a function of applied field. It has been observed that as the applied voltage increases, the electrical field increases which corresponds to the increase in energy density as a parabolic curve for all BOPP and its nanocomposites. Moreover, it has been observed that as the applied voltage increases the loss factor increases in 3 different slopes. The loss factor slope between 30 MV/m and 75 MV/m is less steep whereas the loss factor increases a lot after 75 MV/m with steep slope.

This thesis has set some standards for future experiments using the Novocontrol device. Some recommendations based on the analysis and limitations of the thesis could be made e.g. sample electrodes should be made using either a sputtering device equipped with cooling system or it can be made by evaporation method to avoid plasma heating effects. Careful selection of sample electrode diameter and top electrode diameter should be made. Edge correction should be taken into consideration in future experiments. Every prepared sample should be annealed before dielectric spectroscopy to reduce the defects. A detailed calibration session should be essentially carried out before using Novocontrol device. As discussed in Chapter 7 about the issues related to thermal expansion, an extensive study could be made to figure out the thermal expansion behavior and measures to reduce this effect. Moreover, in future careful scanning should be done to figure out the morphological changes in BOPP at different stages of sample preparation and experiments. A study based on the aspects of degradation of an insulating material during testing could be a part of any future project or thesis. This thesis has already made outlines for carrying out dielectric spectroscopy using Novocontrol device and these guidelines and procedures could be followed for studying dielectric behavior and characteristics of different polymers and nanocomposites.

9. REFERENCES

[1] J. K. Nelson, "Overview of Nanodielectrics- Insulating materials of the future," in *Electrical Insulation Conference and Electrical Manufacturing Expoi*, 2007, pp. 229–235.

[2] R. Hackam, "Outdoor high voltage polymeric insulators," in *Proceedings of 1998 Intlernational Symposium on Electrical Insulating Materials, in conjunction with 1998 Asian International Conference on Dielectrics and Electrical Insulation and the 30th Symposium on Electrical Insulating Materials.*, 1998, pp. 1–16.

[3] C. Zou, J. C. Fothergill, and S. W. Rowe, "A 'water shell' model for the dielectric properties of hydrated silica-filled epoxy nano-composites," in *2007 International Conference on Solid Dielectrics, ICSD*, 2007, pp. 389–392.

[4] L. A. Dissado and J. C. Fothergill, *Electrical Degradation and Breakdown in Polymers*, First ed. London, UK: IET (The institude of engineering and technology), 1992.

[5] M. Roy, J. K. Nelson, R. K. Maccrone, L. S. Schadler, C. W. Reed, and R. Keefe, "Polymer nanocomposite dielectrics-the role of the interface," *IEEE Trans. Dielectr. Electr. Insul.*, vol. 12, no. 4, pp. 629–643, 2005.

[6] G. Picci and M. Rabuffi, "Status quo and future prospects for metallized polypropylene energy storage capacitors," *PPPS 2001 - Pulsed Power Plasma Sci. 2001*, vol. 1, no. 5, pp. 417–420, 2015.

[7] I. Rytöluoto, K. Lahti, M. Karttunen, M. Koponen, S. Virtanen, and M. Pettersson, "Large-area Dielectric Breakdown Performance of Polymer Films – Part II: Interdependence of Filler Content, Processing and Breakdown Performance in Polypropylene-Silica Nanocomposites," *IEEE Trans. Dielectr. Electr. Insul.*, vol. 224, no. 2, pp. 2196–2206, 2015.

[8] P. Ghosh, *Polymer Science and Technology: Plastics, Rubbers, Blends and Composites*, Second ed. New Delhi: Tata McGraw-Hill Education, 2002.

[9] J. V E. Desmond Goddard, *Principles of Polymer Science and Technology in Cosmetics and Personal Care*, Second edi. Newyork: Marcel Dekker Inc, 1999.

[10] D. K. Matyjaszewsk, "Encyclopedia Of Polymer Science and Technology," *Wiley Online Library*. Wiley Online Library, p. 1123, 2015.

[11] M. Ritamäki, "Effects of Thermal Aging on Polymer Thin Film Insulations for Capacitor Applications," M.Sc. Thesis, Tampere University of Technology, 2014.

[12] I. Rytöluoto, "Application of polypropylene nanocomposites in metallized film capacitors under DC voltage," M.Sc. Thesis, Tampere University of Technology, Tampere, 2011.

[13] F. Guastavino, A. S. Thelakkadan, G. Coletti, and A. Ratto, “Electrical tracking in cycloaliphatic epoxy based nanostructured composites,” *Annu. Rep. - Conf. Electr. Insul. Dielectr. Phenomena, CEIDP*, pp. 701–704, 2009.

[14] C. Maier and T. Calafut, “Morphology and Commercial Forms,” in *Polypropylene The Definitive User’s Guide and Databook*, First ed., USA: William Andrew, 1998, pp. 12–25.

[15] A. R. Blythe and D. Bloor, *Electrical Properties of Polymers*, Second ed. Edinburg, UK: Cambridge University Press, 2005.

[16] Robert O. Ebewele, *Polymer Science and Technology*, First ed. Newyork: CRC Press, NY, 2000.

[17] David Clifford Bassett, *Principles of polymer morphology*, First ed. London: Cambridge University Press, 1981.

[18] A. Helgeson, “High Voltage Dielectric Response Measurement Methods.” Department of Electric Power Engineering, KTH, Stockholm, 2000.

[19] Gorur Govinda Raju, *Dielectrics in Electric Fields*, First ed. ON, Canada: CRC Press, 2003.

[20] J. K. Nelson, *Dielectric Polymer Nanocomposites*, First edit. Newyork: Springer, 2010.

[21] Teruyoshi Mizutani, “Techniques and Space Charge in Polyethylene,” *IEEE Electr. Insul. Mag.*, vol. 1, no. 5, pp. 923–933, 1994.

[22] M. S. Naidu, *High Voltage Engineering*, Second edi. USA: Tata McGraw-Hill Education, 2009.

[23] H. A. Maddah, “Polypropylene as a Promising Plastic: A Review,” *Am. J. Polym. Sci.*, vol. 6, no. 1, pp. 1–11, 2016.

[24] C. Maier and T. Calafut, “Polypropylene Chemistry,” in *Polypropylene The Definitive User’s Guide and Databook*, First ed., USA: William Andrew, 1998, p. 452.

[25] L. Qi, L. Petersson, and T. Liu, “Review of Recent Activities on Dielectric Films for Capacitor Applications,” *J. Int. Counc. Electr. Eng.*, vol. 4, no. 1, pp. 1–6, 2014.

[26] Tervakoski_Films, “Tervakoski Film RER.” Data Sheet, pp. 1–4, 2008.

[27] C. Maier and Teresa Calafut, “Extrusion,” in *Polypropylene.The Definitive User’s Guide and Databook*, First ed., USA: William Andrew, 1998, pp. 205–221.

[28] Richard Fitzpatrick, “Energy Stored by Capacitors,” *lecture*, 2007. [Online]. Available: http://farside.ph.utexas.edu/teaching/302l/lectures/node47.html.

[29] K. Y. Lau and M. A. M. Piah, “Polymer Nanocomposites in High Voltage Electrical Insulation Perspective: A Review K. Y. Lau, M. A. M. Piah,” *Malaysian*

Polym. J., vol. 6, no. 1, pp. 58–69, 2011.

[30] M. Takala, "Electrical Insulation Materials towards Nanodielectrics," D.Sc Thesis, Tampere University of Technology, 2010.

[31] W. A. Izzati, Y. Z. Arief, Z. Adzis, and M. Shafanizam, "Partial discharge characteristics of polymer nanocomposite materials in electrical insulation: A review of sample preparation techniques, analysis methods, potential applications, and future trends," *Sci. World J.*, p. 14, 2014.

[32] T. Tanaka, G. C. Montanari, and R. Mulhaupt, "Polymer nanocomposites as dielectrics and electrical insulation-perspectives for processing technologies, material characterization and future applications," *IEEE Trans. Dielectr. Electr. Insul.*, vol. 11, no. 5, pp. 763–784, 2004.

[33] K. Y. Lau, A. S. Vaughan, and G. Chen, "Nanodielectrics: Opportunities and challenges," *IEEE Electr. Insul. Mag.*, vol. 31, no. 4, pp. 45–54, 2015.

[34] D. Pitsa and M. Danikas, "Interfaces Features in Polymer Nanocomposites: a Review of Proposed Models," *Nano Br. reports Rev.*, vol. 6, no. 6, pp. 497–508, 2011.

[35] S. Li *et al.*, "Short-term breakdown and long-term failure in nanodielectrics: A review," *IEEE Trans. Dielectr. Electr. Insul.*, vol. 17, no. 5, pp. 1523–1535, 2010.

[36] Montanari *et al.*, "Polarization processes of nanocomposite silicate-EVA and PP materials," *IEEE Electr. Insul. Mag. Trans. Fundam. Mater.*, pp. 1090–1096, 2006.

[37] T. Imai, Y. Hirano, H. Hirai, S. Kojima, and T. Shimizu, "Preparation and properties of epoxy-organically modified layered silicate nanocomposites," in *Conference Record of the 2002 IEEE International Symposium on Electrical Insulation*, 2002, pp. 379–383.

[38] S. Fujita, M. Ruike, and M. Baba, "Treeing breakdown voltage and TSC of alumina filled epoxy resin," in *Proceedings of Conference on Electrical Insulation and Dielectric Phenomena - CEIDP '96*, 1996, vol. 2, pp. 7–10.

[39] S. Singha and M. J. Thomas, "Permittivity and tan delta characteristics of epoxy nanocomposites in the frequency range of 1 MHz-1 GHz," *IEEE Trans. Dielectr. Electr. Insul.*, vol. 15, no. 1, pp. 2–11, 2008.

[40] J. Lu and C. P. Wong, "Recent Advances in High-k Nanocomposite Materials for Embedded Capacitor Applications," *IEEE Trans. Dielectr. Electr. Insul.*, vol. 15, no. 5, pp. 1322–1328, 2008.

[41] T. Kozako, M., Fuse, N., Ohki, Y., Okamoto, T., and Tanaka, "Surface Degaradation of polyamide nanocomposites caused by partial discharges using IEC (b) electrodes," *IEEE Trans. Dielectr. Electr. Insul.*, vol. 0, no. 0, pp. 833–839, 2004.

[42] P. Maity, S. Basu, V. Parameswaran, and N. Gupta, "Degradation of polymer

dielectrics with nanometric metal-oxide fillers due to surface discharges," *IEEE Trans. Dielectr. Electr. Insul.*, vol. 15, no. 1, pp. 52–61, 2008.

[43] A. H. El-Hag, L. C. Simon, S. H. Jayaram, and E. A. Cherney, "Erosion resistance of nano-filled silicone rubber," *IEEE Trans. Dielectr. Electr. Insul.*, vol. 13, no. 1, pp. 122–128, 2006.

[44] B. Venkatesulu and M. J. Thomas, "Erosion Resistance of Silicone Rubber Nanocomposite At Low Filler Loadings," in *16th International Symposium on High Voltage Engineering*, 2009, pp. 1–6.

[45] Zhang Peihong, Zhang Weiguo, Liu Yan, Fan Yong, and Lei Qingquan, "Study on corona-resistance of polyimide-nano inorganic composites," in *Proceedings of the 7th International Conference on Properties and Applications of Dielectric Materials (Cat. No.03CH37417)*, 2003, vol. 3, pp. 1138–1141.

[46] Q. Wang and G. Chen, "Effect of nanofillers on the dielectric properties of epoxy nanocomposites," *Adv. Mater. Res.*, vol. 1, no. 1, pp. 93–107, 2012.

[47] A. Boone, "Definition of Capacitors." pp. 1–63, 2009.

[48] A. Kahouli *et al.*, "Structure effect of thin film polypropylene view by dielectric spectroscopy and X-ray diffraction: Application to dry type power capacitors," *J. Appl. Polym. Sci.*, vol. 42602, p. 42602, 2015.

[49] S. Kume, M. Yasuoka, N. Omura, and K. Watari, "Effects of annealing on dielectric loss and microstructure of aluminum nitride ceramics," *J. Am. Ceram. Soc.*, vol. 88, no. 11, pp. 3229–3231, 2005.

[50] T. C. M. Chung, "Functionalization of Polypropylene with High Dielectric Properties : Applications in Electric Energy Storage," *Green Sustain. Chem.*, vol. 1, no. 2, pp. 29–37, 2012.

[51] Gianni Monaco, "Coating Technology : Evaporation Vs Sputtering," *AR coating technologies*, vol. 1. Satisloh, Italy, pp. 1–8, 2016.

[52] A. Doolittle, "Lecture 12 Physical Vapor Deposition : Evaporation and Sputtering," *Tech, Georgia*. Georgia Institude of Technology, Georgia, p. 12, 2012.

[53] Jeff Sauro, "How To Measure The Reliability Of Your Methods And Metrics," 2015. [Online]. Available: http://www.measuringu.com/blog/measure-reliability.php. [Accessed: 20-Nov-2016].

[54] William M.K. Trochim, "Types of Reliability," 2006. [Online]. Available: http://www.socialresearchmethods.net/kb/reltypes.php. [Accessed: 20-Nov-2016].

[55] G. Rankin and M. Stokes, "Reliability of assessment tools in rehabilitation: an illustration of appropriate statistical analyses," *Clin. Rehabil.*, vol. 12, no. 3, pp. 187–199, 1998.

[56] R. Landers, “Computing (ICC) as Intraclass Estimates Correlations of Interrater Reliability in SPSS,” *The Winnower*, vol. 4, no. 2, pp. 1–4, 2015.

[57] University of Pennsylvania Department of Physics & Astronomy, “Averaging , Errors and Uncertainty,” *Undergrad. Labs*, vol. 1, p. 8, 2015.

[58] Novcontrol, “Alpha-A High Resolution Dielectric , Conductivity , Impedance and Gain Phase Modular Measurement System,” *USER’s Manual*, no. 7. Novocontrol Technologies GmbH & Co. KG, Hundsangen, pp. 1–184, 2005.

[59] Novocontrol Technologies, “N o v o c o o l C r y o s y s t e m,” *Brochure*. GmbH & Co. KG, Hundsangen, Germany, pp. 1–2, 2009.

[60] H. Zhao and R. K. Y. Li, “Effect of water absorption on the mechanical and dielectric properties of nano-alumina filled epoxy nanocomposites,” *Compos. Part A Appl. Sci. Manuf.*, vol. 39, no. 4, pp. 602–611, 2008.

[61] W. S. Chow, “Water absorption of epoxy/glass fiber/organo-montmorillonite nanocomposites,” *Express Polym. Lett.*, vol. 1, no. 2, pp. 104–108, 2007.

[62] H. D. Chandrashekara, D. Kumar, and L. C. S. Murthy, “Effect of the Temperature and Humidity on the Dielectric Properties of TiO 2 Thin Films Prepared by Spray Pyrolysis Technique,” *Int. J. Sci. Technol. Vol.*, vol. 2, no. 5, pp. 377–381, 2013.

[63] D. Qiang, G. Chen, T. Andritsch, and A. Material, “Influence of Water Absorption on Dielectric Properties of Epoxy SiO 2 and BN Nanocomposites,” pp. 439–442, 2015.

[64] C. Zou, J. C. Fothergill, and S. W. Rowe, “The Effect of Water Absorption on the Dielectric Properties of Epoxy Nanocomposites,” *IEEE Trans. Dielectr. Electr. Insul.*, vol. 15, no. 1, pp. 106–117, 2008.

[65] V. Yadav, D. Sahu, Y. Singh, and D. Dhubkarya, “The Effect of Frequency and Temperature on Dielectric Properties of Pure Poly Vinylidene Fluoride (PVDF) Thin Films,” in *Proceedings of the international multiconference of engineers and computer scuentists 2010*, 2010, vol. 3, pp. 17–20.

[66] J. K. Nelson and Y. Hu, “The impact of nanocomposite formulations on electrical voltage endurance,” *Proc. 2004 IEEE Int. Conf. Solid Dielectr. ICSD 2004.*, vol. 2, no. 4, pp. 832–835, 2004.

[67] M. Nagao and T. Tokoro, “High-field Dissipation Current Waveform in e-beam Irradiated XLPE Film at High Temperature,” *IEEE Trans. Dielectr. Electr. Insul.*, vol. 3, no. 3, pp. 375–379, 1996.

[68] M. Fujii, K. Tohyama, T. Tokoro, M. Kosaki, Y. Muramoto, and M. Nagao, “Increment of capacitive current and space charge formation of PP film near breakdown field,” in *1999 Conference on Electrical Insulation and Dielectric Phenomena Increment*, 1999, pp. 128–131.

[69] M. Fujii, M. Fukuma, T. Tokoro, Y. Muramoto, N. Hozumi, and M. Nagao, “Numerical analysis of space charge distribution in polypropylene film under AC

high field," in *Proceedings of 2001 International Symposium on Electrical Insulating Materials (ISEIM 2001).*, 2001, pp. 156–159.

[70] Novcontrol, "Alpha-A High Resolution Dielectric , Conductivity , Impedance and Gain Phase Modular Measurement System," *User's Man.*, no. 1, pp. 1–184, 2005.

[71] M. a Vasilyeva, I. V Lounev, and Y. a Gusev, "The Methodology of the Experiment on the Dielectric Spectrometer Novocontrol BDS Concept 80 Novocontrol BDS Concept 80 Study guide," *KAZAN Fed. Univ.*, vol. 2, pp. 1–65, 2013.